The moment-curvature relation of reinforced concrete

Th. Monnier
I.B.B.C.

Summary

This paper describes both experimental and theoretical research performed on the moment-curvature relation of reinforced concrete. The investigation concerns rectangular cross-sections in bending. The shape of the M-$\varkappa$ diagram under different conditions of loading-history is fully discussed, including rules to determine the idealised diagram. Furthermore, the theoretical determination of the M-$\varkappa$ diagram is taken into consideration. Therein, the relation is concluded from the properties of uncracked concrete and from the properties of the cracked cross-section. The "exact" analysis-procedure for the latter as well as approximation formulas concerning the properties of the cracked cross-section are discussed.

A complete survey of the tests performed is represented in Appendix I and II.

This investigation is only partly worked out in this paper. However, it leads to the conclusions that:

- the real bending stiffness of reinforced concrete in the cracked state and for a first-time loading is a rather simple function of the percentage of tensile reinforcement;
- the M-$\varkappa$ diagram for more complicated cases of "loading history" can be concluded in a satisfactory way from the diagram concerning a first-time loading;
- the CEB-formula for the bending stiffness in the cracked state under-estimates the real value of beams with low concrete qualities and for higher percentages of tensile reinforcement.

CONTENTS

NOTATIONS

A	area of tensile reinforcement
A'	area of compressive reinforcement
b	width of rectangular section or width of flange for flanged beams
E_a	modulus of elasticity of steel
E'_b	modulus of elasticity of concrete
E'_{bo}	$= E'_b$ in the origin of the concrete stress-strain diagram
E'_{be}	$= 2/3\ E'_{bo}$, defined in fig. 40
$(EI)_o$	bending stiffness in the uncracked state
$(EI)_g$	bending stiffness in the cracked state $(= \frac{\Delta M}{\Delta \varkappa})$
$(EI)_{gs}$	bending stiffness of a cracked section
$(EI)_t$	stiffness belonging to a retrograde branch or "unloading line"
f_c	deflection measured with a curvimeter in the region of constant moment
f_m	deflection at mid-span
h	distance from extreme compressive fibre to centroid of tensile reinforcement
h_t	total depth of the cross-section
I_{bo}	moment of inertia of an uncracked cross-section including the quantity of steel
K	quality of the concrete (for K 300 $\rightarrow \sigma'_w = 300$ kg/cm^2)
$k_{bo}.b$	web thickness of flanged beams
$k'_d.h$	distance from extreme compressive fibre to centroid of compressive reinforcement
$k_{ho}.h$	flange thickness of flanged beams
$k_{ht}.h$	depth of the cross-section $(= h_t)$
$k_x.h$	depth of neutral axis $(= x)$
$k_{xgr}.h$	depth of neutral axis at simultaneous attainment of concrete strain ε'_{be} and steel strain ε_{ae}
$k_{x_{max}}.h$	depth of neutral axis at simultaneous attainment of concrete strain ε'_{bu} and steel strain ε_{ae}
ℓ	span length
$\Delta\ell$	crack distance
M	bending moment
M_c	moment in the mid-span (region of constant moment)
M_e	yield moment
M_r	cracking moment
M_u	ultimate moment according to the G.B.V.-1962

ΔM total bending moment less M_r

N_a resultant steel tensile force

N'_a resultant steel compressive force

N'_b resultant concrete compressive force

n ratio of modulus of elasticity of steel to that of concrete ($= \frac{E_a}{E'_b}$)

n_o ratio $\frac{E_a}{E'_{bo}}$

n_e ratio $\frac{E_a}{E'_{be}}$

P point load

r_a ratio $\frac{\varepsilon_{ae}}{\varepsilon'_{be}}$

r_d ratio $\frac{\varepsilon'_b}{\varepsilon'_{be}}$

W_{bo} section modulus of an uncracked cross-section including the quantity of steel

W_{ag} section modulus in the cracked state ($= \frac{\Delta M}{\Delta \sigma_a}$)

x depth of neutral axis ($= k_x.h$)

z lever arm

$\emptyset$ diameter in mm of a bar of the reinforcement or stirrup

ε_a strain of tensile reinforcement

ε'_a strain of compressive reinforcement

$\varepsilon_{ae}; \varepsilon'_{ae}$ strain at commencement of yielding of tensile reinforcement and compressive reinforcement respectively ($= \sigma_{ae}/E_a$; σ'_{ae}/E_a)

ε'_b strain of extreme compressive fibre

ε'_{be} concrete compressive strain at maximum compressive stress σ'_{be}

ε'_{bu} maximum concrete compressive strain ($= 3.5\,‰$ according to the G.B.V.-1962)

φ angular rotation

$\varkappa$ curvature (average curvature in a region of constant moment)

$\varkappa_e$ curvature at the yield moment

$\varkappa_r$ curvature at the cracking moment

$\varkappa_{pl}$ plastic curvature

$\Delta\varkappa$ total curvature less $\varkappa_r$

σ_a stress in tensile reinforcement

σ'_a stress in compressive reinforcement

σ_{ae};σ'_{ae} yield stress of tensile reinforcement and compressive reinforcement respectively

σ_{ar} stress in tensile reinforcement at cracking moment

σ_{au} ultimate tensile stress

$\Delta\sigma_a$ total stress in tensile reinforcement less σ_{ar}

σ_b tensile stress (in bending) of concrete *)

σ'_b concrete compressive stress

σ'_{be} maximum concrete compressive stress ($=\alpha\sigma'_w$)

σ'_{bu} concrete compressive stress belonging to the strain ε'_{bu}

σ'_w concrete compressive stress determined on 20 cm cubes

ω tensile steel ratio $\frac{A}{bh}$

ω' compressive steel ratio $\frac{A'}{bh}$

ω_o percentage of tensile reinforcement (= 100 ω)

ω'_o percentage of compressive reinforcement (= 100 ω')

ω_{gr} tensile steel ratio ω of a cracked section (without compressive reinforcement) at which $\varepsilon'_b = \varepsilon'_{be}$ and $\varepsilon_a = \varepsilon_{ae}$

ω_{max} ditto, but with $\varepsilon'_b = \varepsilon'_{bu}$ and $\varepsilon_a = \varepsilon_{ae}$

*) σ_{bt} mentioned in table I-1 and II-2 is the tensile strength measured on prisms according to a 3-point bending test with $\ell = 2\ h_t$ ($\sigma_b = 0.75\ \sigma_{bt}$).

1. Introduction

Knowledge of the real distribution of moments and the possible redistribution of bending moments after cracking in statically indetermined reinforced concrete structures is especially of importance if:

- deformations are imposed upon the structure;
- the distribution of the quantity of reinforcement in the structure does not conform the disposition required by the distribution of the moments in accordance with the elastic theory. *)

For studying the above-mentioned subjects it is necessary to have reliable moment-curvature diagrams of reinforced concrete at one's disposal. Having regard to these considerations the M-$\varkappa$ diagram of reinforced concrete was investigated by means of both experimental and theoretical research. The M-$\varkappa$ diagrams in this paper concern rectangular cross-sections, in which only a bending moment occurs.

In this paper the discussions will enclose at first the shape of the M-$\varkappa$ diagram obtained from test-beams under the different conditions of loading. After the experimental investigation a number of empirical formulas were developed in order to apply the test results as quick as possible in (computer-) calculations concerning the real behaviour of reinforced concrete structures. The empirical formulas, the idealised M-$\varkappa$ diagram and the rules with which the latter can be found are fully discussed. More data concerning the experimental investigation, enclosing two groups of beams, are represented in detail in Appendix I and II.

The real, measured M-$\varkappa$ diagram in the cracked state of the concrete is in fact an average of the properties of both the cracked cross-sections and the uncracked concrete between two cracks. The theoretical considerations started with a method to derive directly the measured M-$\varkappa$ diagram for a first-time loading from the properties of the cracked and uncracked cross-sections. Furthermore, a calculation procedure is developed, which is programmed for the computer, to calculate the stresses and strains in concrete and steel completely, also in the region between two cracks. These calculations are until now applied only for a first-time loading; however, the programme is suitable for more variation. It has been deve-

*) This subject is discussed in a separate paper: The behaviour of continuous beams in reinforced concrete (results of experimental and theoretical investigation)
Heron, vol. 17 (1970), no. 1

loped to collect more knowledge by calculation. The analysis procedure and the results obtained will be published in a separate paper.

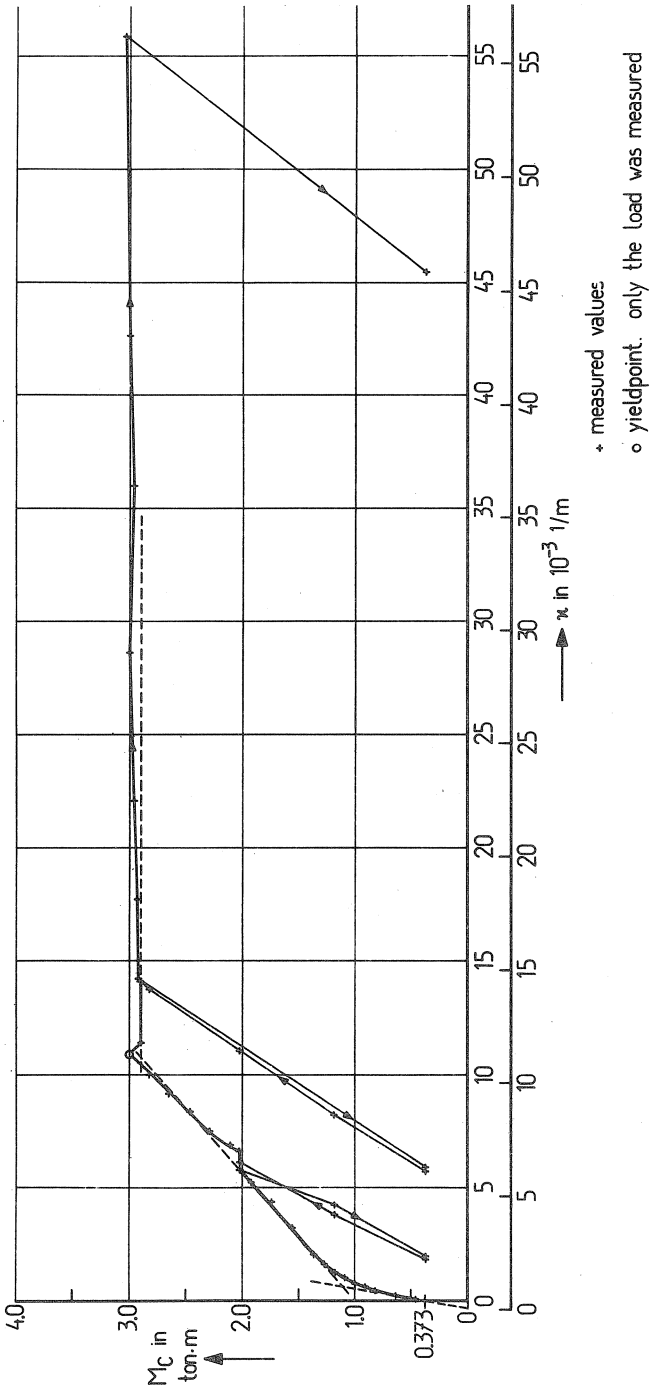

Fig. 1 A measured M-$\varkappa$ diagram. (Beam VII, see Appendix I)

2. The shape of the M-$\varkappa$ diagram (discussion of the test results and practical rules to determine the idealised diagram)

The desired moment-curvature relations are obtained from beams tested according to the well-known four-point bending test. For every load increment the lengthenings and shortenings were measured along the total length of the region of constant moment, that occurs in those test-beams. Finally the (average) curvature calculated from these data is plotted against the moment concerned, as represented in Fig. 1. All the measured M-$\varkappa$ diagrams are given in the Appendixes I and II together with the complete description of the investigation performed.

From the results of the measurements it appears that the relation between moment and curvature for a first-time loading can be approximated by means of three straight lines. Fig. 2 presents examples of diagrams for 4 different percentages of tensile reinforcement.

The first branch of the M-$\varkappa$ diagram is related to uncracked concrete. The concerning flexural stiffness $(EI)_o$ is equal to the modulus of elasticity of the concrete multiplied by the moment of inertia of the entire cross-section, including the reinforcement:

$$(EI)_o = E'_{bo} \cdot I_{bo}$$

The modulus of elasticity of the concrete can, for practical use, be related with the cube strength of the concrete according to:

$$E'_{bo} = (1/3\ \sigma'_w + 200) \cdot 10^3 \text{ kg/cm}^2$$

In every measured M-$\varkappa$ diagram produced in this paper the $(EI)_o$, calculated in this way, is drawn too. In general, the agreement with the measured values appears to be good.

At the fictitious cracking moment M_r the influence of the crack formation becomes noticeable. In reality, the first branch of the M-$\varkappa$ diagram shades off into the second branch concerning the flexural stiffness $(EI)_g$ in the cracked state. Cracks, however, arise already before the moment M_r is reached in the test beams; that is why M_r was called fictitious in the first instance.

An exact calculation of this cracking moment M_r appears to be impossible as yet. Therefore this moment is approximated with the formula:

$$M_r = \sigma_b \cdot W_{bo}$$

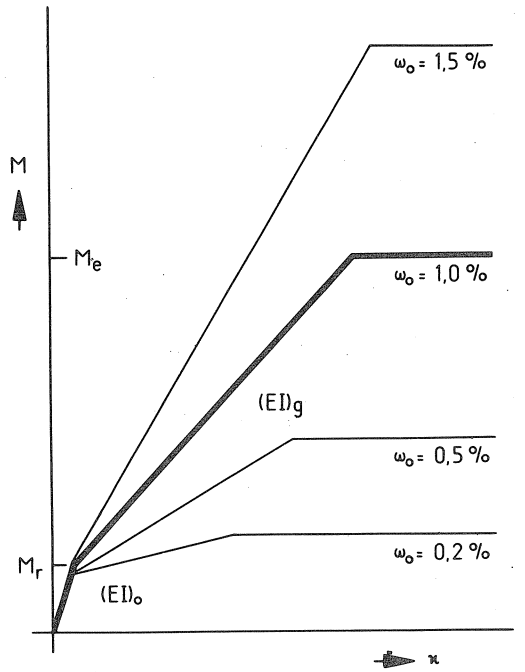

Fig. 2 Some examples of idealised M-$\varkappa$ diagrams.

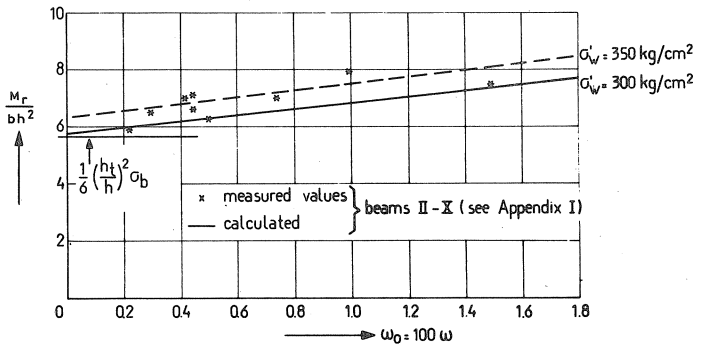

Fig. 3 The 'cracking' moment M_r.

In which

σ_b = tensile strength of the concrete which can be found for this purpose according to $\sigma_b = 1.2\ (1/20\ \sigma'_w + 10)$ kg/cm^2, where σ'_w is the cube strength of the concrete

W_{bo} = section modulus, including the reinforcement

In consequence of the normal variation of the tensile strength of the concrete and of shrinkage stresses in the concrete, the measured values for the cracking moments in the various tests can differ rather considerably from one another. Nevertheless, the approximation mentioned above, appears to be in reasonable good agreement with reality as shown in Fig. 3. In this figure a comparison is made for measured and calculated values, concerning the test-beams discussed in Appendix I.

The bending stiffness $(EI)_g$ in the cracked state of the concrete is as said before, an average of both cracked cross-sections and uncracked reinforced concrete between the cracks. A realistic calculation taking everything which plays a part into account is very intricate. That was the main reason why experiments were performed. Fig. 4 presents the measured $(EI)_g$ as a function of the percentage of tensile reinforcement in the cross-section (see Appendix I). This figure shows already that the stiffness $(EI)_g$ is rather simply connected with the percentage of tensile reinforcement, limited on the one hand by the minimum percentage of reinforcement and on the other hand by a percentage at which $(EI)_g = (EI)_o$. Fig. 4 shows also that both the grade of steel and the diameter of the bars (with a given reinforcement percentage) have no noticeable effect upon the stiffness in the cracked state. The data concerned, completed with experimental data published in literature, confirm the indication discovered. All the collected data are plotted down in Fig. 5. Although these data comprise qualities of concrete ranging in strength from 150 to 500 kg/cm^2, a number of steel grades and different percentages of compressive reinforcement, all the points are found to be situated reasonably close together, with regard to one percentage of tensile reinforcement. The empirical expression

$$(EI)_g = (-\ 2.5\ \omega_o^{\ 2} + 13.9\ \omega_o - 1.1)\ bh^3\ .\ 10^3\ \text{kgcm}^2$$

where ω_o is the percentage of tensile reinforcement, appears to be in reasonable good agreement with the data obtained. The empirical curve

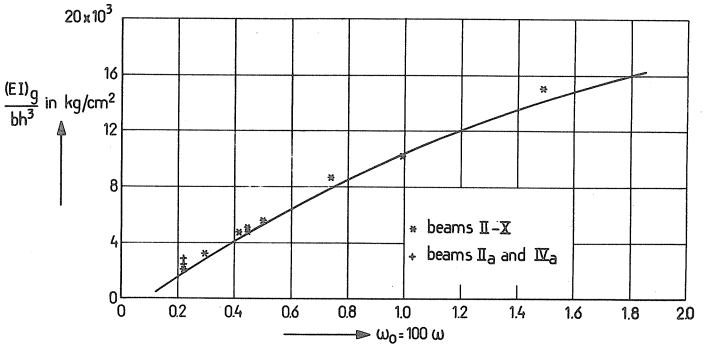

Fig. 4
The stiffness $(EI)_g$ concerning beams of Appendix I.

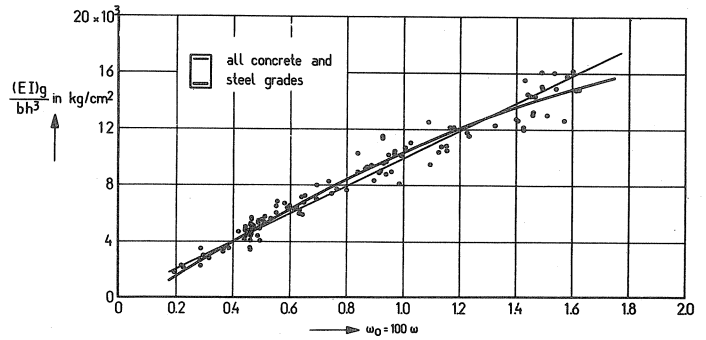

Fig. 5
The stiffness in the cracked state $(EI)_g$ as a function of the percentage of tensile reinforcement.

is drawn thick in Fig. 5.

For practical use even a simpler formula is available for the bending stiffness in the cracked state, namely:

$$(EI)_g = \omega_o \, bh^3 \, 10^4 \text{ kg cm}^2$$

The empirical line representing this expression is drawn thin in Fig. 5. From the figure it seems to be necessary to limit the validity of the latter at $\omega_o \approx 1.5\%$. Nevertheless, the range of ω_o's in which that simple formula can be used is much greater, as will be pointed out in the theoretical considerations later on in this paper.

The influence of load alternations, applied while the load is being increased, can be neglected with regards to the resultant value of $(EI)_g$. In those cases the resultant second branch of the M-$\varkappa$ diagram moves a little parallel to itself to the right, as is shown in Appendix II.

The horizontal third branch of the M-$\varkappa$ diagram occurs when the (tensile) stress of the steel reinforcement attains the yield stress concerned. It is assumed here that with regard to the "hyperstatique" structures under discussion the cross-section will always be designed as an under-reinforced one (e.g. yielding occurs before the concrete crushes). The concerning yield moment M_e can be approximated with a calculation of M_u according to the well-known ultimate-load method for a cross-section.

The conditions at that state (ultimate moment M_u) according to the Dutch Code of Practice GBV are represented in Fig. 6. Fig. 7 shows the agreement between the measured moment M_e and the calculated values (both M_e and M_u) for the beams discussed in Appendix I (average steel grade QR 44). Near yield moment the agreement between idealised and measured M-$\varkappa$ diagrams remains perfect for beams containing steel with a definite yield point. If cold-drawn steel is applied, the second branch of the diagram shades off into the third one by a smooth curve. In accordance with normal design-practice for cold-drawn steel so far, this difference will be neglected. At yielding, reinforced concrete turns out to be a very tough material in most cases (see Fig. 8 and 9).

Finally, the cross-section fails when the cube-strength of the concrete is reached. Thus, the curvature-capacity available depends in general on the percentage of reinforcement, the steel grade and the concrete quality applied.

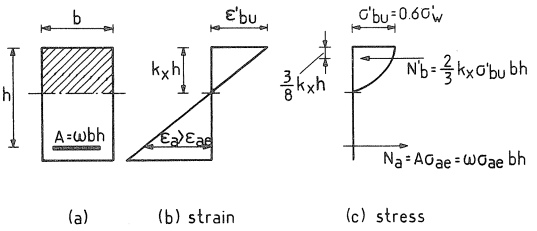

Fig. 6
Conditions at ultimate moment according to the G.B.V.

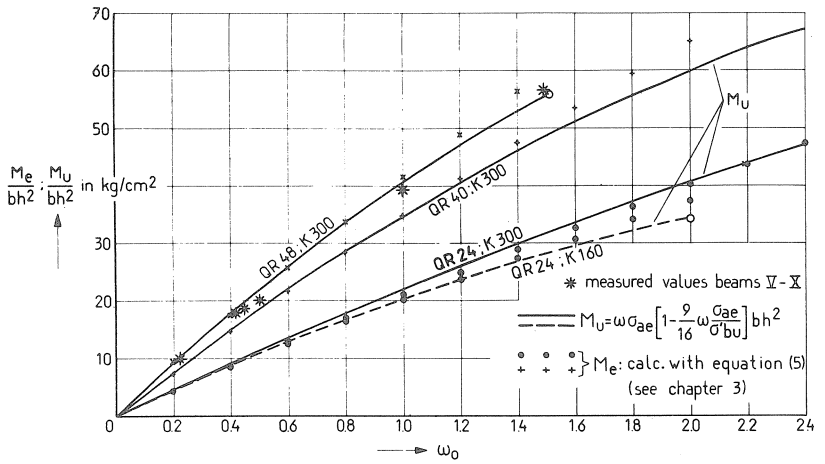

Fig. 7
Comparison of measured and calculated yield moments and the ultimate moment according to the G.B.V.

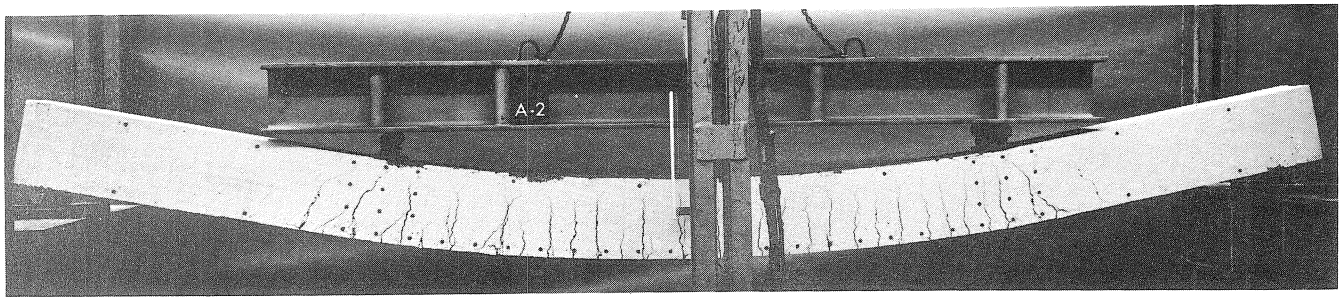

Fig. 8
Beam A_2 after yielding.

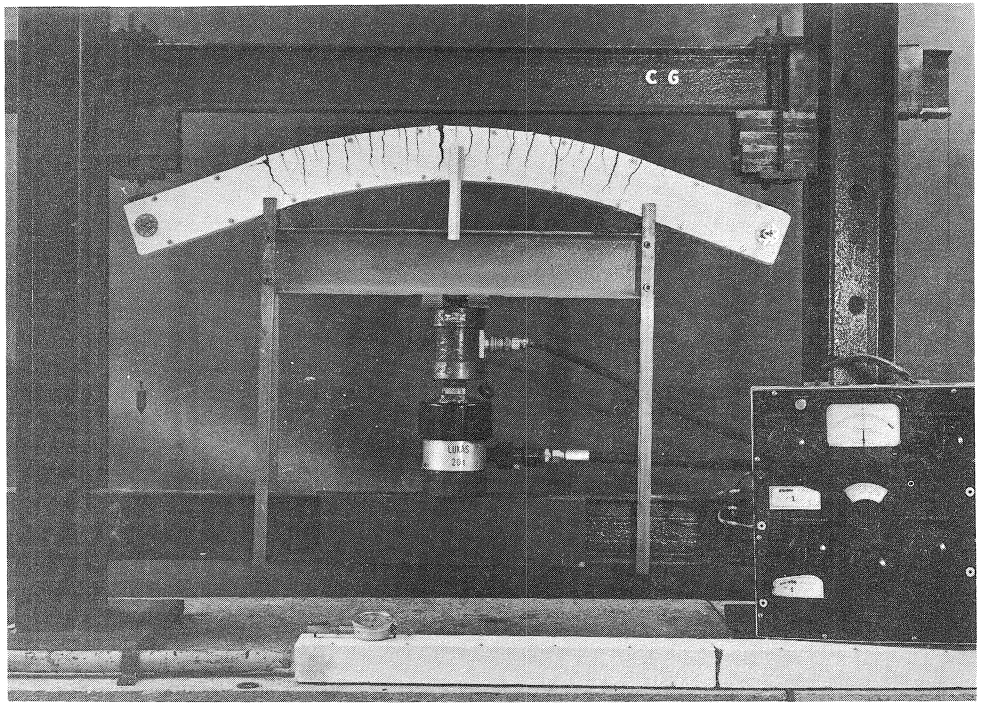

Fig. 9
Beam C_6 after yielding.

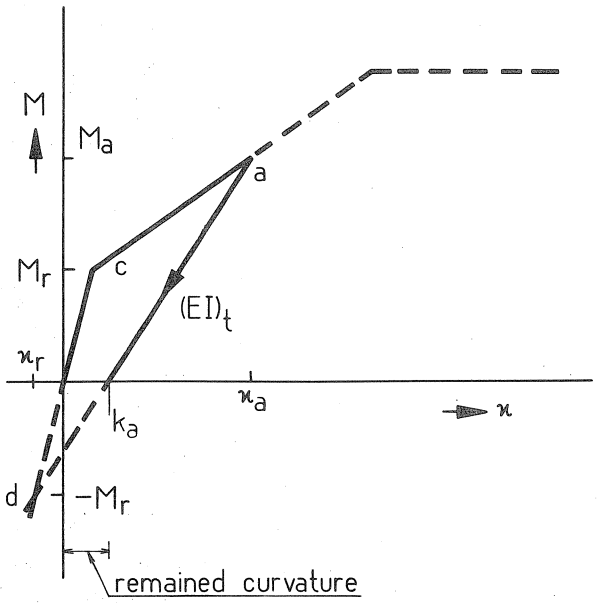

Fig. 10 Retrograde branch in the M-$\varkappa$-diagram

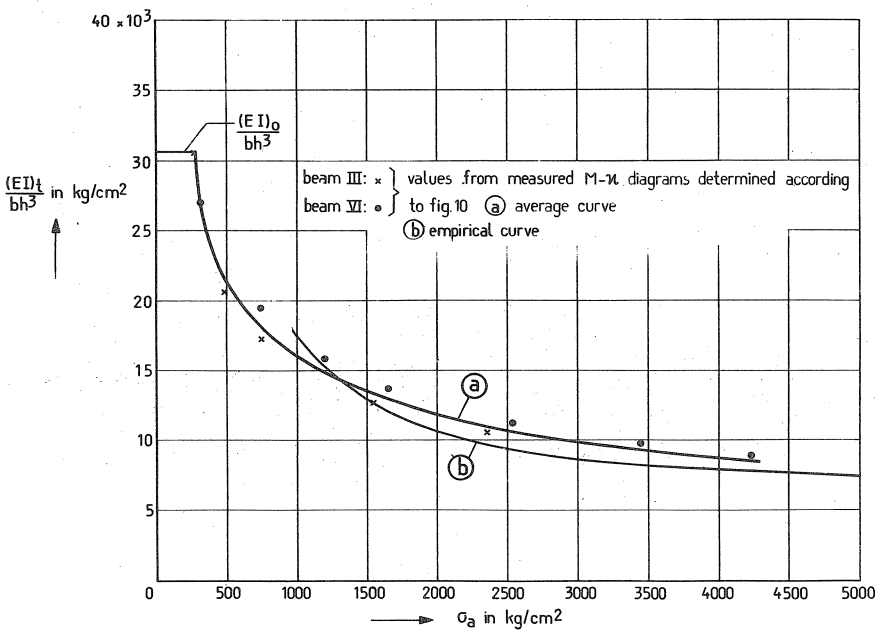

Fig. 11 The stiffness $(EI)_t$ of retrograde branches.

Of course it is possible that the moment occurring in a cracked part of a beam decreases. After increasing again to the original value, the relationship between bending moment and curvature will have the form of a loop in reality (see Fig. 1 and the figures in Appendix I). The difference between these loops and a straight line are only small. Therefore, they have been schematised as straight lines, which everywhere represent the average stiffness of the loop. These lines are designated as retrograde branches or unloading lines. The associated stiffness is $(EI)_t$, which shows all in all a reasonable agreement with reality. The stiffness $(EI)_t$ concerned appears to be a rather simple function of the percentage of tensile reinforcement and the value of the moment or steel stress reached, when the loading reduced. An empirical expression is presented in Appendix I. From the results of the measurements (concerning rectangular sections), it appears also that the unloading line can be represented by a straight line a-d, as drawn in Fig. 10. Point a is related to the moment where the loading decreased; the other point d corresponds with the mirror image of point c, the intersection of the first and the second branch of the original $M-\varkappa$ diagram, as shown in the figure. All the retrograde branches of the diagram can be assumed to have that common point of intersection d. From this figure it appears also that a remaining curvature exists when the moment reaches zero again. This finds an origin in the bond-slip occurring between reinforcement and concrete, which is a nearly complete permanent, plastic deformation. Fig. 11 shows the reasonable good agreement between the empirical curve (b) concerning "unloading lines" (from Appendix I) and the curve (a) representing an average of $(EI)_t$ values determined according to a-d as drawn in Fig. 10. The latter have been used in our calculations carried out so far.

If the moment decreases to such an extent that the original compressive zone becomes cracked, the stiffness at that bending moment becomes equal to $(EI)_{g1}$ corresponding to the original compressive reinforcement. This value can therefore directly be calculated by means of the given formula for the stiffness in the cracked state. The diagram is shown in Fig. 12. If the moment then decreases - at M_b, for example, see Fig. 13 - the previously given rules are again valid for the retrograde branch in question, up to the abscissa $M = 0$. On passing this, the relation between moment and curvature is best approximated by the straight line connecting this intersection point to that point in the

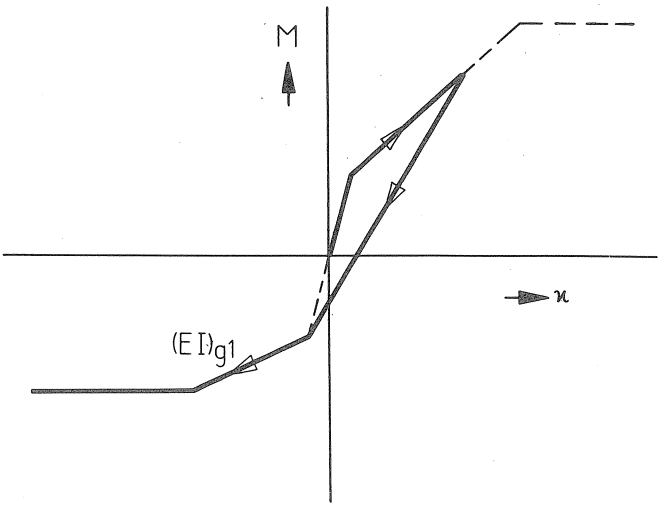

Fig. 12

Change of sign of
the moment after cracking

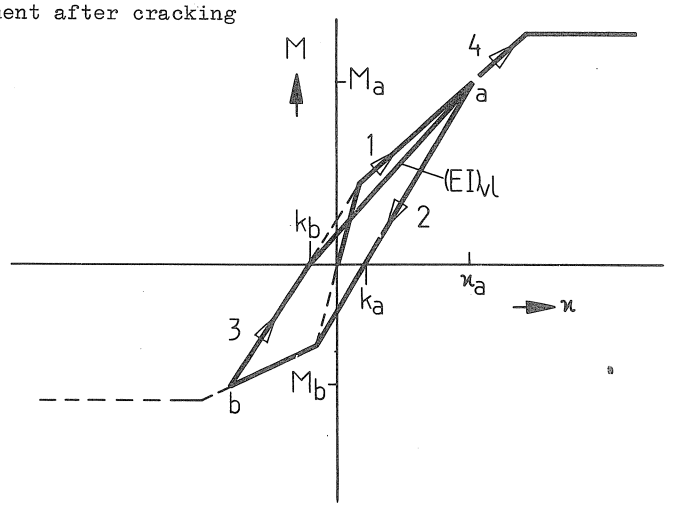

Fig. 13

Change of sign of the moment before occurence of yielding

original M-$\varkappa$ diagram where the moment began to decrease. Thereafter the original diagram is followed.

If the yield moment is exceeded in the M-$\varkappa$ diagram, it is found that the direction of the retrograde branch undergoes no further change. All the plastic deformations in that case are indeed permanent deformations. This state of affairs is indicated in Fig. 14.

If the moment then changes its sign, as in Fig. 15, then there are two possible directions for the branch after passing through the axis of abscissae (in Fig. 15 the branch in question is provided with arrow No. 3) which provide good approximations to the measured branches in the conditions concerned:

1. If the point of intersection S2 (see Fig. 15) is located between the origin of the diagram and the intersection S1 of the extended second branch (associated with the original compressive reinforcement) with the axis of abscissae, then the relevant branch below this axis has the same direction as that of the retrograde branch corresponding to the yield moment of the original compressive reinforcement.

2. The second possibility is that S2 is located to the right of S1. In that case the branch below the axis of abscissae has the same direction as that of the second branch of the M-$\varkappa$ diagram corresponding to the original compressive reinforcement.

If the original compressive reinforcement is plastically strained in tension to such an extent that the point where yield of the steel first occurred is passed, then the branch will, on reduction of this moment, again follow the direction of the corresponding retrograde branch. If the plastic deformation of the original compressive reinforcement is less than this, then the direction of the second branch of the diagram will be retained. These behaviour patterns are shown in Fig. 16. Above the axis of abscissae the relation between moment and curvature is represented by the connecting line from the point of intersection with the axis of abscissae to the point of the diagram where the "loop" had started. In the loops envisaged here the directions of most of the lines are now known; only the directions of the connecting lines remain to be determined. The other lines in the loop are parallel to lines for which rules defining them have already been found.

Of course, the designations "above" and "below" the axis of abscissae

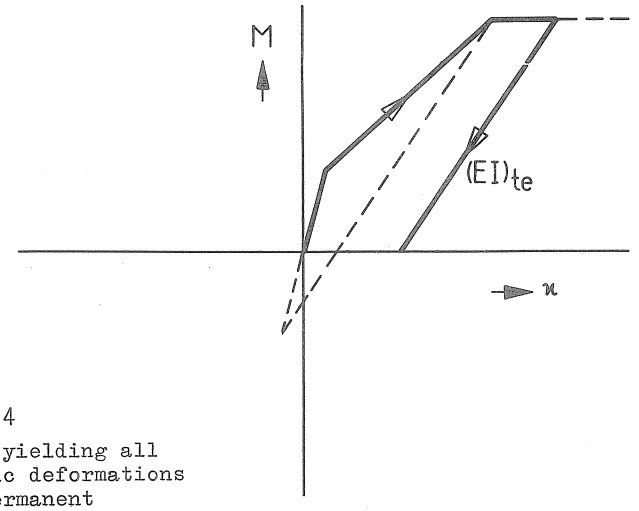

Fig. 14

After yielding all plastic deformations are permanent

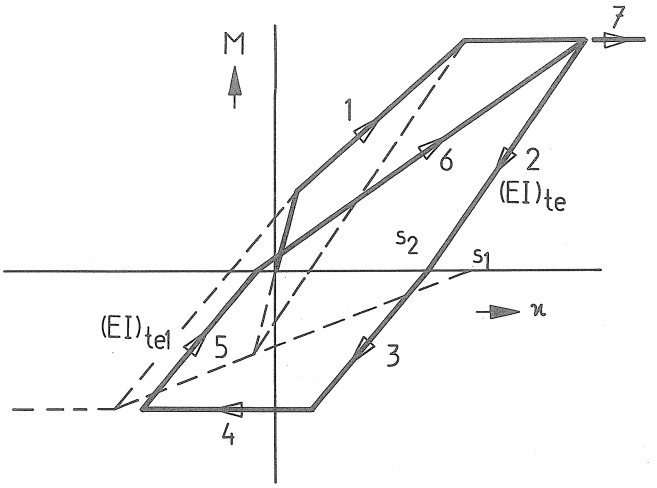

Fig. 15

M-$\varkappa$ diagram for change of sign of the moment after yield moment has been exceeded.

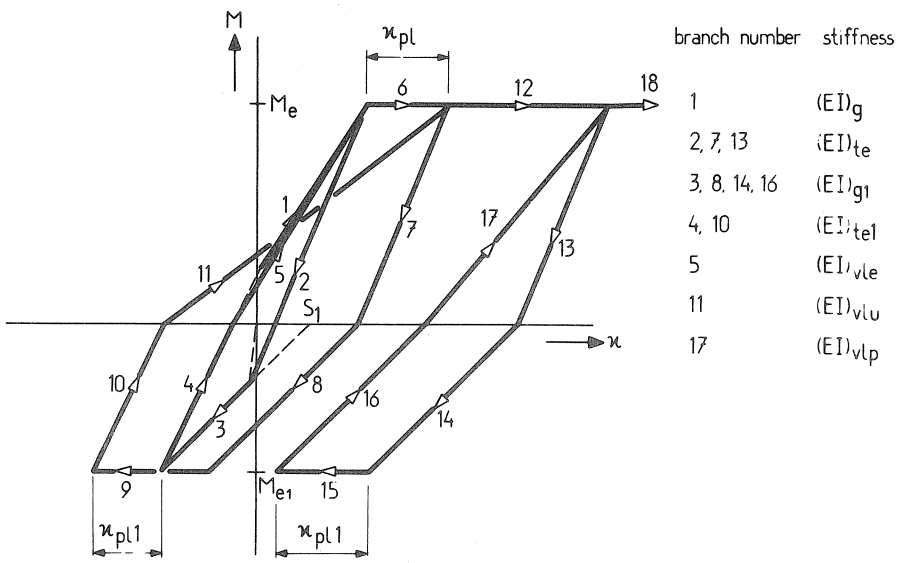

Fig. 16 Schematised M-$\varkappa$ diagram for change of sign of the moment

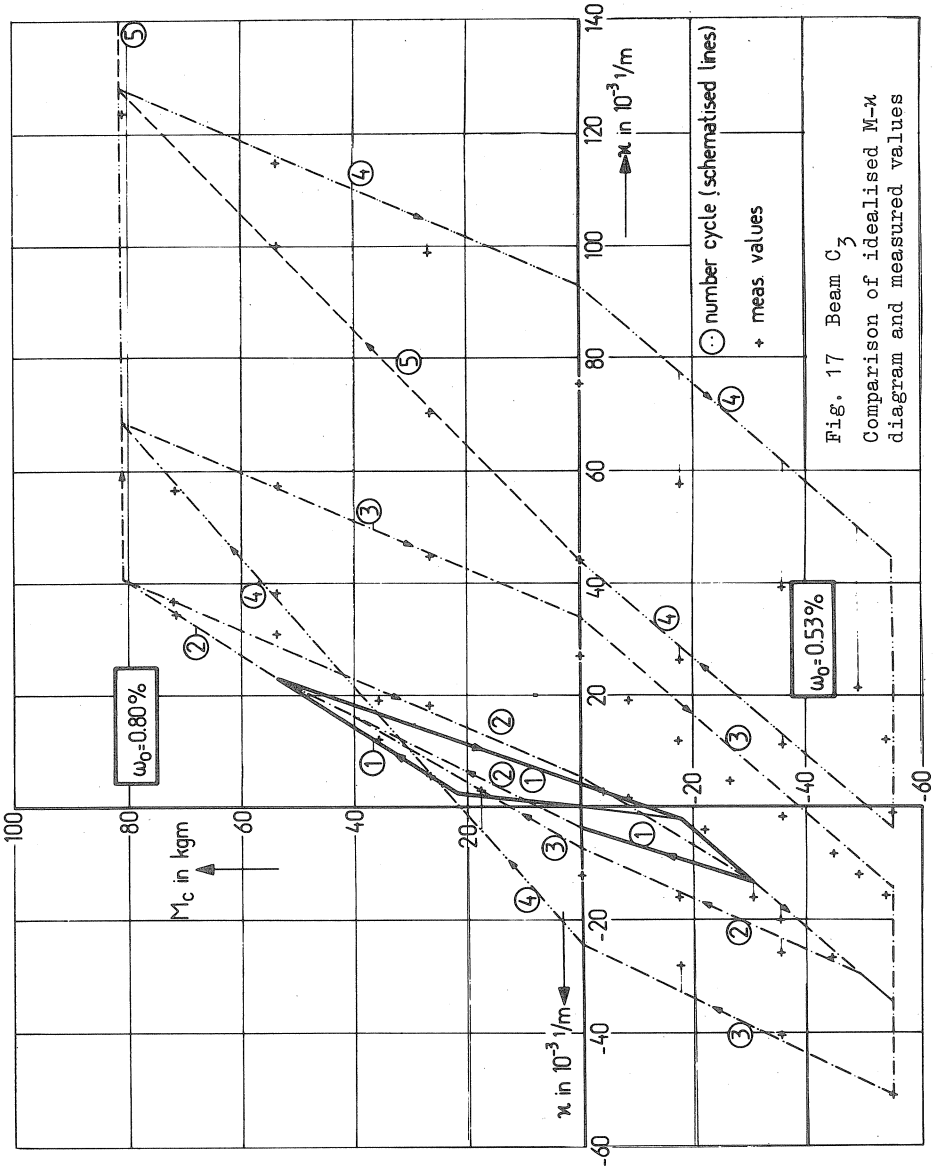

Fig. 17 Beam C_3
Comparison of idealised M-$\varkappa$ diagram and measured values

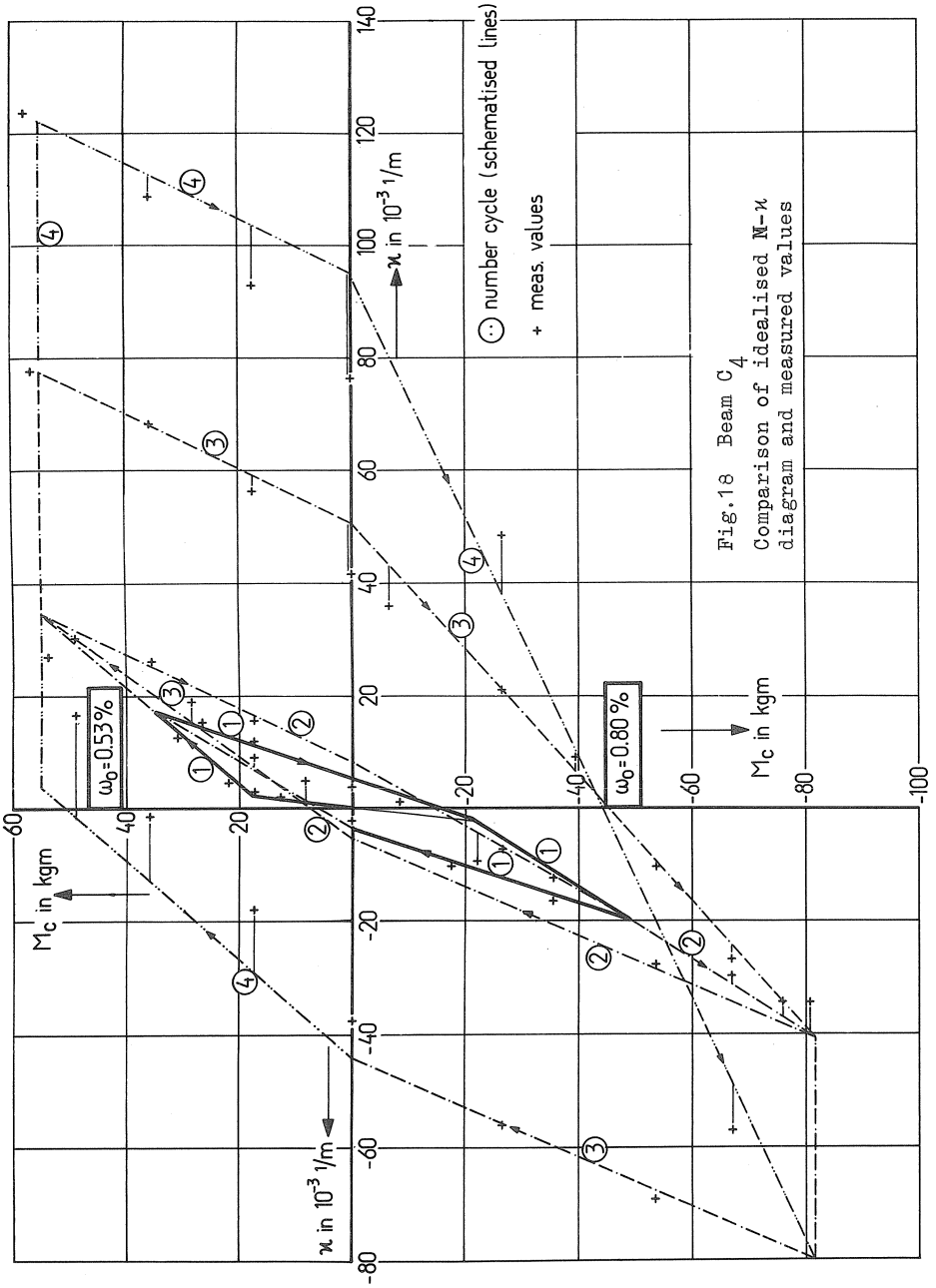

Fig.18 Beam C_4
Comparison of idealised M-$\varkappa$ diagram and measured values

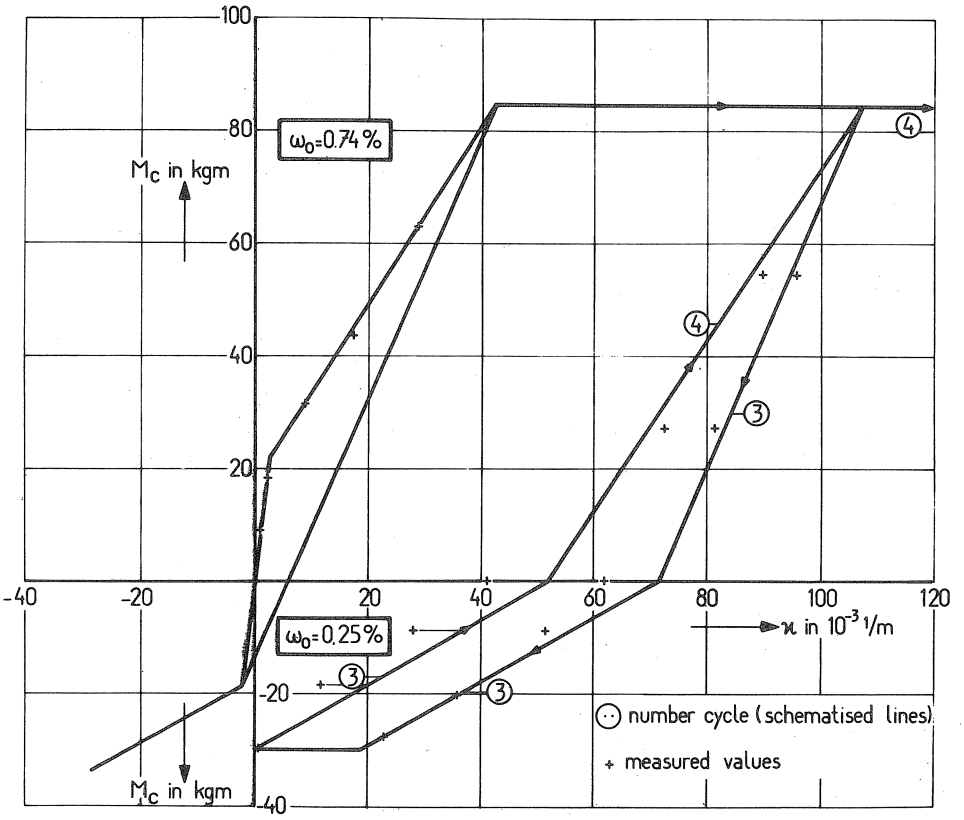

Fig. 19 Beam D_1

Comparison of idealised M-$\varkappa$ diagram and measured values

relate only to the case represented in Fig. 16. In general, this should be taken to mean "on that side of the axis of abscissae where the loop begins and where the loop ends, respectively."

In Figs 17, 18 and 19 the schematised diagrams are compared with the measured values. There is seen to be reasonable good agreement. The measured data are derived from an experimental investigation discussed in Appendix II. In the appendix a complete survey is given of the tests themselves and the results obtained.

A fortunate circumstance in this connection is that the M-$\varkappa$ diagram for a first-time loading, which diagram can be calculated with the aid of empirical equations given before, continues to form part of the diagram in which the moment changes its sign. From the results of the measurements it further appeared that the relation between moment and curvature can, in the case of a change in the sign of the moment, also be approximated by means of a number of straight lines. In Fig. 20 these lines are generally associated with the three straight branches of the M-$\varkappa$ diagram for a loading applied for the first time. This figure presents also a number of empirical equations expressed in those data, by means of which the desired diagram can be established.

With the above schematisation of the M-$\varkappa$ diagram and the associated rules it therefore becomes possible to utilise the measured data for calculations concerning shake-down analysis. Although the equations look somewhat forbidding, they are adequately suited for use in the computer programme.

Branch no.	Stiffness	Formula	Remarks
1	$(EI)_0$		
2, 7, 20, 22	$(EI)_g$	$= (-2.5\,\omega_o^2 + 13.9\,\omega_o - 1.10)\ bh^3 \cdot 10^3\ kgcm^2$	$g = (EI)_g/(EI)_0$
3	$(EI)_t$	$t = \dfrac{g(M_a + M_r)}{M_a + (2g - 1)M_r}$	$t = (EI)_t/(EI)_0$
4. 11	$(EI)_{g_1}$		$g_1 = (EI)_{g_1}/(EI)_0$
5	$(EI)_{t_1}$	$t_1 = \dfrac{g_1(M_b + M_r)}{M_b + (2g_1 - 1)M_r}$	$t_1 = (EI)_{t_1}/(EI)_0$
6	$(EI)_{vl}$	$vl = \dfrac{g.g_1.t_1.M_a}{g_1.t_1.M_a + g(t_1 - g_1)M_b - t_1(g + g_1 - 2g.g_1)M_r}$	$vl = (EI)_{vl}/(EI)_0$
9, 14, 16	$(EI)_{te}$	$te = \dfrac{g(M_e + M_r)}{M_e + (2g - 1)M_r}$	$te = (EI)_{te}/(EI)_0$
10	$(EI)_{vlu_1}$	$vlu_1 = \dfrac{g.g_1.te.M_b}{g.te.M_b + g_1(te-g)M_e - te(g+g_1-2g.g_1)M_r + \varkappa_{pl}.g.g_1.te(EI)_0}$	$\varkappa_{pl}$ = plastic curvature of branch 8
13, 19	$(EI)_{te_1}$	$te_1 = \dfrac{g_1(M_{e_1} + M_r)}{M_{e_1} + (2g_1 - 1)M_r}$	$te_1 = (EI)_{te_1}/(EI)_0$
17	$(EI)_{vlu_1}$	same as branch 10 but with $M_b = M_{e_1}$	$\varkappa_{pl}$ = sum of plastic curvatures of branch 12, 8 and the partion of 15 after 8
23	$(EI)_{vlp_1}$	$vlp_1 = \dfrac{t_{e_1}.M_{e_1}}{M_{e_1} + t_{e_1}(EI)_0.\varkappa_{pl}}$	$\varkappa_{pl}$ = plastic curvature of branch 21

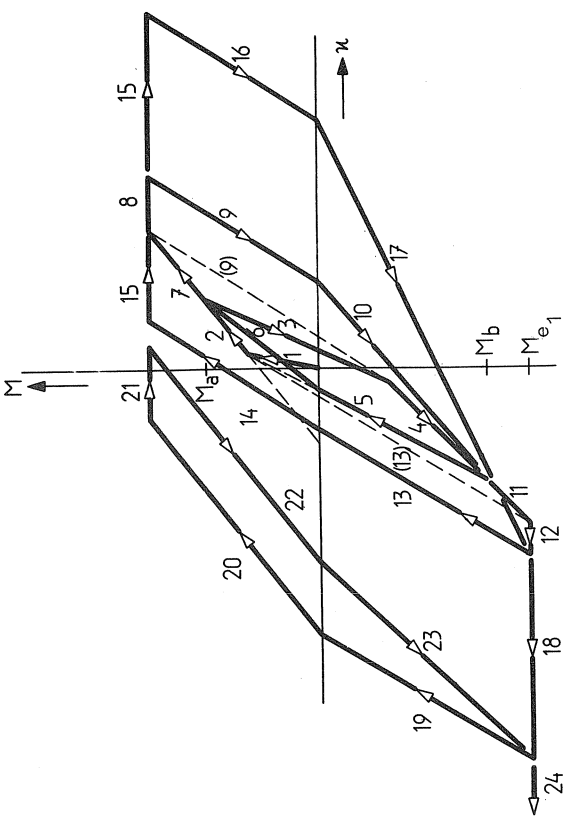

Fig. 20 Expression for the M-$\varkappa$ diagram of reinforced concrete.

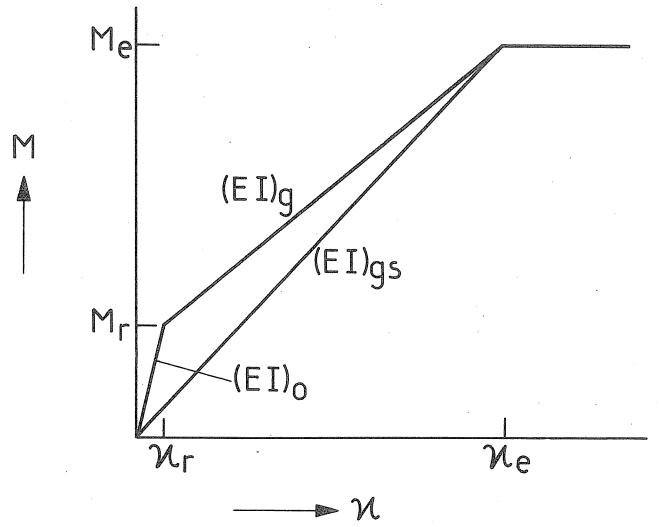

Fig. 21

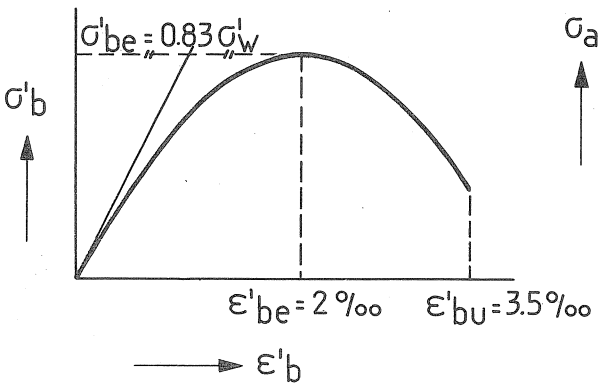

Fig. 22

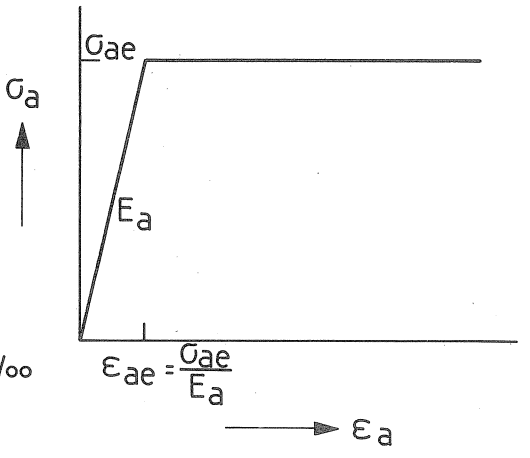

Fig. 23

3. Theoretical considerations

From the tests performed a clear insight has been obtained, which shape the M-$\varkappa$ diagram of reinforced concrete has under different conditions of "loading history". Still, a further theoretical interpretation of the results seems to be necessary. At first for a better understanding of the measured data. Secondly with the purpose to find an analysis-procedure that gives the opportunity to extend the knowledge obtained by calculations.

In this paper the accent of the interpretation will be led on the M-$\varkappa$ diagram for a first-time loading with special regard to rectangular beams in bending alone.

As mentioned in the introduction, the measured M-$\varkappa$ diagram, after cracking, is an average of the properties of both cracked sections and uncracked concrete between the cracks. The stiffness of a cracked section alone $(EI)_{gs}$ is represented in the M-$\varkappa$ diagram as a straight line connecting the origin of the diagram and the curvature where the yield moment is reached, see Fig. 21. In general this appears to be a reasonable good approximation, although especially for lower percentages of tensile reinforcement, a rather unimportant difference occurs. In those cases, $\omega_o < 0.5\%$, the above-mentioned line is "stiffer" than according to a calculation.

Two methods can be distinguished with regard to the theoretical determination of the M-$\varkappa$ diagrams.
At first, the real stiffness $(EI)_g$ in cracked state can be calculated directly, using the idealised diagram as a basis and with:
the stiffness of the uncracked section $(EI)_o$, the fictitious cracking moment M_r, the stiffness of the cracked cross-section $(EI)_{gs}$ and the yield-moment M_e, according to:

$$(EI)_g = \frac{M_e - M_r}{\varkappa_e - \varkappa_r} = \frac{M_e - M_r}{\frac{M_e}{(EI)_{gs}} - \frac{M_r}{(EI)_o}} \qquad (1)$$

Calculations concerning $(EI)_o$ and M_r have been discussed before; thus for this interpretation additional calculations with regard to the cracked section are still necessary. This design determines the stiffness $(EI)_g$ "over the head of" the stresses and the deformation of the reinforced concrete between the cracks.

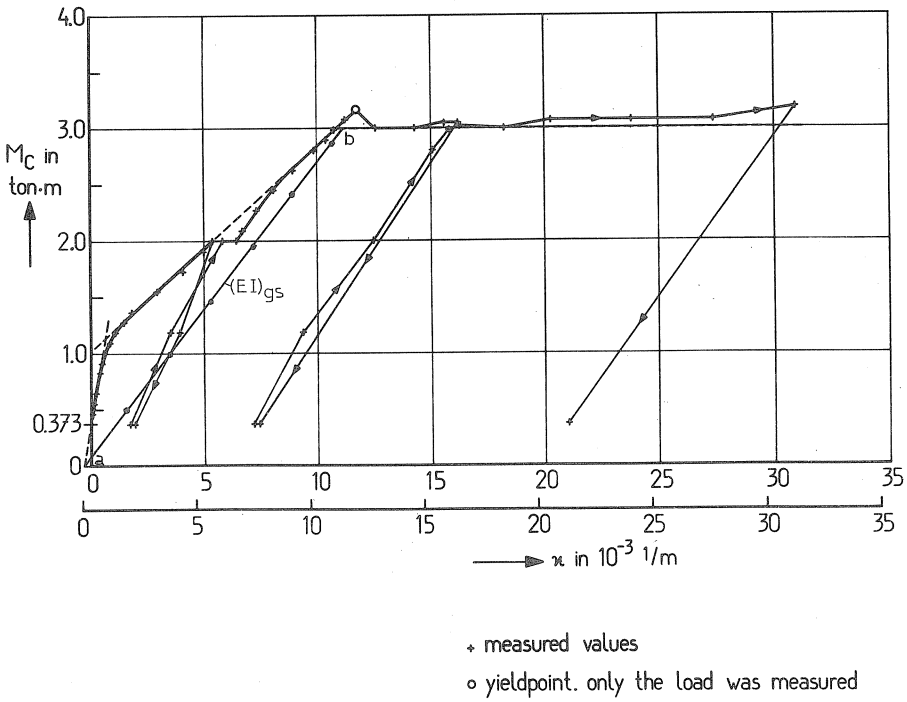

Fig. 24
Comparison of a calculated stiffness $(EI)_{gs}$ and a measured M-$\varkappa$ diagram. (Beam VI, ω_0 = 0.44%, see Appendix I)

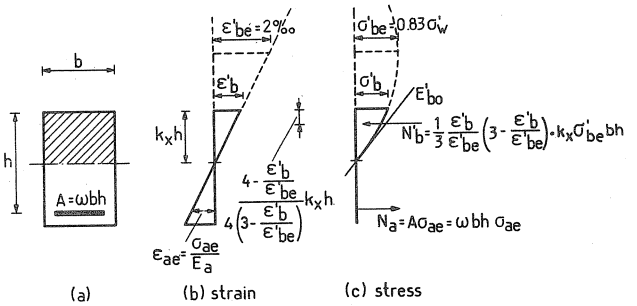

Fig. 25 Conditions at yield moment Me.

The calculation of the latter is performed in another analysis procedure. However, those calculations are rather complicated, the advantages are attractive. Therefore this calculation is developed and programmed for the computer. Only the cracked section and the additional considerations, however, will be discussed in this paper.

3.1. Calculations concerning the cracked section

In order to approach reality as close as possible, the calculations will be carried out for a parabolic stress-strain diagram of the concrete (Fig. 22). As usual, the stress-strain diagram of steel is assumed to be as drawn in Fig. 23. The tensile strength of the concrete is neglected. The basic assumptions used and the derivation of the formulas is presented in Appendix III. Because the interpretation under consideration concerns short-time loading tests, the calculations are mainly performed with regard to the σ'_b-ε'_b diagram of concrete where $\varepsilon'_{be} = 2‰$ and $\sigma'_{be} = 0.83\ \sigma'_w$ ($\equiv$ prism strength). *)

From calculations in this way, the relation between curvature and moment of the cracked cross-section appears to be a very smooth curve. On the scale of Fig. 24 the deviation from the straight line a-b is even invisible. Therefore, in the further consideration the latter will be used as the right one. As a consequence, all our calculations are performed at the moment, where the yield stress σ_{ae} of the steel is reached (see Fig. 25). This yield moment M_e and the concerning curvature $\varkappa_e$ are sufficient to find the sought stiffness $(EI)_{gs}$ from

$$(EI)_{gs} = \frac{M_e}{\varkappa_e} \qquad (2)$$

Because of the parabolic stress-strain relation of the concrete, the solution of the problem can only be found by solving a 3rd degree equation in k_x ($\equiv$ ratio of the depth of the neutral axis), namely

$$-k_x^3 \left(3 + \frac{\varepsilon_{ae}}{\varepsilon'_{be}}\right) + 3\, k_x^2 (1 - 2\, n_o\omega) + 12\, k_x \cdot n_o\omega - 6\, n_o\omega = 0 \qquad (3)$$

*) The rather general derivation of the formulas in Appendix III allows the substitution of other values for ε'_{be} and σ'_{be}. Furthermore, the theory is applied to flanged beams and provides also with regard to the shape of the section more possibilities.

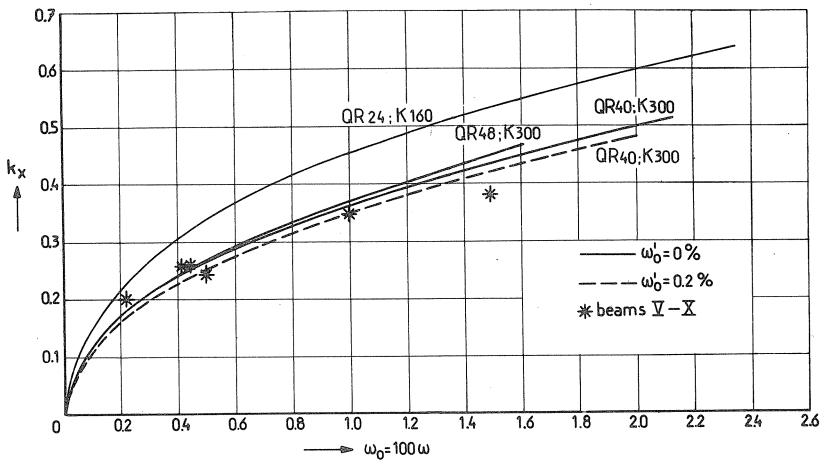

Fig. 26

Ratio k_x at yield moment, comparison of 'exactly' calculated and measured values.

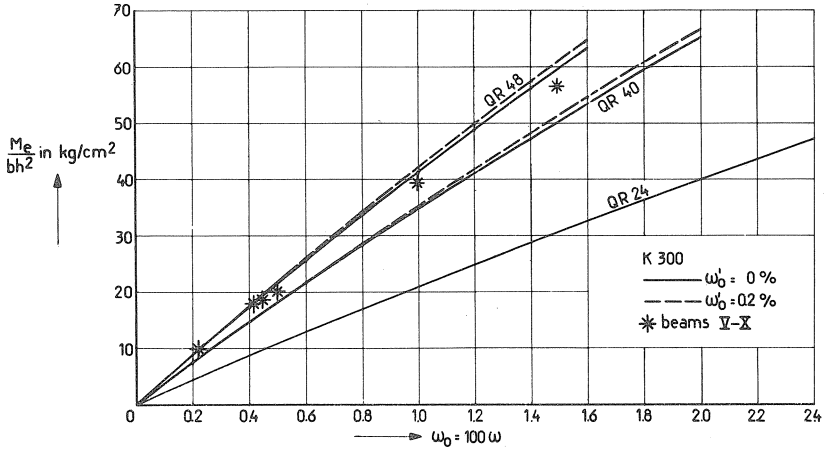

Fig. 27

The yield moment M_e, 'exactly' calculated values and measured values.

in which $n_o = \frac{E_a}{E'_{bo}}$ $(= E_a \cdot \frac{\varepsilon'_{be}}{2\sigma'_{be}}$, as a consequence of the parabolic stress-strain relation).

This formula follows from equilibrium of horizontal forces, after expressing the deformations of the section as functions of the strains ε_{ae} and ε'_{be}. The expression concerns a rectangular cross-section without compressive reinforcement. Fig. 26 presents some results of the calculations for the ratio k_x (with $\varepsilon'_{be} = 2‰$ and $\sigma'_{be} = 0.83\ \sigma'_w$); the comparison of those ones with measured values (from Appendix I) is satisfactorily.

After solving the equation presented above, at yield moment, the actual concrete strain follows from:

$$\varepsilon'_b = \varepsilon_{ae} \cdot \frac{k_x}{1 - k_x} \tag{4}$$

Further, the yield moment can be found according to:

$$M_e = \omega\, \sigma_{ae}\, bh^2 \left[1 - \frac{4 - \frac{\varepsilon'_b}{\varepsilon'_{be}}}{4\left(3 - \frac{\varepsilon'_b}{\varepsilon'_{be}}\right)} \cdot k_x \right] \tag{5}$$

Calculated values for M_e are plotted down in Fig. 27; measured values are presented too in this figure for the beams discussed in Appendix I (average steel grade QR 44). The latter having a compressive reinforcement of which $\omega'_o = 0{,}2‰$.

Finally the stiffness of the cracked section follows from:

$$(EI)_{gs} = \frac{M_e}{\varkappa_e} = \frac{M_e}{\frac{\varepsilon_{ae}}{(1 - k_x)h}}$$

or

$$(EI)_{gs} = \omega\, E_a\, bh^3 \left[1 - k_x \right] \left[1 - \frac{4 - \frac{\varepsilon'_b}{\varepsilon'_{be}}}{4\left(3 - \frac{\varepsilon'_b}{\varepsilon'_{be}}\right)} \cdot k_x \right] \tag{6}$$

Fig. 28 represents the results of those calculations for a number of combinations for concrete and steel grades; the stiffness $(EI)_{gs}$ is plotted

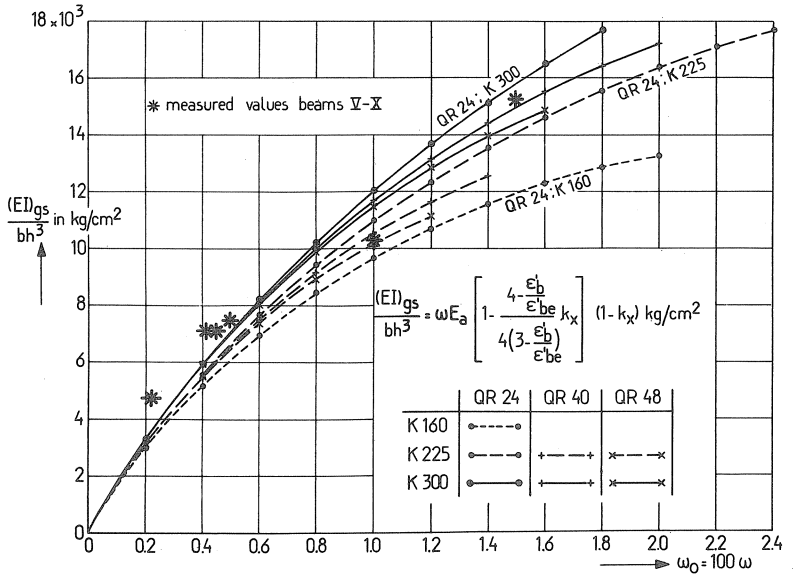

Fig. 28

The stiffness $(EI)_{gs}$ of rectangular cracked sections without compressive reinforcement.

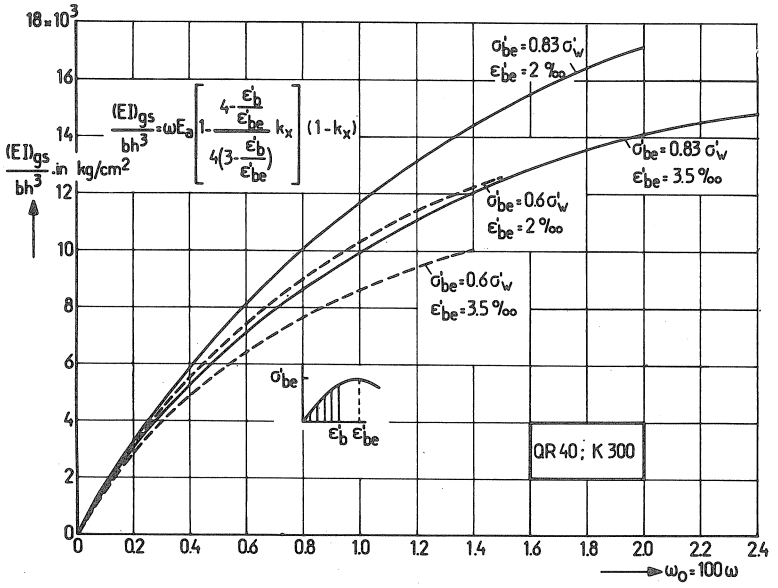

Fig. 29

Influence of σ'_{be} and ε'_{be} on the stiffness $(EI)_{gs}$.

against the percentage of tensile reinforcement. This figure too shows some measured values which are in reasonable good agreement with the calculated ones. The influence of changing the data of stress-strain diagram of concrete is clearly apparent from Fig. 29. This figure is presented to give an idea what the theoretical effect of long-term loading could be. That circumstance has been included, e.g. in the Dutch Code of Practice, in the data $\varepsilon'_{be} = \varepsilon'_{bu} = 3{,}5‰$ and $\sigma'_{be} = \sigma'_{bu} = 0{,}6\ \sigma'_w$.

The calculations necessary to determine the ratio of the depth of the neutral axis k_x and thereafter the stiffness of the cracked section are difficult to perform. Therefore, a number of expressions will be produced leading approximately to the same results, but without the necessity to solve a 3rd degree equation. The approximation formulas express k_x, ε'_b, ν_e, M_e and $(EI)_{gs}$ as functions of ω, σ_{ae}, ε'_{be} and of course also b and h. They are derived from a number of computer calculations, in which $\varepsilon'_{be} = 2‰$ and $\sigma'_{be} = 0.83\ \sigma'_w$. The tensile steel ratio ω_{gr}, figuring in the expressions also, is defined as: the ratio of tensile reinforcement where both steel and concrete reach at the same time the top of their idealised σ-ε diagram, respectively the yield stress and the crushing strength.

The depth of the compression zone occurring at yielding when this tensile steel ratio ω_{gr} is applied, is:

$$k_{xgr} = \frac{\varepsilon'_{be}}{\varepsilon'_{be} + \varepsilon_{ae}} \qquad (7)$$

From horizontal equilibrium follows for the cross-sections concerned:

$$\omega_{gr} = \frac{2}{3} k_{xgr} \frac{\sigma'_{be}}{\sigma_{ae}} = \frac{2}{3} \frac{\varepsilon'_{be}}{\varepsilon'_{be} + \varepsilon_{ae}} \cdot \frac{\sigma'_{be}}{\sigma_{ae}} \qquad (8)$$

Table 1 gives on the left a survey of the value of ω_{gr} for a number of concrete and steel grades. On the right-hand side the attention is paid to the real maximum percentage of reinforcement for the complete σ'_b-ε'_b diagram reaching ultimate concrete strain. In that case, more tensile reinforcement will not yield before failure of the cross-section concerned where compressive reinforcement is missing.

All the approximation formulas are valid only for a ratio of tensile reinforcement less ω_{gr}.

Table 1

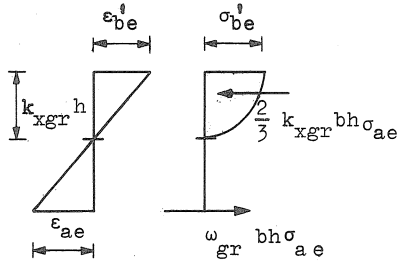

$\varepsilon'_{bu} = 3.5$ °/oo
$\varepsilon'_{be} = 2$ °/oo
$\sigma'_{be} = 0.83\,\sigma'_{w}$

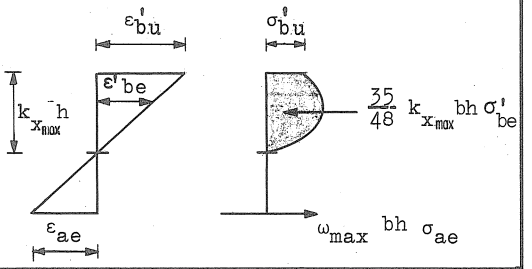

steel quality	$k_{xgr}=\frac{0.002}{0.002+\varepsilon_{ae}}$	$\omega_{gr}=\frac{2}{3}k_{xgr}\frac{\sigma'_{be}}{\sigma_{ae}}$			$k_{x_{max}}=\frac{0.035}{0.035+\varepsilon_{ae}}$	$\omega_{max}=\frac{35}{48}k_{x_{max}}\frac{\sigma'_{be}}{\sigma_{ae}}$		
		K 160	K 225	K 300		K 160	K 225	K 300
QR24 (σ_{ae} = 2400 kg/cm^2, ε_{ae} = 1.143 °/oo)	0.636	0.0235	0.0330	0.0440	0.754	0.0304	0.0418	0.0570
$QR^{40}_{(n)}$ (σ_{ae} = 4000 kg/cm^2, ε_{ae} = 1.905 °/oo)	0.512		0.0159	0.0213	0.648		0.0220	0.0294
$QR^{48}_{(n)}$ (σ_{ae} = 4800 kg/cm^2, ε_{ae} = 2.286 °/oo)	0.467		0.0121	0.0161	0.605		0.0172	0.0229
$n_o=\frac{Ea}{E'_{bo}}=\frac{1}{2}\frac{E_a\,\varepsilon'_{be}}{\sigma'_{be}}$:		15.81	11.24	8.43				
$n_e=\frac{3}{2}n_o$:		23.72	16.87	12.65				

3.1.1. Approximation formulas

These expressions concern, at yield moment: the depth of the compression zone k_x, the concrete strain ε'_b, the curvature $\varkappa_e$ and further: the yield moment M_e itself and the stiffness $(EI)_{gs}$ of the cracked cross-section. A number of figures present the results; most of the mentioned characters are plotted against the percentage of tensile reinforcement. The exact values are plotted with points, -dots or similar things; drawn lines represent the approximations obtained. The expressions concerning the latter are printed in the figures.

The depth of the compression zone

Fig. 30 shows for a number of combinations of concrete and steel grades the ratio k_x at the yield moment. The drawn curves approximate the exactly calculated values very good.

The concrete strain ε'_b

The calculated concrete strain, when the yield moment is reached, appears to be a practical, linear function of the tensile reinforcement index: $\frac{\omega}{\sigma'_{be}}$, as given in Fig. 31.

The curvature $\varkappa_e$

This curvature stands of course for a given depth of the beam h, in the same relation to the reinforcement-percentage as the concrete strain ε'_b does,

$$\varkappa_e \cdot h = \varepsilon'_b + \varepsilon_{ae}$$

The steel strain at the commencement of yielding ε_{ae} is there in a constant value for each steel grade. Fig. 32 represents the comparison of exact and approximated, calculated values. The agreement with **measured** data appears to be good also for this character (measured values concern the beams discussed in Appendix I).

The yield moment M_e

The values obtained from an exact calculation agree reasonably well with the approximation given in Fig. 33. The concerning expression is derived from equation 5 by substituting:

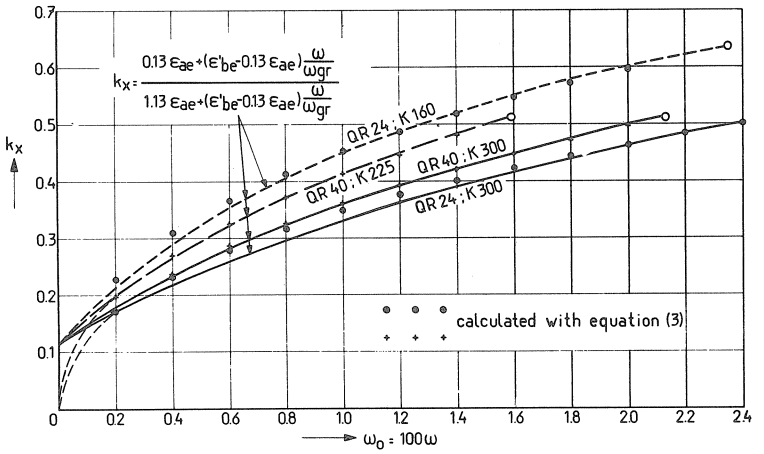

Fig. 30

Ratio k_x at yield moment, comparison of 'exactly' calculated values and the approximation formula.

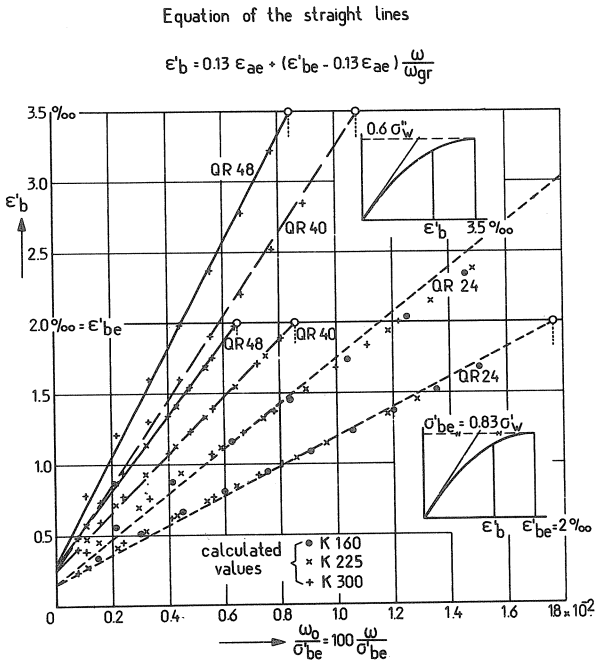

Fig. 31

The concrete strain ε'_b at the yield moment, comparison of 'exactly' calculated values and the approximation formula.

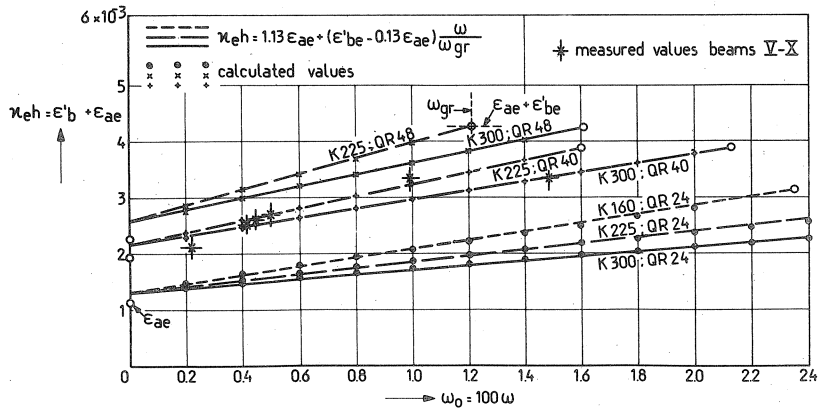

Fig. 32

The curvature at yield moment, measured values, 'exactly' calculated values and the approximation formula.

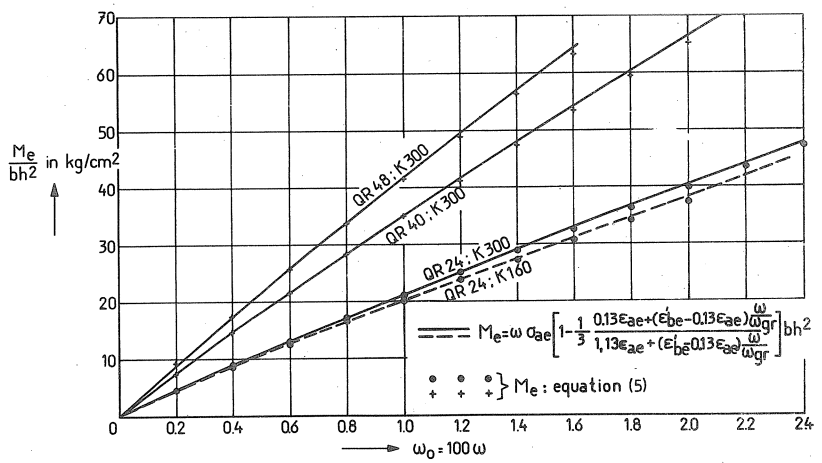

Fig. 33 Approximation for the yield moment M_e.

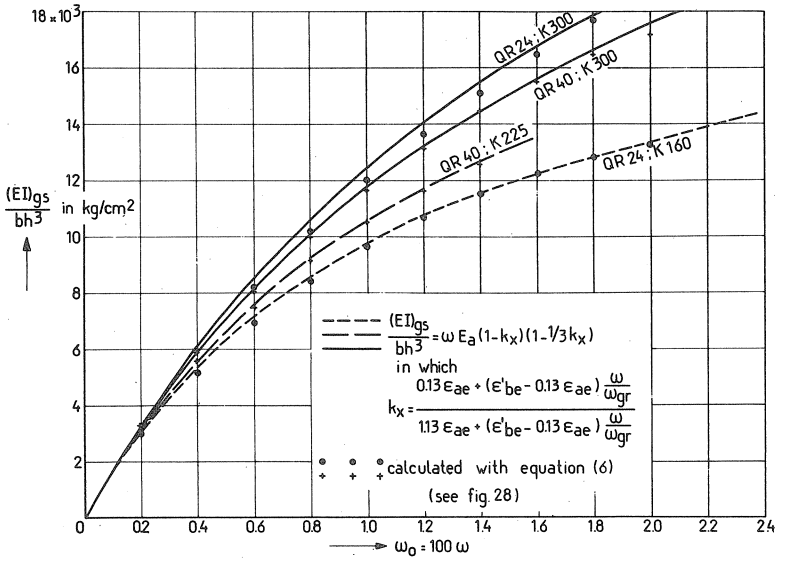

Fig. 34

The stiffness $(EI)_{gs}$, comparison of the approximation and the 'exactly' calculated values.

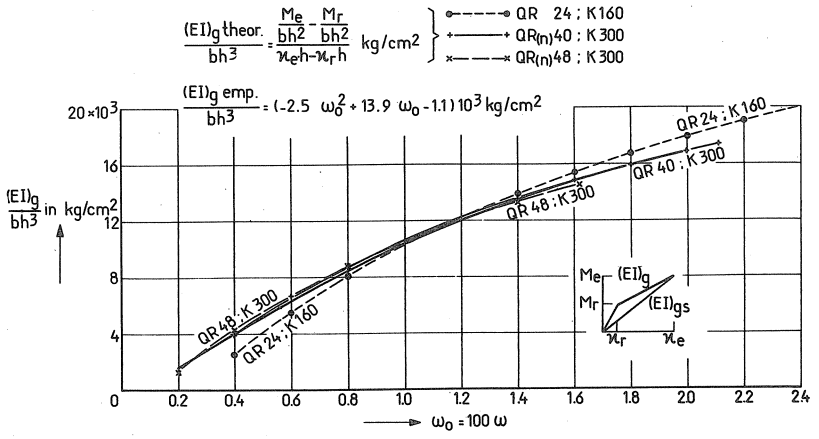

Fig. 35

Stiffness in the cracked state $(EI)_g$ directly calculated.

- 1/3 in stead of $\dfrac{4 - \dfrac{\varepsilon'_b}{\varepsilon'_{be}}}{4\left(3 - \dfrac{\varepsilon'_b}{\varepsilon'_{be}}\right)}$

- k_x according to the expression given in Fig. 30.

The stiffness $(EI)_{gs}$

Finally, the sought stiffness $(EI)_{gs}$ is expressed in the approximation formula

$$\frac{(EI)_{gs}}{bh^3} = \omega E_a (1 - k_x)(1 - 1/3\, k_x) \qquad (9)$$

and plotted in Fig. 34 against the percentage of reinforcement. The values k_x are therefore obtained from the equation given in Fig. 30. The agreement between the approximations and the exact calculations is good.

3.1.2. Determination of the flexural stiffness $(EI)_g$

The main purpose of the above "wandering around in the cracked section" was to determine the real flexural stiffness $(EI)_g$ in the cracked state, according to

$$\frac{(EI)_g}{bh^3} = \frac{\dfrac{M_e}{bh^2} - \dfrac{M_r}{bh^2}}{\varkappa_e h - \varkappa_r h} \qquad (10)$$

With the approximation-expressions derived before, in both chapter 2 and 3, all terms in the right-hand side of this equality can now be calculated quite simply. The $\varkappa_r$ can be found from $\varkappa_r = \dfrac{M_r}{(EI)_o}$, with the help of the expressions presented in chapter 2.

Values for $(EI)_g$ calculated in this way are given in Fig. 35 as a function of the percentage of tensile reinforcement ω_o. Three combinations of concrete and steel grades are considered. The curve representing the empirical formula for $(EI)_g$ (chapter 2), also drawn in Fig. 35, agrees very well with the average of the calculated values for $(EI)_g$. This figure

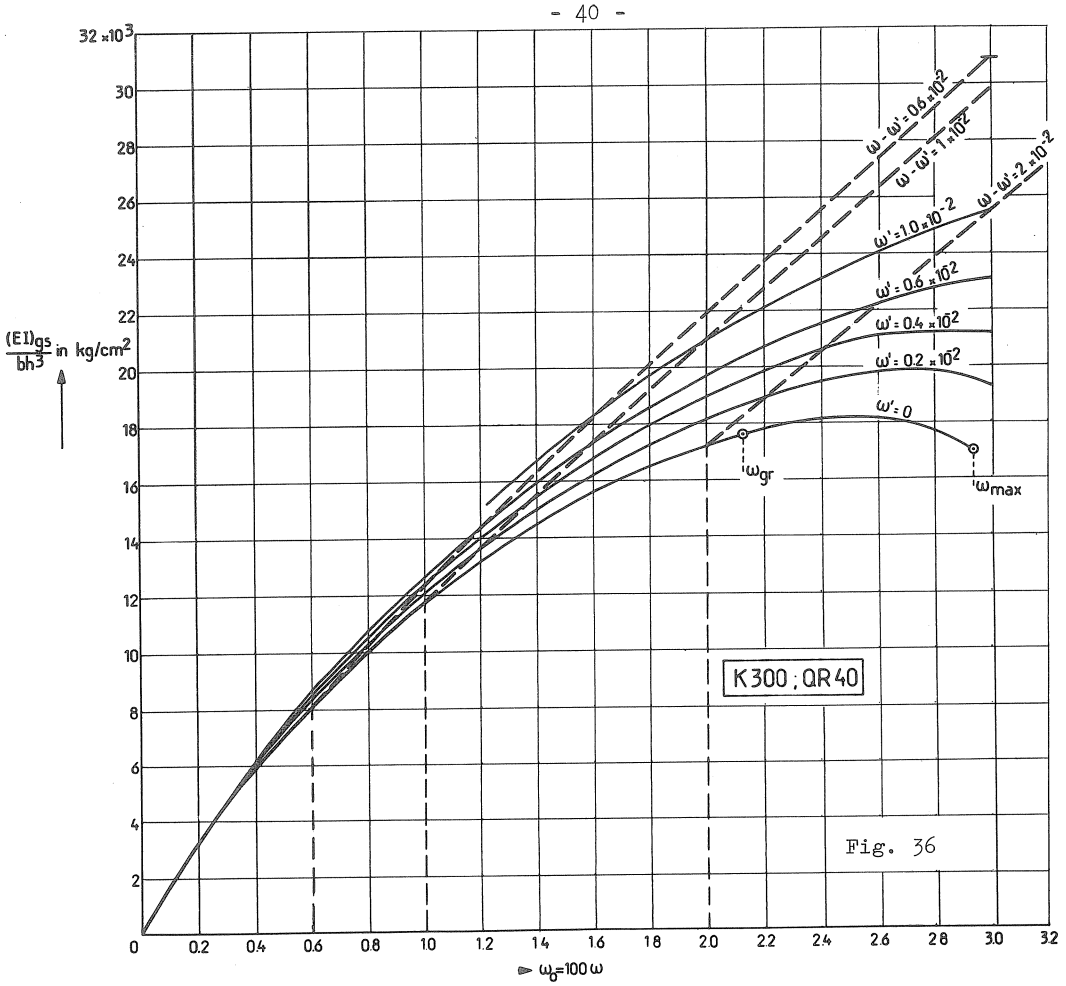

Fig. 36

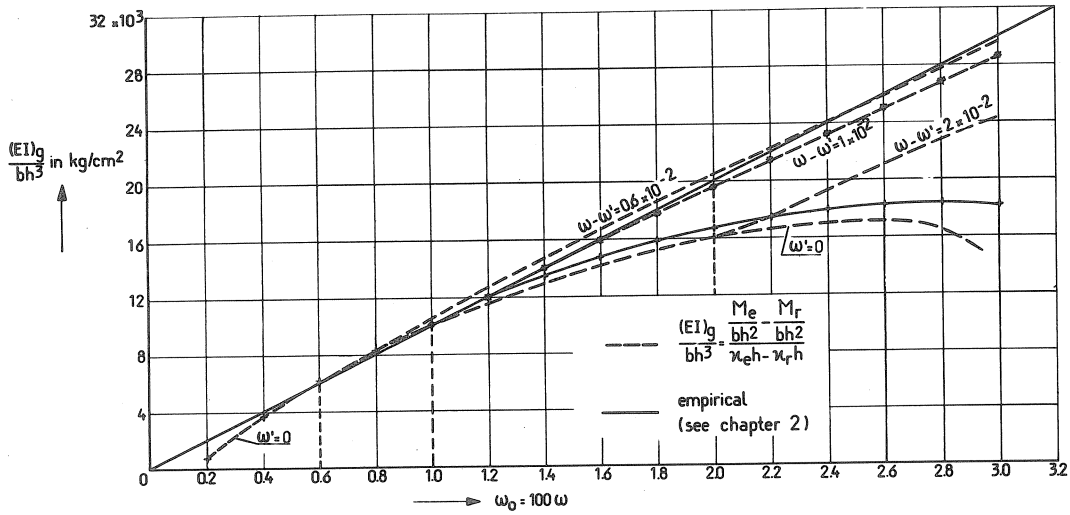

Fig. 37

Influence of compressive reinforcement on the stiffness in the cracked state.

justifies the conclusion that indeed, as an overall view, the stiffness $(EI)_g$ in cracked state, hardly depends on the concrete and steel grade applied. With regards to Fig. 35 the concerning empirical formula

$$\frac{(EI)_g}{bh^3} = \left(- 2.5\ \omega_o^2 + 13.9\ \omega_o - 1.1 \right) \cdot 10^3\ kg/cm^2 \qquad (11)$$

seems to be the most simple way to determine the sought $(EI)_g$ reasonable satisfactorily. Even the same statement is valid for the approximation of the empirical formula, namely

$$\frac{(EI)_g}{bh^3} = \omega_o \cdot 10^4\ kg/cm^2 \qquad (12)$$

Summarising can be said, that for the rectangular cross-section concerned, the second branch of the M-$\varkappa$ diagram (for a first-time loading) can be determined by either a calculation as demonstrated (exact one or with help of the approximation formulas discussed), or by the two empirical formulas mentioned above. Without further discussion this statement holds for percentages of tensile reinforcement respectively $\omega_o < 2\%$ concerning equation 11 and $\omega_o < 1.5\%$ with regard to equation 12. That means most of the practical cases are included above. Besides, for the cross-sections without compressive reinforcement, the percentage of tensile reinforcement will normally be limited about in that range, because of the maximum percentage with regard to yielding.

As said before, dealing with "hyperstatique" structures, it is preferable to design the cross-section in such a manner, that the reinforcement yields before the concrete crushes. The belonging maximum percentage of reinforcement is in fact, as well-known, the difference between the percentages of tensile less compressive reinforcement of the cross-section. This maximum, of course, depends on the concrete and steel grades also (see table 1). So, in order to be able to make some remarks with regards to the bending stiffness $(EI)_g$ for higher percentages of tensile reinforcement than mentioned above, the influence of the compressive reinforcement should be taken into consideration.

Therefore, Fig. 36 shows the stiffness of the cracked cross-section for some compressive reinforcement. The influence of compressive reinforcement appears to increase with the percentage of tensile reinforcement.

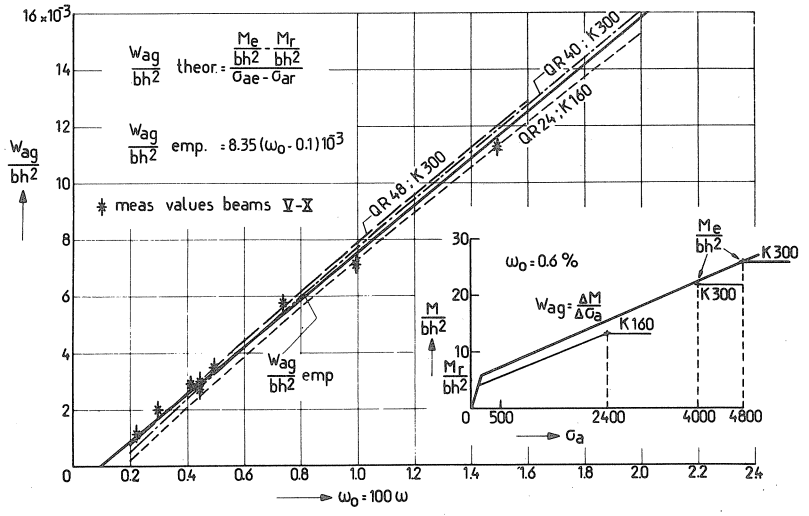

Fig. 38

The section modulus with respect to the tensile reinforcement.

This is logical because of the increasing distance of the compressive reinforcement with respect to the neutral axis. An interesting conclusion from Fig. 36 is further, that a constant difference between compressive and tensile reinforcement-percentage gives a nearly straight line, when the latter increases. This concerns a certain ratio of concrete and steel grades.

The consequence of this for the real, flexural stiffness $(EI)_g$ is presented in Fig. 37. This character is also about a linear function of the percentage of tensile reinforcement under the above-mentioned conditions. Keeping in mind that one will be obliged to keep the meant difference in reinforcement-percentages constant from a certain maximum on, the linear empirical formula is preferable in those cases. With regard to Fig. 36 (and Fig. 5 also) this formula

$$\frac{(EI)_g}{bh^3} = \omega_o \cdot 10^4 \text{ kg/cm}^2$$

is a satisfactory average. On the other hand, it is of course always possible to calculate the flexural stiffness in that range of percentages of reinforcement, according to the analysis-procedure discussed.

3.1.3. Further evaluation of calculated data

As a further interpretation of the measured data, at first some attention will be paid to the average steel stress in cracked concrete. From the measurements discussed in Appendix I, it appears that the average steel tensile stress in the region of constant moment was, after cracking, linearly related with the percentage of tensile reinforcement. From the calculations discussed in 3.1.1 the ratio $W_{ag} = \frac{\Delta M}{\Delta \sigma_a}$ is determined according to:

$$\frac{W_{ag}}{bh^2} = \frac{\frac{M_e}{bh^2} - \frac{M_r}{bh^2}}{\sigma_{ae} - \sigma_{ar}}$$

The results are plotted down in Fig. 38. The ratio W_{ag} indeed appears to be a linear function of the percentage of tensile reinforcement for different combinations of concrete and steel grades. The narrow bundle of the lines concerned can be replaced by an average straight line according

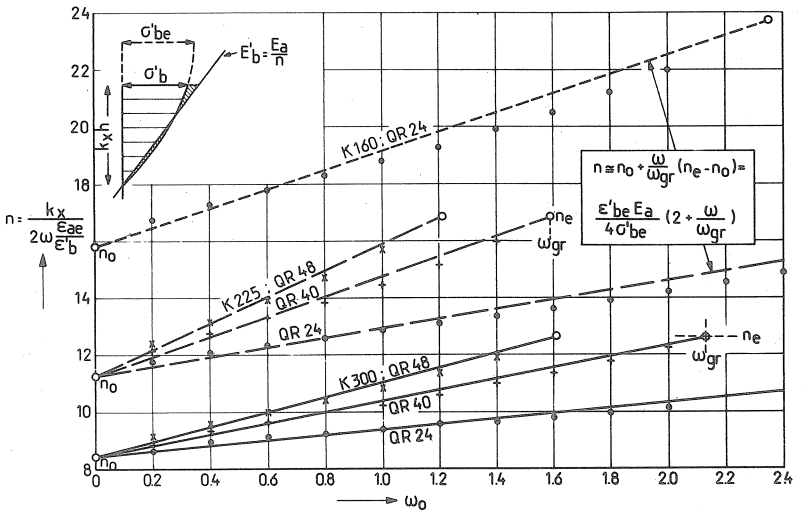

Fig. 39 The equivalent n (for $\varepsilon'_{be} = 2‰$ and $\sigma'_{be} = 0.83\ \sigma'_{w}$).

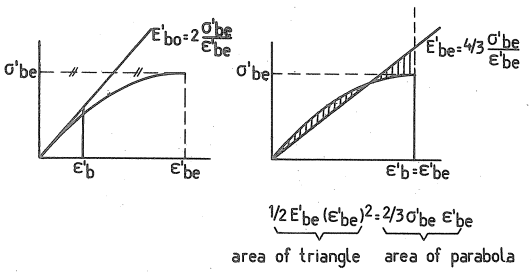

Fig. 40
Conditions to determine the equivalent n.

to:

$$\frac{W_{ag}}{bh^2} = 8{,}35\ (\omega_o - 0.1)\ 10^{-3}$$

The measured values agree well with the calculated values.

As second "further evolution" the ratio of modulus of elasticity of concrete and steel is taken into consideration. One could ask which $n = \frac{E_a}{E'_b}$ should be taken into account in calculations according to the old n-method, to get the same results as discussed before. This can be obtained on the conditions that, when yield moment M_e is reached:

- the concrete compression-resultant in both calculations is equal (the approximation of the lever arm by $z = (1 - 1/3\ k_x)\ h$ is already shown to be good, see p. 35: The yield moment M_e);
- the deformations are equal, i.e. the curvature.

From the first condition:

$$1/2\ k_x \cdot \varepsilon'_b \cdot \frac{E_a}{n} \cdot bh = \omega \cdot \varepsilon_{ae}\ E_a\ bh$$

or

$$n = \frac{k_x}{2\,\omega \cdot \frac{\varepsilon_{ae}}{\varepsilon'_b}} \qquad (13)$$

The exactly calculated values of equation 13 (with k_x and ε'_b from eq. 3 and 4 resp.) are plotted in Fig. 39 against the percentage of tensile reinforcement (with points or similar things). The relation of n appears to be a practically linear one to that percentage of reinforcement. This can be approximated by

$$n = n_o + (n_e - n_o)\ \frac{\omega}{\omega_{gr}} \quad (\omega_{gr}, \text{ see equation 8, p. 33})$$

or after substituting

$$n_o = \frac{E_a}{E'_{bo}} = \frac{\varepsilon'_{be} \cdot E_a}{2\sigma'_{be}}$$

and

$$n_e = \frac{E_a}{\frac{4}{3}\,\frac{\sigma'_{be}}{\varepsilon'_{be}}} = \frac{3}{4}\,\frac{\varepsilon'_{be}\ E_a}{\sigma'_{be}} = \frac{3}{2}\ n_o \qquad \text{(see Fig. 40)}$$

by:

$$n = \frac{\varepsilon'_{be}\ E_a}{4\ \sigma'_{be}}\ \left(2 + \frac{\omega}{\omega_{gr}}\right) \qquad (14)$$

The results of Fig. 39 lead to the conclusion that the equivalent n depends on both the concrete and the steel grade. Thus, with those values for n the calculation of $(EI)_{gs}$ according to the n-method gives the same values as if $(EI)_{gs}$ was exactly calculated. The equation 14 will be used, in the "complete analysis procedure" mentioned in the introduction where also the concrete between two cracks is taken into consideration.

3.1.4. Comparison with some calculation methods known in literature

The flexural stiffness of the cracked cross-section can easily be calculated according to the n-method. The concerning formula is presented in literature in different forms:

$$(EI)_{gs} = E_a \cdot \omega \, (1 - 1/3 \, k_x) \, (1 - k_x) \, bh^3 \qquad (15a)$$

$$(EI)_{gs} = \frac{E_a}{n} \left\{ 1/3 \, k_x^3 + n \, \omega \, (1 - k_x)^2 \right\} bh^3 \qquad (15b)$$

$$(EI)_{gs} = \frac{E_a}{n} \left\{ 1/2 \, k_x^2 \, (1 - 1/3 \, k_x) \right\} bh^3 \qquad (15c)$$

Herein is:

$$k_x = - n \, \omega + \sqrt{(n \, \omega)^2 + 2 \, n \, \omega} \qquad (16)$$

and

$$n = \frac{E_a}{E'_b} = \text{constant}$$

The other form is:

$$(EI)_{gs} = E_a \omega \left(1 - \frac{2}{3} \omega \frac{\sigma_{ae}}{\sigma'_{be}} \right) \left(1 - 2 \omega \frac{\sigma_{ae}}{\sigma'_{be}} \right) \qquad (17)$$

The above-mentioned formulas $15^{a \text{ to } c}$ all follow from:

$$(EI)_{gs} = \frac{M}{\varkappa} = \frac{M(1 - k_x)h}{\varepsilon_a} \qquad (18)$$

respectively by taking the moment M with respect to the concrete compression resultant, the neutral axis and the tensile reinforcement. The ratio k_x (eq. 16) to be substituted in equations 15 follows from the assumption that plane sections remain plain and from equilibrium of horizontal forces. Equation 17 might be found from eq. 15a after substitution of the ratio k_x belonging to equilibrium of horizontal forces in the ultimate state,

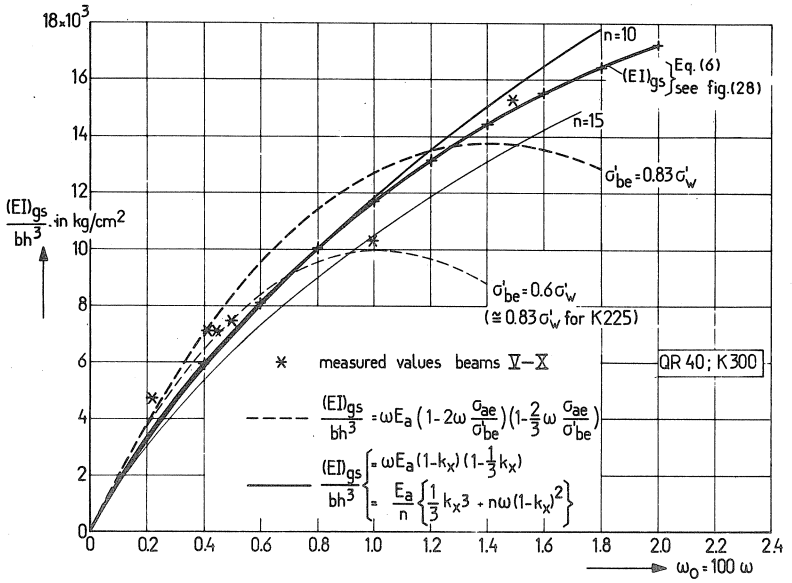

Fig. 41
Comparison of $(EI)_{gs}$ determined in different ways.

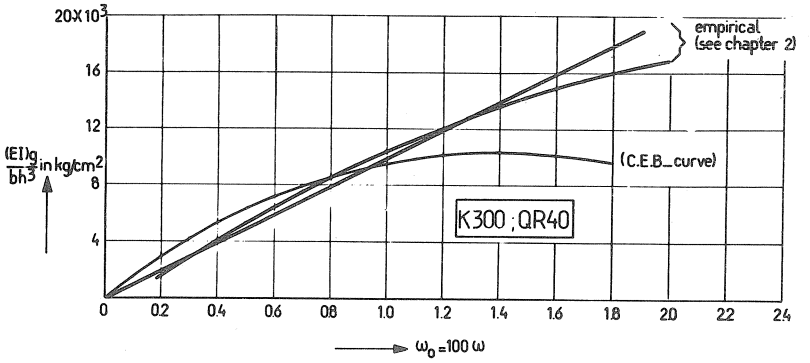

Fig. 42
Comparison between C.E.B.- and empirial curves.

$k_x = 2\,\omega\,\frac{\sigma_{ae}}{\sigma'_{be}}$. The assumption herein is, that the stress-strain diagram of concrete remains linear, also in the ultimate state. Fig. 41 presents the results of the mentioned equations 15 and 17. Additionally, the results of exact calculations according to equation 6 and measured values are plotted down in the figure. It is clearly apparent from the figure that the flexural stiffness concerning equations 15 and 17 give only a rough approximation of reality, especially with regard to higher percentages of tensile reinforcement and lower concrete qualities. The assumption of a linear stress-strain diagram thus does not hold in relation with a constant n-value. Especially not with regard to equation 17 where the ratio k_x to be substituted therefore increases too much in relation to the tensile reinforcement percentage.

However, the latter is mentioned in the CEB Recommendations, as

$$(EI)_g = 0.75 \cdot E_a \cdot \omega\left(1 - \frac{2}{3}\,\omega\,\frac{\sigma_{ae}}{\sigma'_{be}}\right)\left(1 - 2\omega\,\frac{\sigma_{ae}}{\sigma'_{be}}\right) \qquad (18)$$

as the second branch of the M-κ diagram. This formula is thus derived from the bending stiffness $(EI)_{gs}$ of the cracked section by multiplying with 0.75: $(EI)_g = 0.75\,(EI)_{gs}$.

It will be evident that also the expression for $(EI)_g$ leads to values which are too small, the bigger the percentage of reinforcement is. Moreover, this is shown by Fig. 42.

Acknowledgments

This investigation was performed in the laboratories of the Institute TNO for Building Materials and Building Structures IBBC-TNO at Delft. The research is partly supported by the Netherlands Committee for Concrete Research CUR. Especially working-group A19 was involved in this subject. P.W.van de Haar, fellow-worker of IBBC-TNO, assisted in both the experimental and the theoretical research.

This paper summarises several TNO-reports, namely:
reports no. BI-65-1, 10 parts (November 1965), BI-66-49 (July 1966), BI-67-106 (October 1967), BI-67-110 (December 1967).

Appendix I

EXPERIMENTAL INVESTIGATION CONCERNING THE M-$\varkappa$ DIAGRAM ESPECIALLY FOR A FIRST-TIME LOADING

I.1 Introduction

A survey of the above mentioned investigation will be presented here. The deformations produced in nine beams by the application of loading were determined and recorded in detail.
Although more data were obtained (relating to the deflections, the position of the neutral axis, average steel stresses, compressive stress in concrete and cracking), attention will be paid especially to the measured M-$\varkappa$ diagrams. The remaining data are shown for one beam (beam VII) only as an illustration of the results obtained.*)

I.2 Test beams

All the beams investigated have cross-sectional dimensions $b \times h_t$ = 29 × 25 cm and an overall length of 400 cm. It was endeavoured to attain a cube strength of 300 kg/cm^2 for the concrete at the time of testing. Each beam contains compressive reinforcement comprising three bars of 8 mm diameter. The variables in the test beams are: the percentage of reinforcement, the bar diameter, and the grade of steel. However, in each beam the quantity of reinforcement does not vary in the longitidinal direction. Stirrups are provided along the entire length of all the beams.

The data relating to all the beams are summarised in Table I-1.

The composition of the concrete is indicated in Table I-2.

Fig. I-1 gives an example of a stress-strain (σ-ε) diagram of the concrete determined on prisms measuring 10 × 10 × 30 cm. The σ-ε diagrams of the grades of steel employed are given in Figs. I-2 and I-3. Both steels were provided with approximately similar bond-increasing profiling (deformed bars).

The cross-sectional shape, concrete composition and reinforcement were not specially determined for these beams. They are associated with the section properties of previously tested portal frames, in which the

*) All measured data are evaluated and presented in TNO-report BI-65-1 (in 10 parts).

Table I-1. General details of test beams.

beam no.	tensile reinforcement		area of tensile reinforcement A in cm^2	perc. of tensile reinforcement ω_o in %	*average cube strength in kg/cm^2		*tensile strength σ_{bt} in kg/cm^2	modulus of elasticity E'_{bo} in kg/cm^2	normal cross-section**	dimensions in cm		
					cubes 10×10×10	cubes 20×20×20				a	b	c
					pressed between 3 mm cardboard		measured in flexure		length of the beams 400 compressive reinforcement 3 Ø 8			
II	4Ø8	Diroc steel+ QRn 40	2.01	0.295	344	291	43.7	2.85×10^5	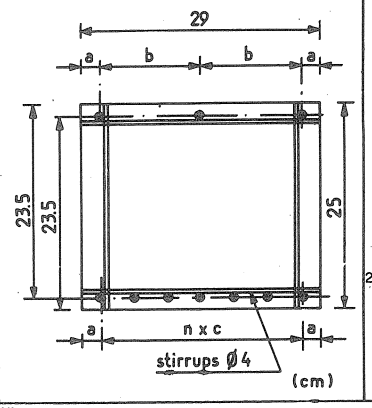	2.5	12.0	8.0
III	6Ø8		3.02	0.443	299	324	47.6	2.78×10^5		2.5	12.0	4.8
IV	10Ø8		5.03	0.738	304	295	43.6	2.70×10^5		1.5	13.0	2.9
V	3Ø8	Hi-bond steel++ QR 40	1.51	0.222	263	298	51.4	2.70×10^5		2.5	12.0	12.0
VI	6Ø8		3.02	0.443	261	298	44.1	2.83×10^5		2.5	12.0	4.8
VII	10Ø6		2.83	0.415	286	304	47.6	2.81×10^5		2.5	12.0	2.6
VIII	3Ø12		3.39	0.497	311	326	50.0	3.00×10^5		2.7/2.5	11.8	12.0
IX	6Ø12		6.78	0.995	309	328	52.7	2.85×10^5		2.5	12.0	4.8
X	9Ø12		10.17	1.492	309	356	44.9	3.40×10^5		2.5	12.0	3.0

*age at test days:

- beam I to IV ~30 days
- beam V to X ~60 days

+steel without yield-point, see Fig. I-2.

++steel with yield-point, see Fig. I-3.

**1) compressive reinforcement of the same kind of steel as the tensile reinforcement

2) distance between the centerlines of the stirrups along the entire length of the beam 25 cm, except:

- beam IX, besides the region of the beam with a constant moment the distance between the centerlines 8 cm
- beam X , besides the region of the beam with a constant moment the distance between the centerlines 6 cm

3) $b \times h = 681.5\ cm^2$

$\frac{1}{6} bh_t^2 = 3020.8\ cm^3$

$\frac{1}{12} bh_t^3 = 37760.4\ cm^4$

Table I-2. Composition of the concrete.

aggregate grading		cement		w/c ratio
sieve diameter (mm)	retained on the sieves, cum. percentages	type	aggregate/cement by dry weight	
5.6	48	Portland cement-A Enci	~ 5.88 (~ 325 kg/m³ concrete)	0.61
2.8	65			
1.4	73			
0.6	78			
0.3	88			
0.15	97			
0	100			

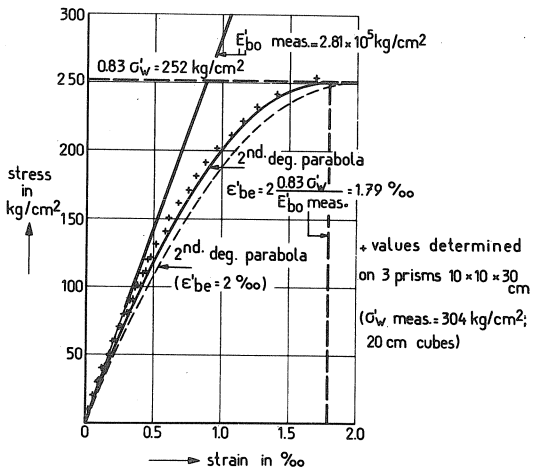

Fig. I-1 Stress-strain diagram for concrete.

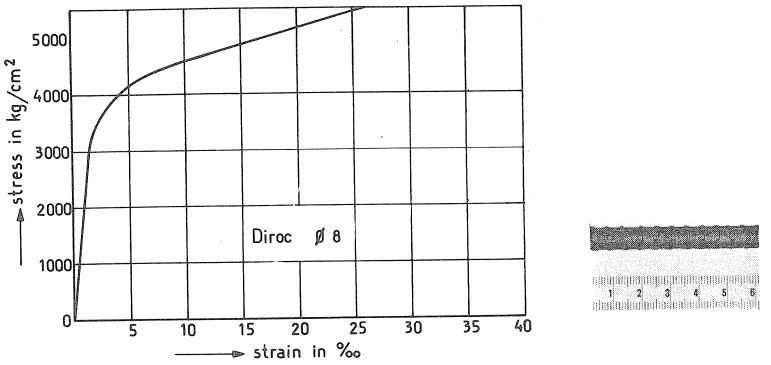

Fig. I-2
Stress-strain diagram for the reinforcement of the beams II-IV.

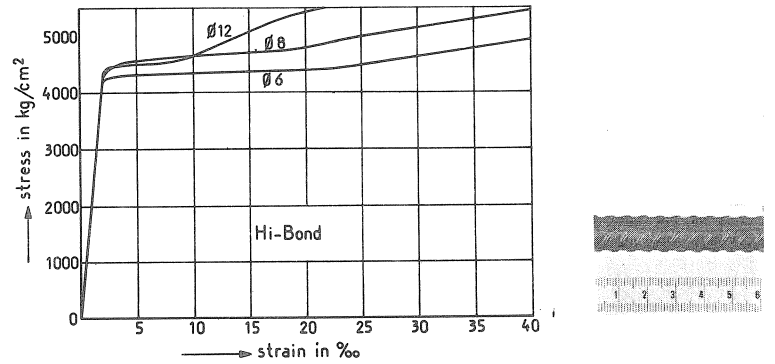

Fig. I-3
Stress-strain diagram for the reinforcement of the beams V-X.

moment redistribution due to applied deformations were measured.

I.3 Execution of the investigation

I.3.1 Test arrangement

Testing comprised the so-called four-point bending test, in which the 4.00 m long beams were supported on two 50 mm diameter rollers spaced at a centre-to-centre distance of 3.80 m. The two concentrated loads constituting the loading were applied at points situated 2.00 m apart and were, of course, like the bearings, disposed symmetrically in relation to the centre of the beam. The concentrated loads were applied through a rolled steel joist and two rollers. This joist was also used - with the aid of springs - as a means of compensating for the dead weight of the beam between the loads. Hence there was a region of really constant bending moment in the beam.

Fig. I-4 schematically shows the test arrangement and the bending moment diagram at the commencement of the measurements.

I.3.2 Measurements performed

For each beam the following measurements were performed at the various loadings:

- The tensile strain at the level of the tensile reinforcement (= 1.5 cm above the underside) and the compressive strain at a distance of 0.5 cm below the top of the beam with a demountable strain gauge with a gauge length of 40 cm. These measurements were performed on both sides of the beam and over the entire length.
- The tensile or the compressive strain at about one-third of the beam depth, both from the underside and from the top, with the aid of a demountable strain gauge with a gauge length of 40 cm. At these levels, measurements were performed on both sides of the beam in the region of constant bending moment.
- The tensile strain at the level of the tensile reinforcement with the aid of a demountable crack measuring gauge with a gauge length of 10 cm. These measurements were performed on one side of the beam in the zone of constant bending moment. They overlapped one another, the measuring points being spaced at intervals of 5 cm.
- The deflection of the region of constant bending moment, in the central part of the beam, over a length of 1.80 m. This measurement was

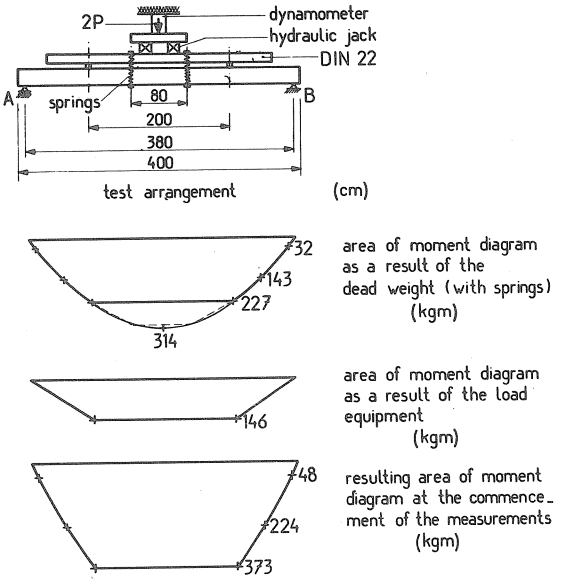

Fig. I-4

Areas of moment diagram at the commencement of the measurements.

performed with a so-called large curvimeter, comprising an aluminium rod supported on two small rollers and provided at the centre with a dial gauge on which the subsidiary deflection can be read.

- The mid-span deflection of the beam. For this purpose a nylon thread was stretched at mid-depth of the beam on one side thereof. The deflection at mid-span was read on a scale with millimetre divisions which was fixed there.

The above-mentioned observations were made at the commencement of the measurements (twice) and thereafter at each load increment.

The measurements on one beam generally extended over a period of three days. In between, measurements were performed two or three times in the unloaded condition of the beam. For each beam a certain loading was on one occasion varied 100 times between zero (i.e., dead weight of the beam plus the weight of the loading equipment) and the loading in question.

Later on, the beams II and IV were moreover also loaded in the reversed position, i.e., with the original underside upwards. The object of this was to ascertain the stiffness of a beam in which, as a result of previous loading, cracking had occurred in the compressive zone. The testing procedure was the same as that already described; also, the same observations were made.

I.4 Evaluation of the measured data, and results

The above-mentioned observations were, in the first place, evaluated and utilised to give the required M-$\varkappa$ diagram. The average tensile strain over the region of constant bending moment and the average compressive strain in that region, measured at the level of the extreme measuring lines, were added together and divided by the distance between those line The values thus obtained were plotted against the magnitude of the associated bending moment M_c in the region of constant moment. Figs. I-6 to I-16 embody the results for the beams II to X, IIa and IVa respectively. The different regions of the test beams are shown in Fig. I-5.

The deflections of the region of constant moment, measured by means of the large curvimeter, were checked with the aid of the M-$\varkappa$ diagrams obtained. There is good agreement between the measured and the calculated values. An example is given in Fig. I-17.

It was verified whether the average curvature, measured in the region of constant moment, would, on being applied to a part of the beam where

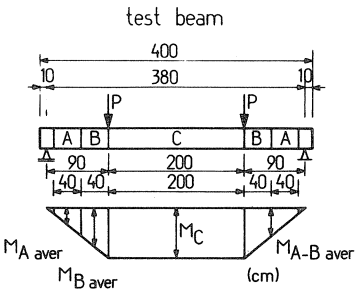

Fig. I-5. Sense of the symbols used.

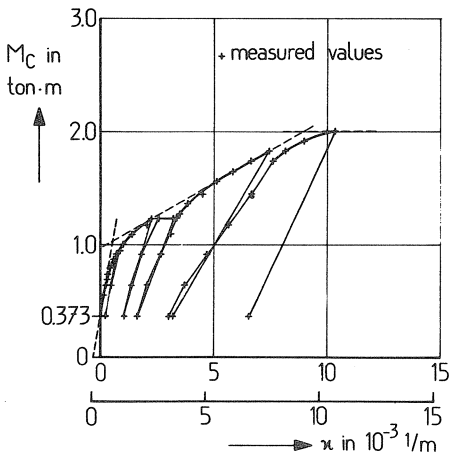

Fig. I-6. Beam II, region C.
Measured M-$\varkappa$ diagram.

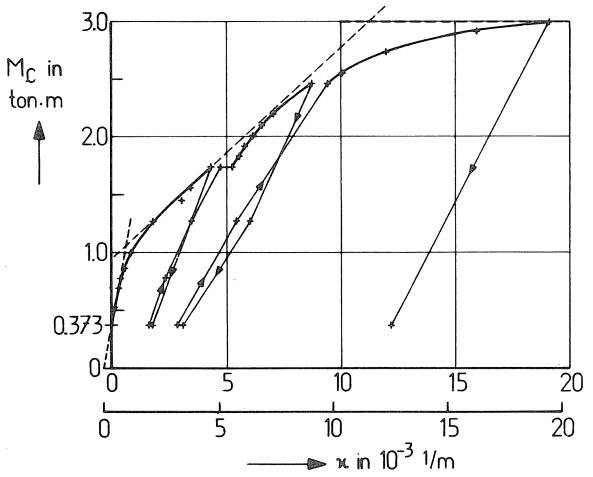

Fig. I-7. Beam III.

+ measured values

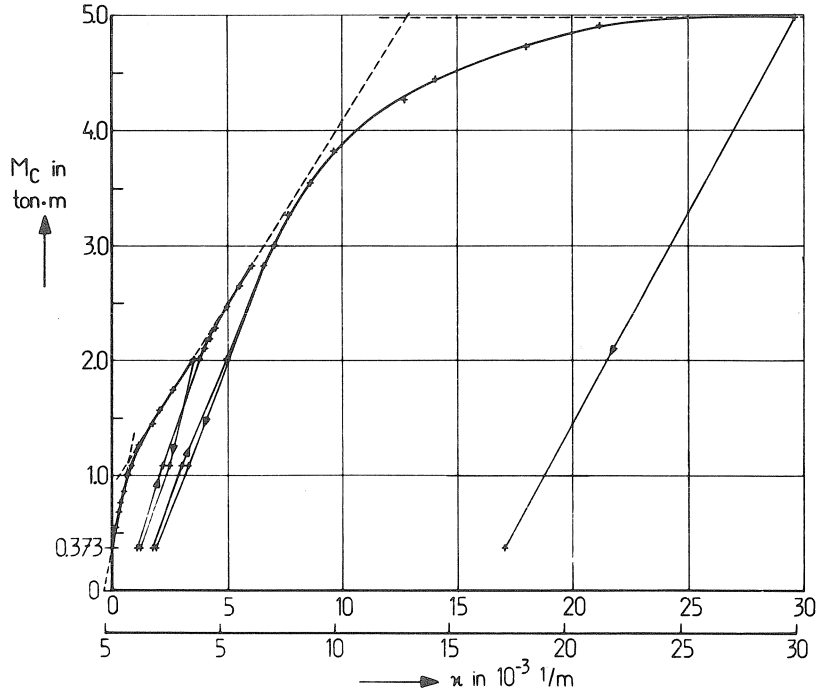

Fig. I-8. Beam IV, region C.
Measured M-$\varkappa$ diagram.

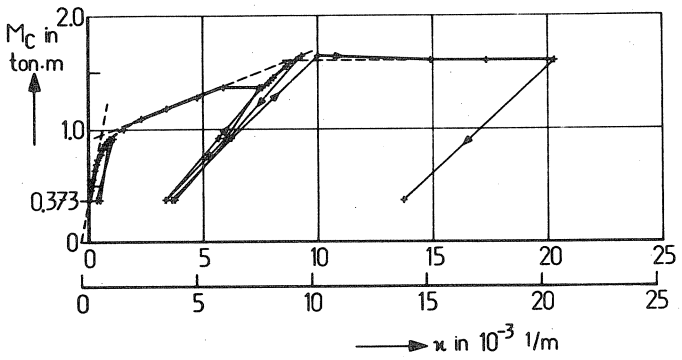

Fig. I-9. Beam V.

+ measured values
o yieldpoint. only the load was measured

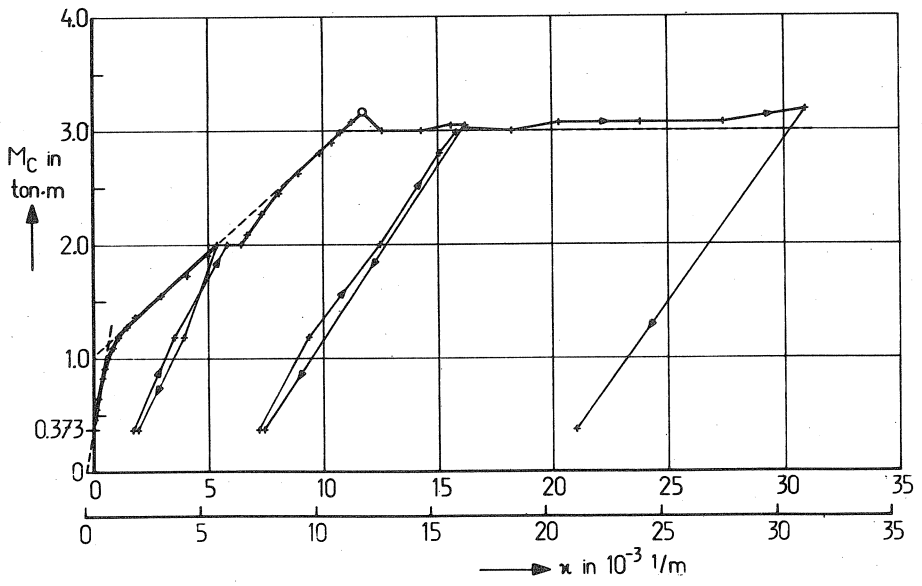

Fig. I-10. Beam VI, region C.
Measured M-$\varkappa$ diagram.

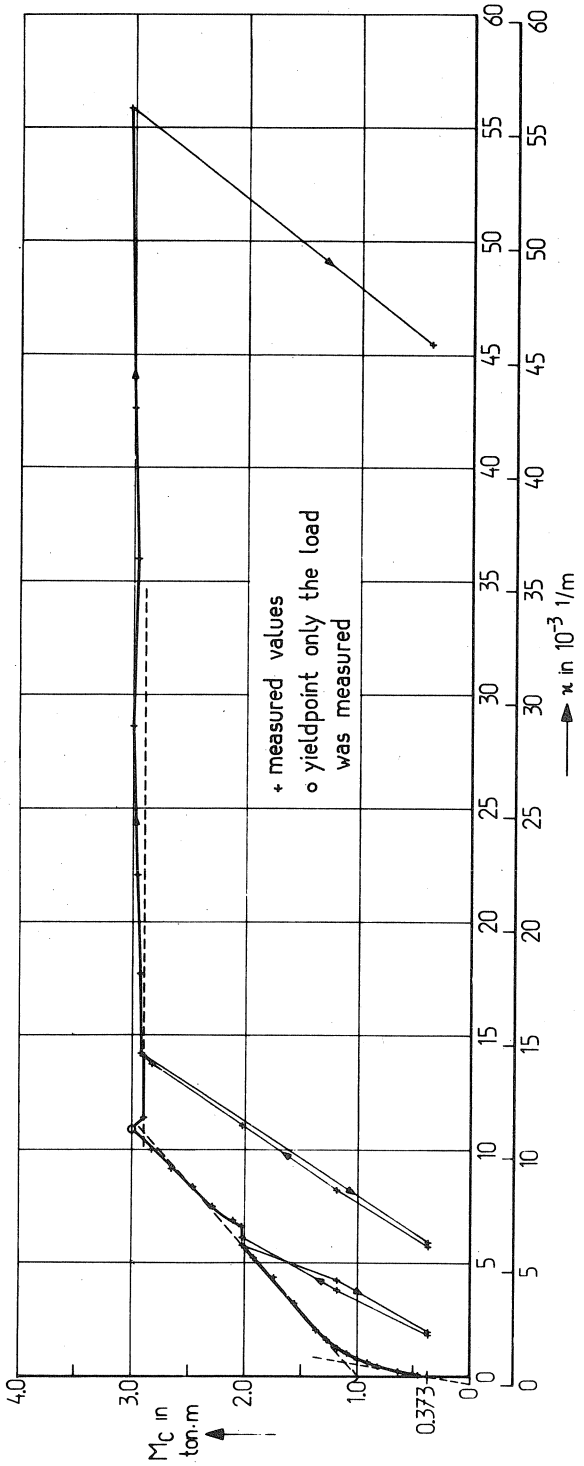

Fig. I-11. Beam VII, region C.
Measured M-$\varkappa$ diagram.

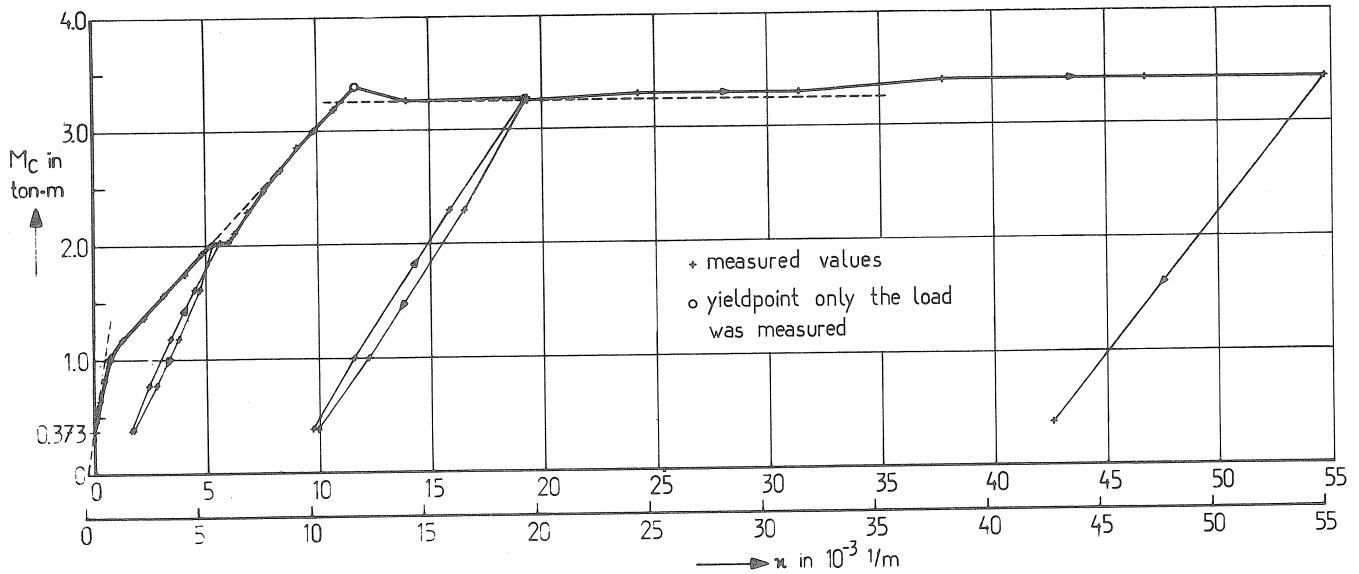

Fig. I-12. Beam VIII, region C.
Measured M-$\varkappa$ diagram.

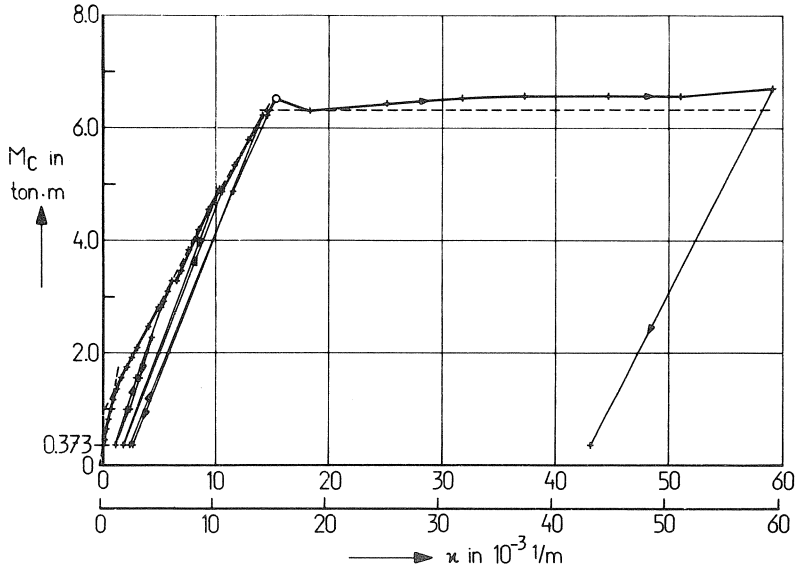

Fig. I-13. Beam IX.

+ measured values
o yieldpoint, only the load was measured

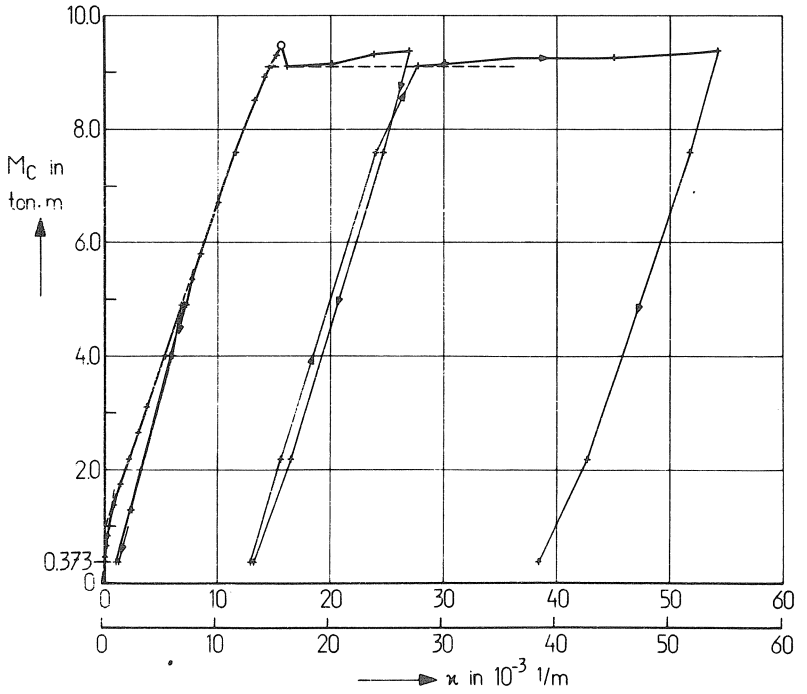

Fig. I-14. Beam X, region C.
Measured M-$\varkappa$ diagram.

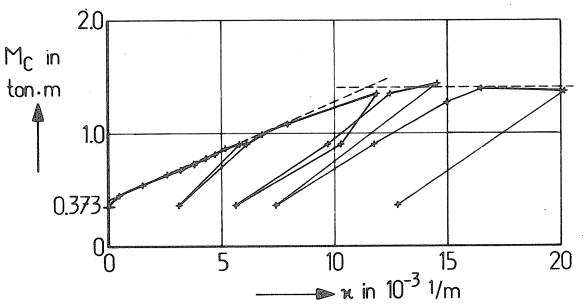

Fig. I-15. Beam IIa.

+ measured values

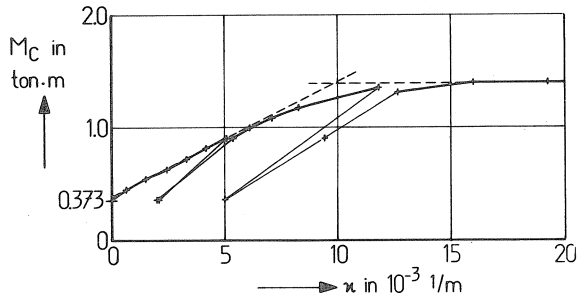

Fig. I-16. Beam IVa, region C.
Measured M-$\varkappa$ diagram.

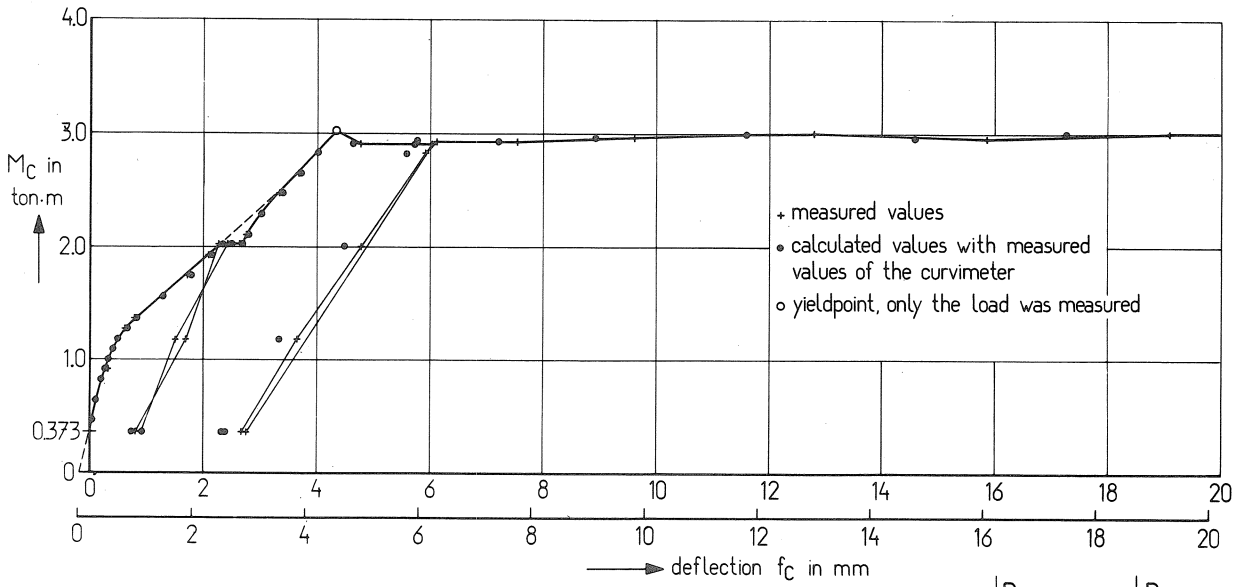

Fig. I-17. Beam VII, region C.
Measured and 'calculated' deflection.

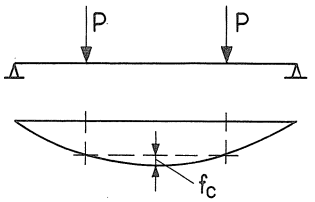

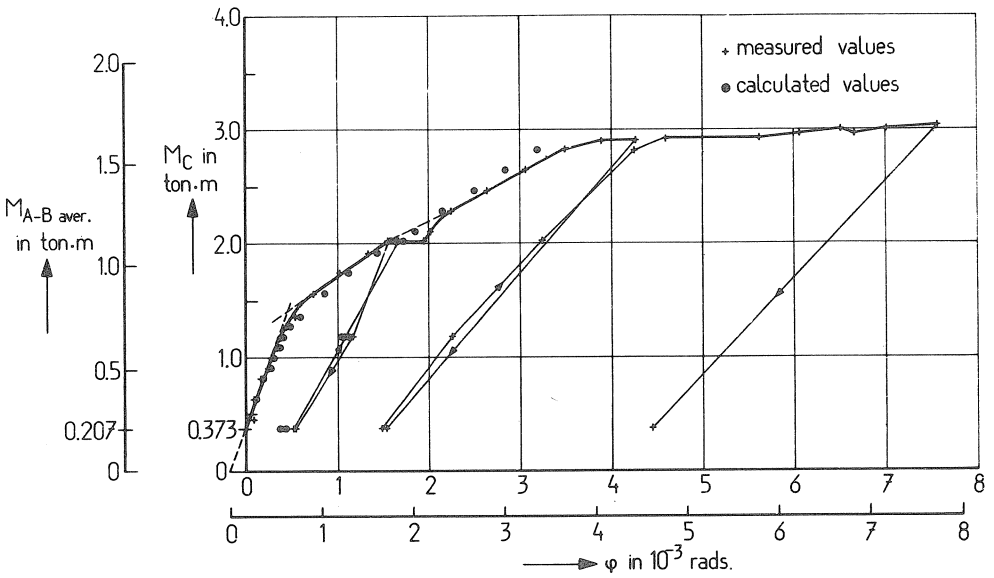

Fig. I-18. Beam VII, region (A + B) (see Fig. I-5).
Average angular rotation φ.

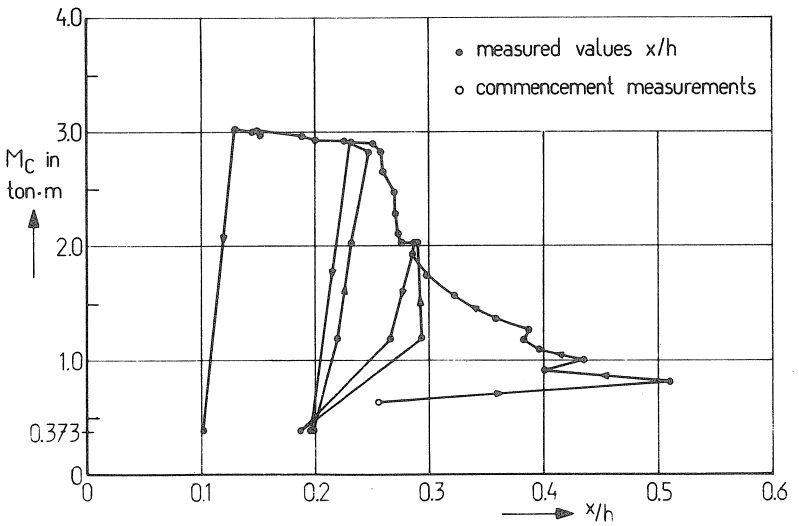

Fig. I-19. Beam VII, region C.
Ratio of neutral axis depth to effective depth.

the moment diminishes in magnitude, yield the correct value of the angular rotation measured there. To this end, in all cases the angular rotations of a part of the beam situated outside the region of constant moment was calculated with the aid of the M-$\varkappa$ diagrams obtained. The compressive strain and tensile strain measured there provide a direct indication of the angular rotations that have occurred. Comparison of the two values showed that there was good agreement, of which Fig. I-18 gives an example. Although the differences are small, the direct measured rotations show the tendency to be bigger than the calculated values. Nevertheless the M-$\varkappa$ diagrams can suitably used there too in the beams concerned.

The average location of the neutral axis was calculated from the measured deformations of the region of constant moment. In general, the average deformations plotted along the depth of the beam yielded a straight connecting line, as was to be expected. An example of this evaluation is given in Fig. I-19.

Fig. I-20 shows the average steel tensile stress in the region of constant moment as a function of the moment there. Those curves are calculated from the measured strain of the tensile reinforcement.

The average and the maximum crack widths were determined from the measurements performed with the small strain gauge (for an example see Fig. I-21). The minimum, average and maximum distances between cracks were also determined as functions of the bending moment in the region of constant moment and are given for one beam in Fig. I-22.

I.5 Further evaluations

As already stated, the object of the investigation was primarily to obtain data concerning the M-$\varkappa$ diagram of reinforced concrete. Observations relating to the other deformations were carried out in order to have the support of additional information in seeking a theoretical basis.

From the shapes of the measured M-$\varkappa$ diagrams it is apparent that they can in general be schematised as a number of straight lines, as Fig. I-23 shows, whereby close approximations are obtained. For this reason the further evaluations will relate to the measured M-$\varkappa$ diagrams schematised in this manner.

In the first place, Fig. I-24 shows the slopes of the second branch of the M-$\varkappa$ diagrams plotted against the percentage of tensile reinforcement. The angles indicated are of course dependent upon the scale;

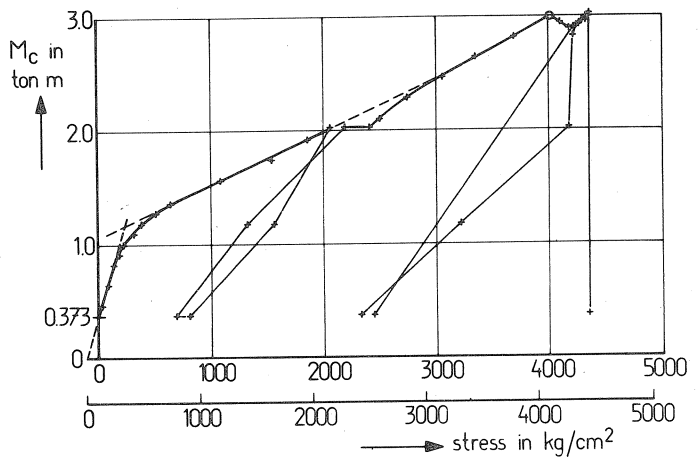

Fig. I-20 Beam VII, region C.
Average steel tensile stress.

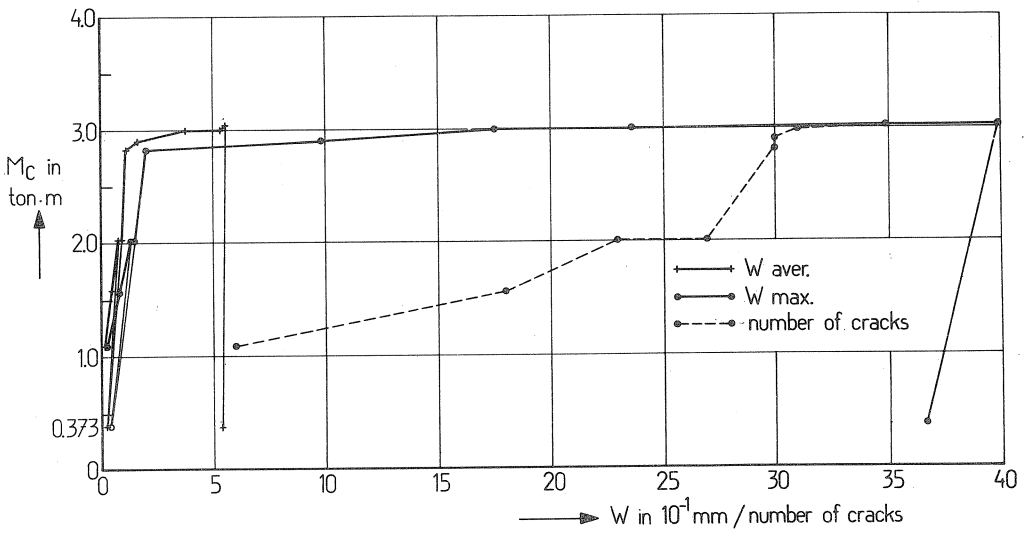

Fig. I-21. Beam VII, region C.
Crack width w and number of cracks (one side of the beam).

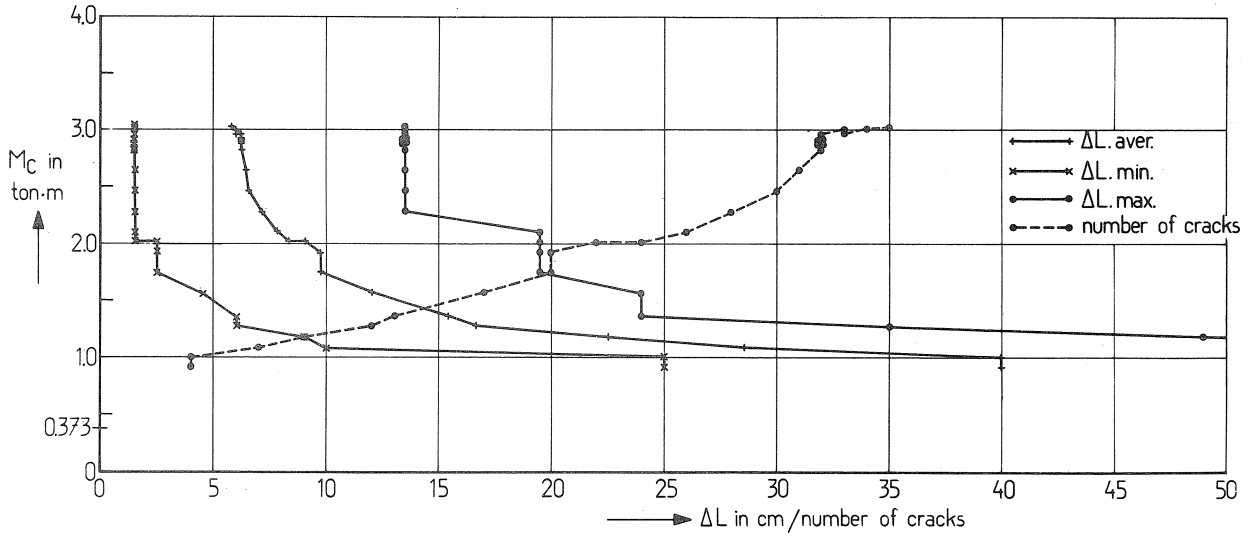

Fig. I-22. Beam VII, region C.
Crack distance $\Delta\ell$ and number of cracks (both sides of the beam).

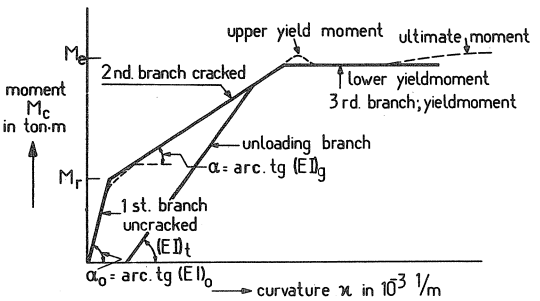

Fig. I-23

Schematised M-$\varkappa$ diagram.

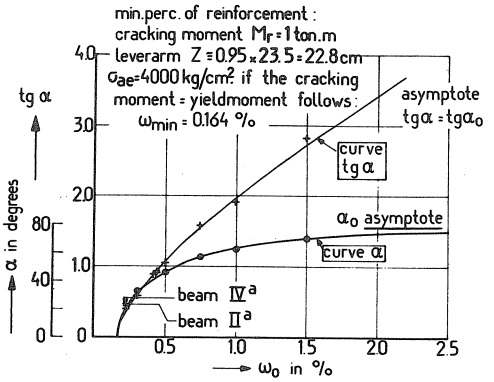

Fig. I-24

Slope of the second branch plotted against the percentage of reinforcement.

in this case they are associated with the scale ratio applied in Figs. I-6 to I-16. The diagram is, however, illustrative because it clearly shows that both the grade of steel and the distribution of the bars have no effect upon the stiffness in the cracked state. Hence for these otherwise similar beams the results of the measurements can be established as a function of the percentage of reinforcement.

The fictitious cracking moment M_r determines the intersection of the two straight branches of the M-$\varkappa$ diagram, which respectively represent the stiffness in the uncracked state and in the cracked state. For the stiffness in the uncracked state the calculated value for $(EI)_o$ has always been adopted. The effect of the reinforcement that was present has been taken into account in this.

If during the measurements the loading is reduced step by step to zero and then increased again, the relationship between bending moment and curvature will have the form of a loop (e.g., see Figs. I-6 to I-16). As already stated, for the purpose of the present report these loops have been schematised as straight lines which everywhere represent the average stiffness of the loop. These lines are designated as 'unloading lines' (retrograde branches); the associated stiffness is $(EI)_t$. For each beam the values $(EI)_t$ of the unloading lines which were determined have been plotted against the average steel stress σ_a of the tensile reinforcement corresponding to the bending moment whereafter the loading was reduced. Fig. I-25 gives the results for the beams II to X, IIa - IVa and results of Belgian experimental investigation*). It appears that the value $(EI)_t$ can be represented by the following expression:

$$(EI)_t = \left[- 5\,\omega_o^2 + 18\,\omega_o + \frac{120}{7 \times 10^{-6}\,\sigma_a^2 + \omega_o + 4} \right] 10^3\ bh^3\ kgcm^2$$

(σ_a in kg/cm^2

bh^3 in cm^4)

In the case of the beams containing steel with a definite yield point the horizontal branch of the diagram was found indeed to occur when the average steel stress attained the yield stress of a single bar. In no case was it possible to determine the end of this branch accurately,

*) H. Lambotte, R. Baus and R. Asselman:
Essais de flexion sur poutres en béton armé;
Rapport de Recherche no. 1, 1963.

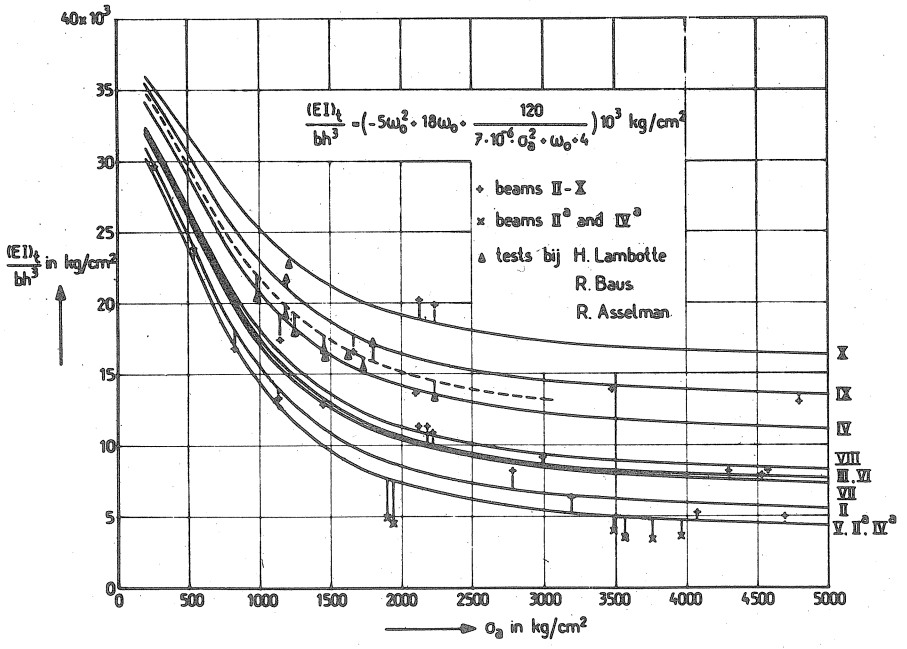

Fig. I-25. Retrograde branches, comparison of measured values $(EI)_t$ with the empirical curves

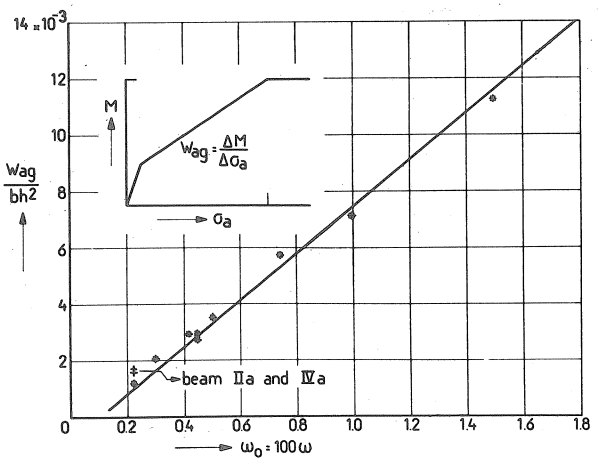

Fig. I-26

Measured values W_{ag} with respect to the tensile reinforcement.

because the test set-up was not so arranged as to be able to cope with the very large attendant deformations.

Finally, the measured average steel stresses call for some comment. The curve which gives the relation between the moment and the average steel stress in the region of constant bending moment can in fact fairly satisfactorily be schematised as three straight lines. If the lines representing this relation $\frac{\Delta M}{\Delta \sigma_a}$ in the cracked state are plotted against the reinforcement percentage ω_0 of the beams concerned, then the average curve is found to be a straight line: see Fig. I-26.

I.6 Conclusions

Within the scope of the variables with which this investigation is concerned the following conclusions can be drawn:

1. The M-$\varkappa$ diagram of reinforced concrete can, with reasonable accuracy, be represented as composed of straight lines.
2. The stiffness in the uncracked state practically corresponds to the calculated $(EI)_0$ in which the presence of reinforcement has been taken into account.
3. The stiffness in the cracked state $(EI)_g$ is, for equal percentage of tensile reinforcement, unaffected by the distribution of the bars (bar diameters employed).
4. For average steel stresses below the limit of proportionality the grade of steel has no significant effect upon the stiffness.
5. The stiffness in the cracked state $(EI)_g$ is, if compressive reinforcement is provided, hardly affected by the presence or absence of cracking in the compressive zone. In this connection the quantity of compressive reinforcement is of relatively minor significance.
6. The stiffness for diminishing magnitude of the loading is a regular function of the reinforcement percentage ω_0 and the highest steel stress that occurred (for equal quality of the concrete).
7. When the M-$\varkappa$ diagram measured in a region of constant bending moment (in a beam with uncracked compressive zone) is applied to parts of the beam where the moment diminishes in magnitude, the values of the angular rotations calculated in such parts are in reasonable good agreement with the measured rotations.
8. In a cracked concrete beam the average steel tensile stress increases proportionally to the bending moment that occurs. The value of that ratio $\frac{\Delta M}{\Delta \sigma_a}$ is linearly related to the percentage of tensile reinforcement for otherwise similar conditions.

Appendix II

EXPERIMENTAL INVESTIGATION CONCERNING THE MOMENT-CURVATURE DIAGRAM FOR
(1) CHANGE OF SIGN OF THE BENDING MOMENT;
(2) LOAD ALTERNATIONS

II.1 Introduction

The M-$\varkappa$ diagram of reinforced concrete has already formed the subject of earlier detailed investigation in the case where the loading is applied for the first time. However, if the loading is applied according to the shake down analysis, it often occurs that the algebraic sign of the bending moment changes. What originally was a tensile zone of the beam then becomes a compressive zone, and vice versa. This effect of the changing of the signs of the moments could not be satisfactorily deduced from the diagrams measured in earlier investigations. Besides this problem there is the fact that as yet little is known concerning the influence of load alternations applied while the load is being increased.

It was decided to obtain data that would provide the required insight into the above-mentioned problems. Measurements were performed on nine reduced-scale test beams. The relation between moment and curvature was determined under various conditions and after various previous sets of conditions (i.e., after such changes as may have occurred in the algebraic sign of the bending moment). The M-$\varkappa$ diagram was in all cases plotted from the observations carried out in the region of constant moment.

The results are summarised here.

II.2 Test beams

The investigation was performed on two series of small beams having a depth h_t = 8 cm and a width b = 5 cm. The overall length of each beam was 100 cm. The beams were made of micro-concrete, the composition of which is indicated in Table II-1.

All the test beams had substantially the same cross-sectional dimensions, as shown in Fig. II-1. Only the main reinforcement differed in the various beams. The six beams of series C were reinforced with six 2.5 mm bars on one side and four 2.5 mm bars on the other. The first two of the three beams comprised in series D were reinforced with six 2.4 mm bars on one side and two 2.4 mm bars on the other, while the third beam

Table II-1. Composition of the concrete.

aggregate grading		cement		w/c ratio
sieve diameter (mm)	retained on the sieves, cum. percentages	type	aggregate/cement by dry weight	
2.8	0	Portland cement-A Enci	~ 4.45 (425 kg/m^3 concrete)	0.50
1.4	40			
0.60	65			
0.300	80			
0.150	95			
0	100			

Table II-2. Strength properties of the concrete.

beam	σ'_w [1] cube strength	[2] compressive strength	[3] prism strength	splitting strength	σ_{bt} flexural (tensile) strength	bulk density	[4] modulus of elasticity E_{bo}	age at testing
	kg/cm^2	kg/cm^2	kg/cm^2	kg/cm^2	kg/cm^2	kg/dm^3	kg/cm^2	days
C_1	227	224	190	-	29.7	2.23	3.23×10^5	7
C_2	249	228	198	-	22.7	2.25	3.02×10^5	6
C_3	249	237	198	-	29.7	2.26	3.12×10^5	6
C_4	272	255	202	-	25.5	2.29	3.02×10^5	6
C_5	247	230	210	-	30.9	2.27	3.15×10^5	7
C_6	266	280	253	-	23.9	2.26	3.30×10^5	8
average	252	244	208	-	27.9	2.26	3.14×10^5	
D_1	219	-	-	21.6	26.0	2.25	2.90×10^5	7
D_2	284	-	211	22.8	30.0	2.29	2.83×10^5	7
D_3	290	-	250	24.0	29.7	2.27	3.23×10^5	7
average	264	-	231	22.8	28.6	2.27	2.99×10^5	

[1] measured on six (series C) or five (series D) 7.1 cm cubes crushed between 3 mm thick cardboard

[2] pressed between two steelplates

[3] measured on one 10 cm × 10 cm × 30 cm prism

[4] measured on two 10 cm × 10 cm × 30 cm prisms

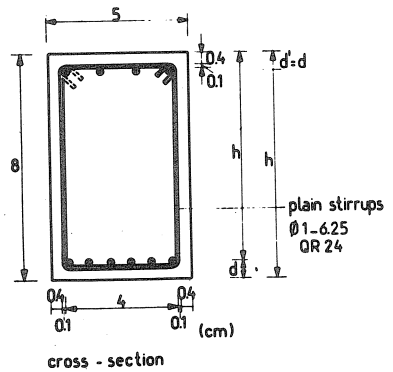

beam	bottem reinf.	top reinf.	d = d' (cm)	h (cm)
C 1	6 Ø 2.5	4 Ø 2.5	0.62^5	7.37^5
C 2	4 Ø 2.5	6 Ø 2.5		
C 3	6 Ø 2.5	4 Ø 2.5		
C 4	4 Ø 2.5	6 Ø 2.5		
C 5	6 Ø 2.5	4 Ø 2.5		
C 6	4 Ø 2.5	6 Ø 2.5		
D 1	6 Ø 2.4	2 Ø 2.4	0.62	7.38
D 2	2 Ø 2.4	6 Ø 2.4		
D 3	6 Ø 2.4	6 Ø 2.4		

serie C

bh = 36.875 cm^2

6Ø2.5 ≡ 0.799 %

4Ø2.5 ≡ 0.533 %

serie D

bh = 36.90 cm^2

6Ø2.4 ≡ 0.736 %

2Ø2.4 ≡ 0.245 %

Fig. II-1 Typical details of the test beams

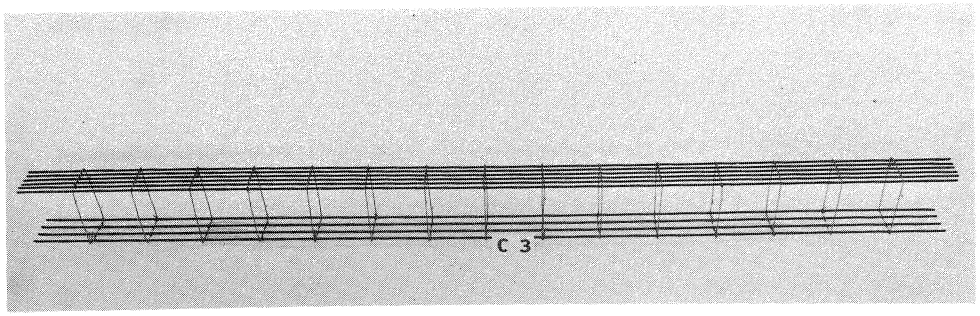

Fig. II-2
Reinforcement cage of testbeam C_3.

(D_3) in this series was provided with six 2.4 mm bars both as top and as bottom reinforcement. The main reinforcement consisted of deformed bars in steel grade QR 40 (hot-rolled steel with minimum elastic limit of 40 kg/mm^2). The location of the reinforcement is shown in the table accompanying Fig. II-1.

Along its entire length each beam was provided with 1 mm diameter stirrups (plain bars of grade QR 24) spaced at 6.25 cm centres. Fig. II-2 shows a typical reinforcement cage.

The properties of the concrete at the time of testing the beams in question are indicated in Table II-2. The stress-strain diagrams and other significant data for the steel are presented in Fig. II-3, which is accompanied by a photograph showing the deformation pattern of the reinforcing steel.

II.3 Execution of the tests

II.3.1 Arrangement

The test beams were loaded in accordance with the so-called four-point bending test. The span was 95 cm. The two load application points were located 50 cm centre-to-centre and symmetrically with respect to mid-span. The arrangement is shown in Fig. II-4, while Fig. II-5 shows testing in progress. For practical reasons the beams were tested in the inverted position.

II.3.2 Testing

The loading was increased in small increments.

The object of testing the beams C_1 and C_2 was to determine the M-$\varkappa$ diagram for loading applied for the first time. In the course of these operations the load was reduced a number of times in order to determine the retrograde branches of the M-$\varkappa$ diagram. This was done because earlier investigations had shown that when such a retrogression occurs only once, the M-$\varkappa$ diagram as a whole is not thereby adversely affected.

The tests performed on the beams C_1 and C_2 therefore determined the M-$\varkappa$ diagrams for tensile reinforcement comprising six 2.5 mm bars (= 0.799%) and four 2.5 mm bars (= 0.533%) respectively.

In the testing of the beams C_3 and C_4 the load was, every time it was reduced to zero as in the preceding cases, reversed in that its algebraic sign was changed. The bending moment then of course also changed to

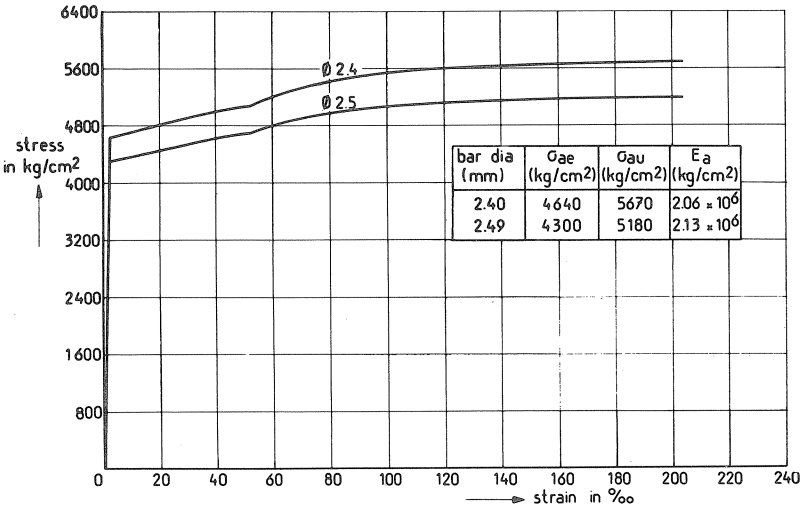

Fig. II-3 Stress-strain diagram of the reinforcement.

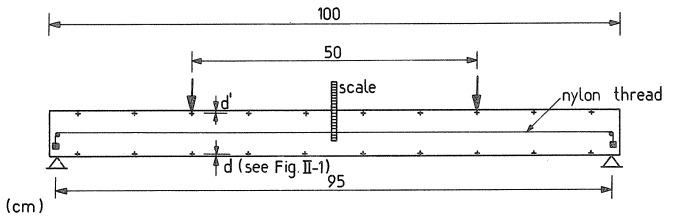

for practical reasons the beams were tested in the inverted position

gauge location points for demountable strain gauge: gauge length 10 cm

Fig. II-4 Schematised diagram of test arrangement.

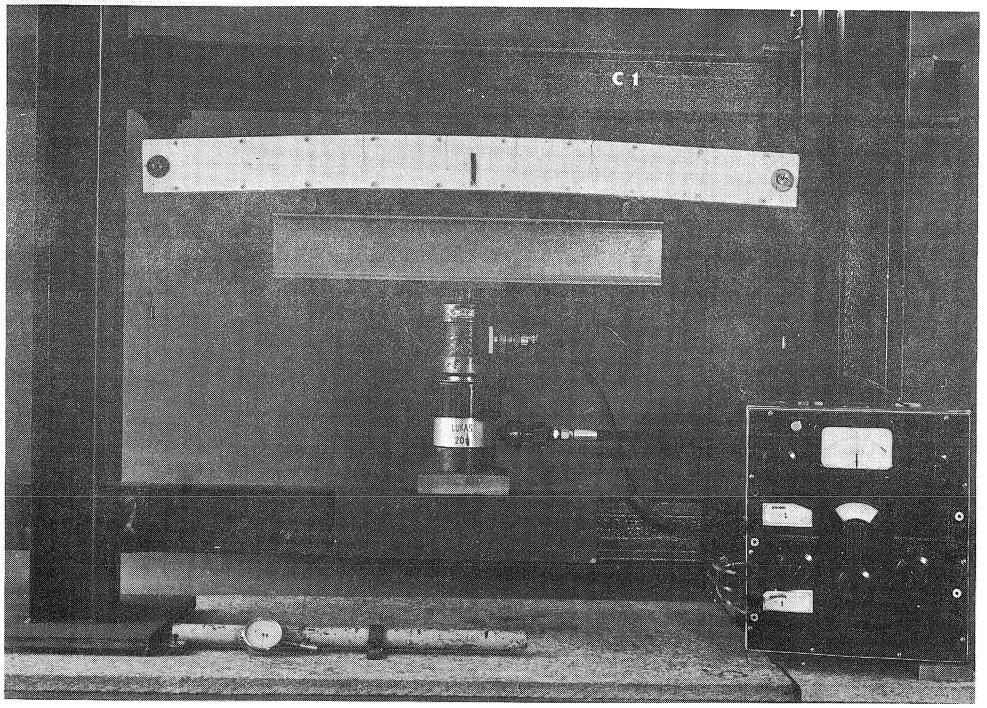

Fig. II-5 Survey of the test equipment

the opposite sign: the original tensile zone became the compressive zone. In this way the sign of the moment was changed at a number of points in the diagram. As appears from Fig. II-1, the testing of beam C_3 started with six 2.5 mm bars as the tensile reinforcement, while in the case of C_4 the original tensile reinforcement consisted of four 2.5 mm bars.

For the last two beams in series C - namely, C_5 and C_6 - the loading applied in the test was increased in conjunction with alternation. More particularly, this procedure was as follows: first, the load was brought up to the desired magnitude; then it was varied ten times between this magnitude and zero. In addition, with each beam the series of ten alternations was repeated three times in order to investigate the influence of the number of alternations.

The three beams of series D were tested in the same manner as C_3 and C_4, i.e., with changing algebraic sign of the moment. In the case of D_1 and D_2 the tensile reinforcement consisted of six 2.4 mm bars (= 0.736%) and two 2.4 mm bars (= 0.245%) respectively. In beam D_3 the top and the bottom reinforcement were identical, so that the quantities of reinforcement in the tensile and in the compressive zone remained unchanged at each change in the sign of the moment.

II.3.3 Measurements performed

The following measurements were performed on the beams:

- The deflection at mid-span. For measuring this deflection a scale with millimetre divisions was affixed to the middle of the side face of the beam. In the longitudinal direction a thin nylon thread was stretched from bearing to bearing. With the aid of a small mirror beside the millimetre scale it was possible to obtain deflection readings that were accurate to within 0.1 mm.

- The tensile and compressive strains at the level of the centre-line of the reinforcing bars. These strains were measured by means of a demountable strain gauge with a gauge length of 10 cm. For this purpose, gauge location points were affixed to both sides of each beam in the positions mentioned. In each series of strain measurements some readings were obtained on an invar calibrating bar and on a non-loaded test beam, in order to enable corrections to be made (in accordance with normal practice) for possible changes affecting the strain gauge or the test beam, e.g., in consequence of temperature influences affecting the

observations.

- The correct load values corresponding to the observations were of course determined.

The necessary means for the execution of the above-mentioned observations are shown in Figs. II-4 and II-5. These observations were performed twice in the zero position of each beam and furthermore once after the application of each load increment.

Since the beams were tested in the inverted position, the dead weight caused negative curvature and deflection. These were, however, so small in comparison with the effects of the other loads ($M_{\text{dead weight}}$ = approx. 1.08 kgm) that they were neglected. When the load had been returned to zero in those case where the algebraic sign of the bending moment was changed, the beam in question was turned upside down. All the observations were made both before and after this inversion.

In the case of those beams on which the load was increased in conjunction with alternation, the measurements were performed directly after the load had been increased and also after this load had undergone ten alternation cycles.

After the yield moment had been reached, the deformations were very large. In this condition the measurements were always performed after the deflection had increased a certain amount. Testing was continued up to a fairly advanced state of deformation, in order to obtain an idea of the greatest plastic curvature. In a number of cases the further application of deformations was stopped already before the occurrence of failure. The deformations which had occurred were then already so large that further testing was not possible with the available equipment. Besides, many of the gauge location points became detached. In those cases the plastic curvature was so great anyway that there would have been little practical significance in accurately determining the extreme value.

II.4 Evaluation of the measured data

From the above-mentioned observations the desired M-$\varkappa$ diagrams were in the first place determined. The average measured compressive strain and tensile strain in the region of constant moment, measured at the level of the tensile and the compressive reinforcement, were for that purpose divided by the distance between the measuring lines. These values were plotted against the corresponding moment M_c occurring in the constant moment

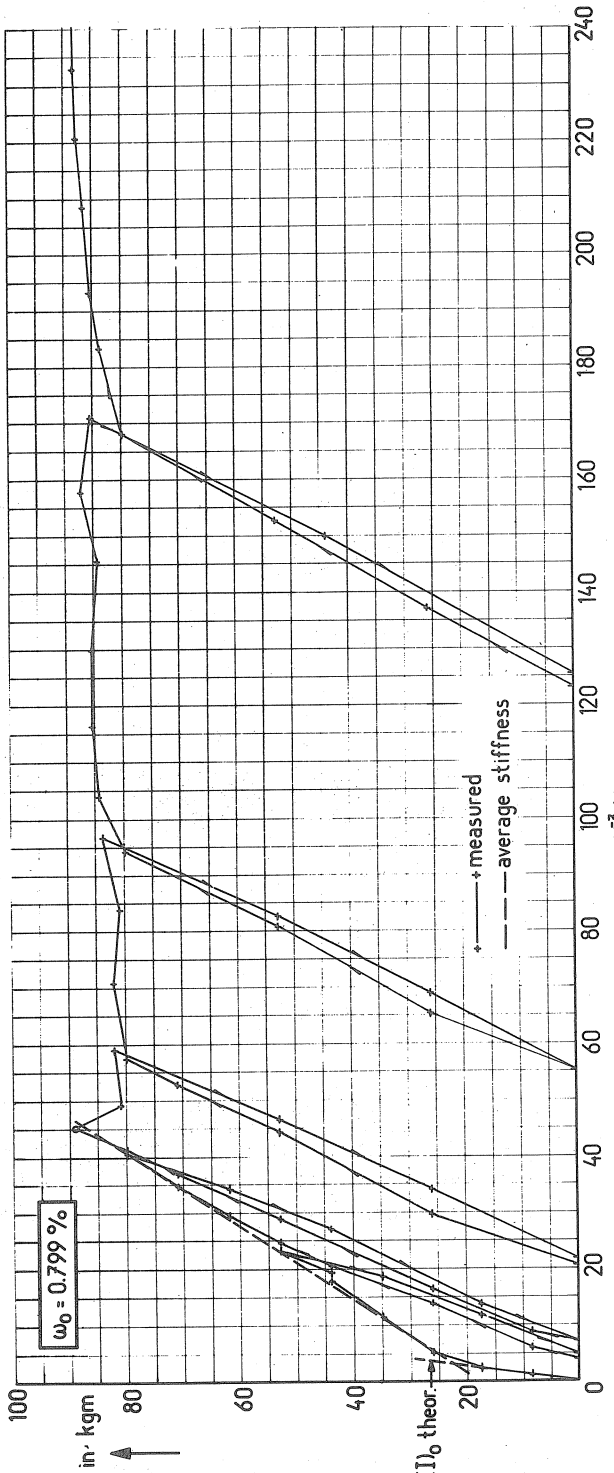

Fig. II-6 Beam C_1

region. Figs. II-6 to II-14 present the results for the beams C_1 to C_6 and D_1 to D_3.

The mid-span deflection was likewise plotted against this moment; these diagrams are not presented here.*) Further evaluation of the measured data has not been carried out.

II.5 Discussion of the M-$\varkappa$ diagrams

II.5.1 Series C

The theoretical stiffness of the uncracked section is $(EI)_o = 7766 \times 10^4$ kgcm^2. In the calculation the effect of the reinforcement was considered, and the average measured value of the modulus of elasticity of the concrete, namely, $E'_{bo} = 3.14 \times 10^5$ kg/cm^2 (see Table II-2), was taken into account. In all the M-$\varkappa$ diagrams presented here this theoretical stiffness is indicated as a thick broken line.

Beam C_1

The measured average stiffness of the cracked reinforced section is $(EI)_g = 1570 \times 10^4$ kgcm^2 (see Fig. II-6). On the basis of the earlier measurements and the empirical formula**) derived therefrom the value of $(EI)_g$ would have had to be 1687×10^4 kgcm^2. The discrepancy is therefore 7.5%.

The measured value of $(EI)_o$ is a little lower than the above-mentioned theoretical value. The retrograde branches conform entirely to the M-$\varkappa$ diagrams measured earlier on. The assumption that these undergo no further change in slope after attaining the yield moment (as previously supposed) is found to be tenable here too.

Beam C_2

The average stiffness in the cracked state measured for this beam is $(EI)_g = 1152 \times 10^4$ kgcm^2 (Fig. II-7). On the basis of the above-mentioned empirical formula the value of $(EI)_g$ would have had to be 1123×10^4 kgcm^2. The discrepancy is 2.5%. The measured value is somewhat greater; in view of the relative great quantity of compressive reinforcement this was to be expected.

---

*) These diagrams are available in TNO-report BI-67-110 (written in dutch)

**) $(EI)_g = (-2.5\,\omega_o^2 + 13.9\,\omega_o - 1.1)\,bh^3 \times 10^3$ kgcm^2

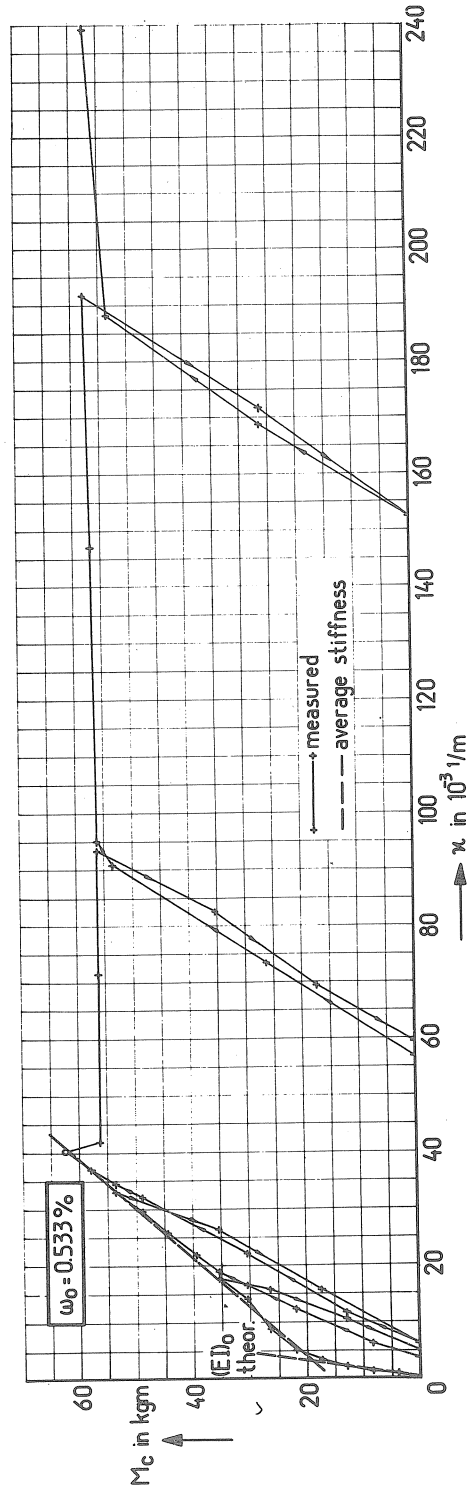

Fig. II-7 Beam C_2

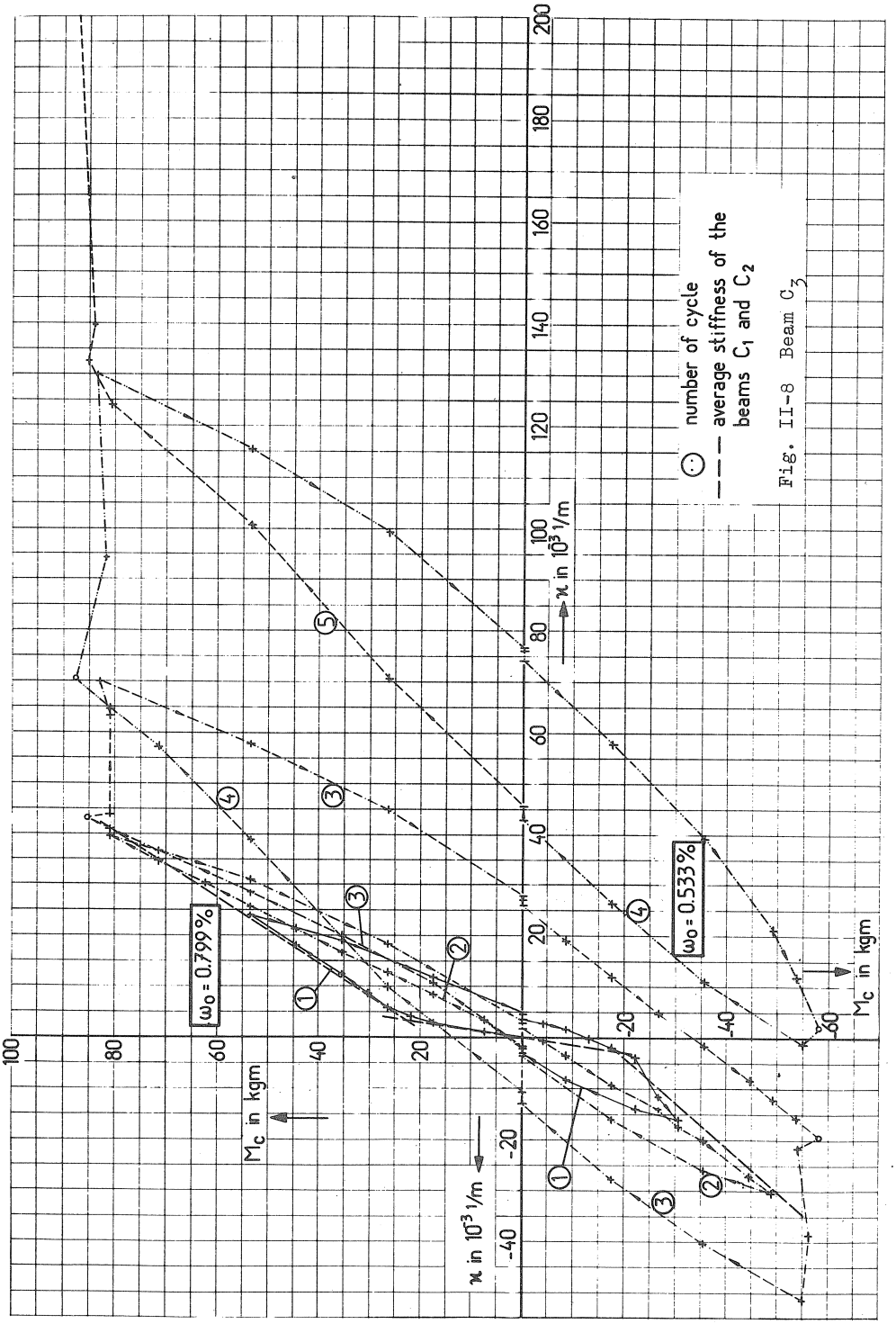

Fig. II-8 Beam C_3

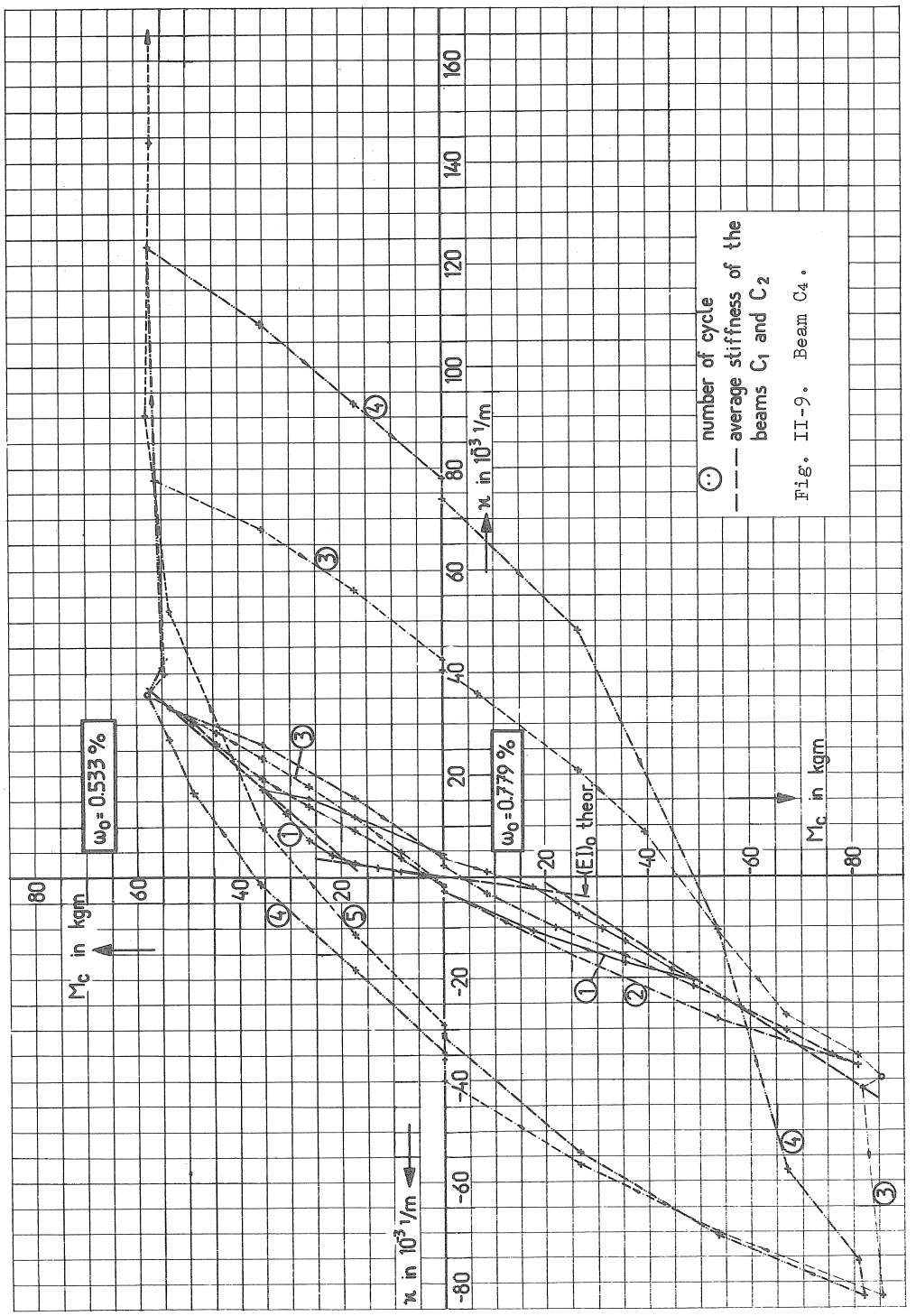

Fig. II-9. Beam C_4.

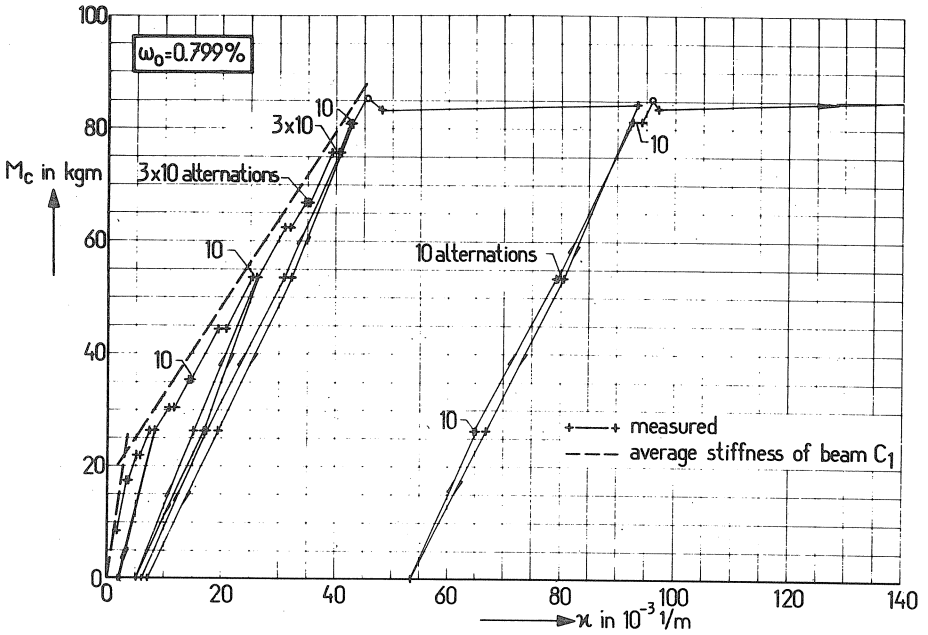

Fig. II-10 Beam C_5

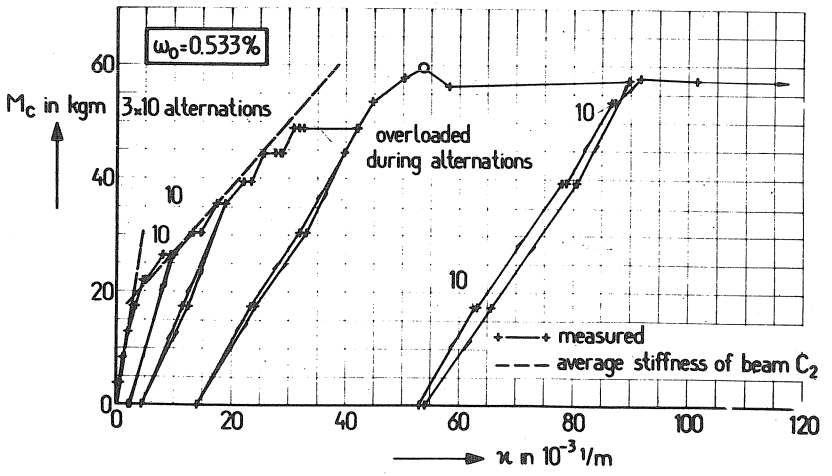

Fig. II-11 Beam C_6

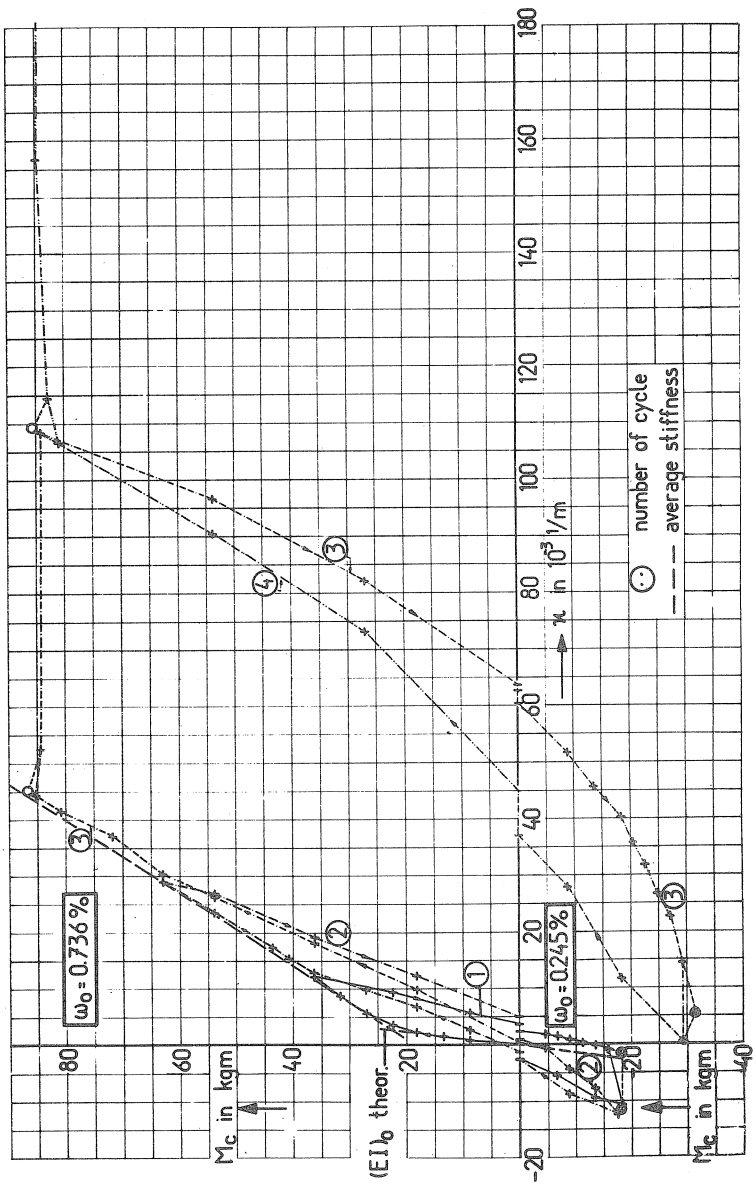

Fig. II-12 Beam D_1

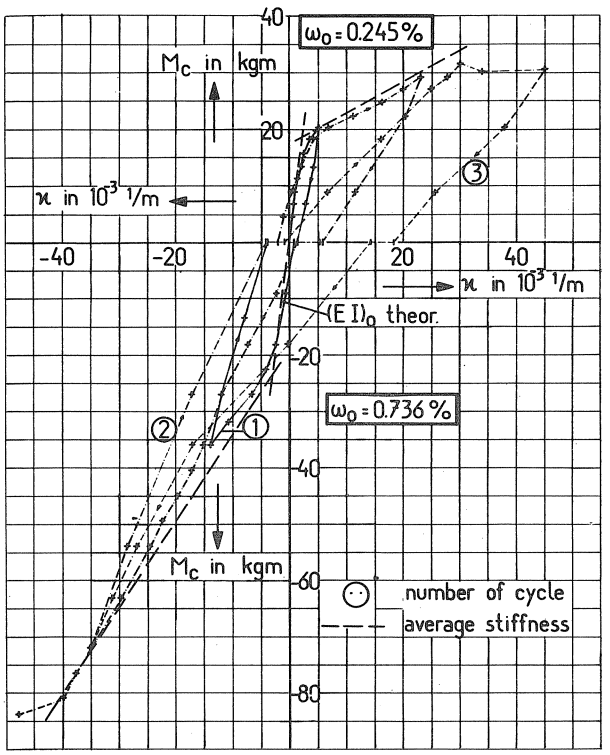

Fig. II-13 Beam D_2

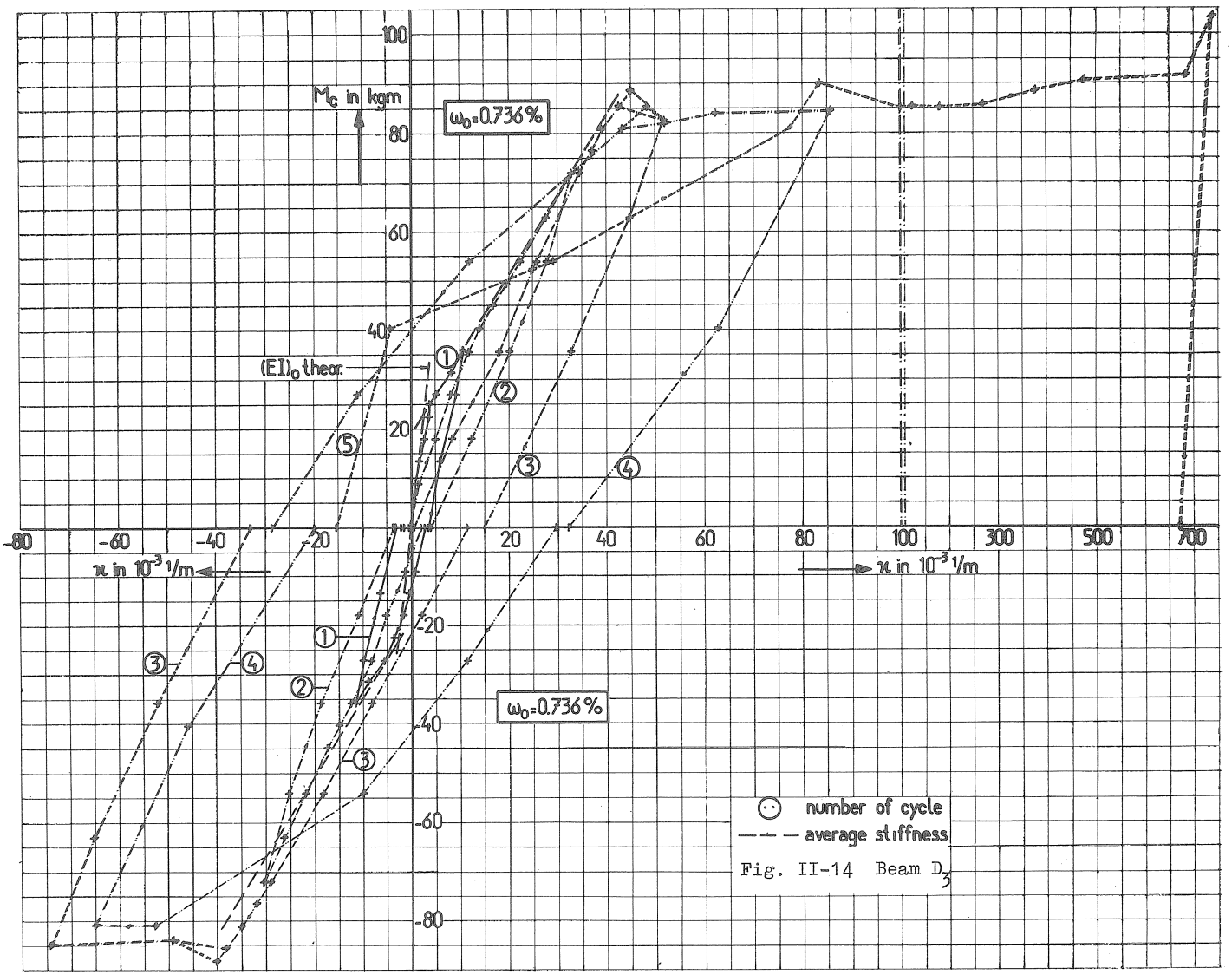

Fig. II-14 Beam D5

For the rest, the comments regarding $(EI)_0$ and the retrograde branches for beam C_1 are valid for beam C_2 also.

Beams C_3 and C_4

In Figs. II-8 and II-9 the average stiffness of the beams C_1 and C_2 is indicated as a thick broken line in the measured M-$\varkappa$ diagrams. It is found that these M-$\varkappa$ diagrams measured for first-time loading remain recognisable for a fairly long time in the diagrams measured for the beams C_3 and C_4.

When the yield moment of the section alternates between "positive" and "negative" the stiffness varies greatly.

Beams C_5 and C_6

When the load is increased in conjunction with alternation, this produces, in the main, a displacement of the "cracked" branch of the curve parallel to itself, as appears from Figs. II-10 and II-11. The cracking moment decreases, as it were. The reason for this effect becomes clear on considering that, as a result of alternation in the tensile zone, the influence of the concrete diminishes. The tensile strength apparently decreases.

Between two load increments, i.e., when the load is increased again after the alternation cycles have been applied, the stiffness tends towards that of the retrograde branch.

The absolute values of these effects are closely linked to the number of alternations applied. The alternations cause no change in the retrograde branches as compared with the retrograde branches of a M-$\varkappa$ diagram for first-time loading.

II.5.2 Series D

The average theoretical stiffness of the uncracked section for the beams D_1 and D_2 is $(EI)_0 = 6800\times10^4$ kgcm^2. This value has been calculated with the average modulus of elasticity for the concrete $E'_{bo} = 2.87\times10^5$ kg/cm^2 for the said beams (see Table II-2). For D_3 the theoretical stiffness is $(EI)_0 = 8065\times10^4$ kgcm^2, calculated with $E'_{bo} = 3.23\times10^5$ kg/cm^2. The reinforcement contained in the beams has of course again been taken into account.

In this series no beams were tested with a view to determining the M-$\varkappa$ diagrams for tensile reinforcement comprising six 2.4 mm and two 2.4 mm bars, respectively, under first-time loading conditions. The

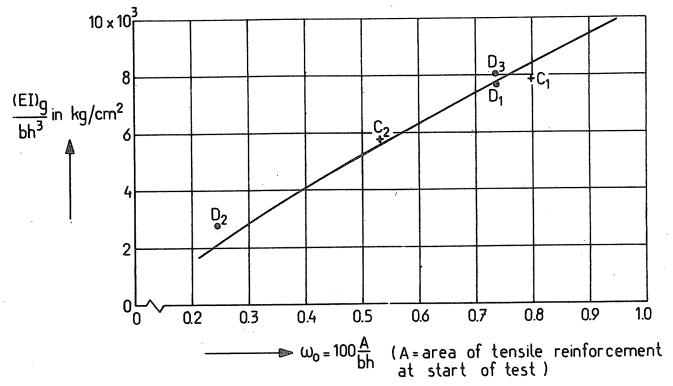

Fig. II-15 The bending stiffness in the cracked state.

stiffnesses represented by thick broken lines in Figs. II-12 to II-14 have in fact been determined from those parts of the measured diagrams which correspond to the original tensile reinforcement (part above the zero line).

The average stiffness in the cracked state, measured on beam D_1 (Fig. II-12), for $\omega_o = 0.736\%$, is $(EI)_g = 1538 \times 10^4$ kgcm^2. The empirical formula gives $(EI)_g = 1563 \times 10^4$ kgcm^2, in relation to which the measured stiffness shows a discrepancy of 1.6%.

From Fig. II-14, relating to beam D_3 with equal top and bottom reinforcement (six bars of 2.4 mm diameter), the stiffness value obtained is $(EI)_g = 1613 \times 10^4$ kgcm^2, in which case the discrepancy is equivalent to 0.3%.

For beam D_2 (Fig. II-13), with $\omega_o = 0.245\%$, the measured stiffness is $(EI)_g = 557 \times 10^4$. This differs by 12.9%, on the stiffer side, from the value calculated from the empirical formula, namely, $(EI)_g = 433 \times 10^4$ kgcm^2.

It has therefore in all cases been taken the portion of the "cracked" branch which has been measured after the first cycle, and is located above the moment at which the load was reduced, extends parallel to the "cracked" branch associated with loading applied for the first time. In Fig. II-15 the measured average stiffnesses $(EI)_g$ have been plotted as a function of the reinforcement percentage ω_o. The said empirical equation has likewise been represented in graph form. As appears from the diagram, for most of the beams the stiffness $(EI)_g$ is in very good agreement with expections based upon the mentioned empirical formula.

II.6 The deflection

The graphes presenting the measured mid-span deflection as a function of the corresponding moment M_c have the same form as the M-$\varkappa$ diagrams.

The deflection in the uncracked state was calculated from:

$$f_m = \frac{Pa}{24\,EI}\,(3\ell^2 - 4a^2)$$

where (see Fig. II-4): $\ell = 95$ cm; $a = 22.5$ cm; $P = \frac{100\,M_c}{22.5}$ kg; EI in kgcm^2; f_m in cm; M_c in kgm

Hence: $f_m = \frac{23,484}{(EI)_o}\,P = \frac{104,375}{(EI)_o}\,M_c$

In the uncracked state the stiffness is $(EI)_0$ for the uncracked section including the reinforcement. In general, the discrepancy between the measured and the calculated deflection in the uncracked state is within the accuracy of measurement.

A rough check of the measured increment of the deflection in the cracked state can be carried out without too much arithmetical effort by assuming the beam to be cracked over its entire length. The deflection calculated in this way:

$$\Delta f_m = \frac{104,375}{(EI)_g} \Delta M_c$$

is in reasonable good agreement with the measured deflection, because of the relatively high ratio $\frac{\ell - 2a}{\ell}$.

II.7 Conclusions

- The M-$\varkappa$ diagrams obtained for first-time loading are in good agreement with the results found in earlier tests.
- When a change of sign occurs in the bending moment to which the beam is subjected, the above-mentioned diagram remains recognisable for a fairly long time, if the percentage of compressive reinforcement at the beginning of the test is not too low in relation to the tensile reinforcement.

For $\omega_o' = 0.245\%$ against $\omega_o = 0.736$ (beam D_1) this is hardly the case.

- Increasing the load in conjunction with alternation thereof causes the "cracked" branch of the curve to be displaced parallel to itself. The tensile strength of the concrete undergoes an apparent decrease. The retrograde branches, however, are not appreciably affected by these alternations.
- As expected, the deflection diagrams exhibit the same trend as the M-$\varkappa$ diagrams under the various conditions.

Appendix III

CALCULATIONS CONCERNING THE CRACKED SECTION

III.1 Theoretical assumptions

To develop the formulas required in the calculations concerning the cracked section, the following wellknown fundamental assumptions are used as a basis:

- The deformations of the fibers are directly proportional to their distances from the neutral axis.
- The tensile resistance of concrete is ignored and the steel reinforcement is depended on to resist all tensile stresses.
- Perfect adhesion exists between the concrete and the steel reinforcement. Deformations of the materials do not break the bond between them.
- The stress-strain relation of the concrete is a 2^{nd} degree parabola with the top at the concrete compressive strain ε'_{be} and the stress σ'_{be}. The ultimate concrete strain is ε'_{bu}. That diagram is drawn in Fig. III-1. For a strain greater than ε'_{be} the real stress-strain diagram of concrete can be schematised in a number of different ways. The formulas developed in this paper, however, are valid only if $\varepsilon'_b \leqq \varepsilon'_{be}$ or in the other case if the stress-strain relation remains a parabola, also between ε'_{be} and ε'_{bu}.
- The stress-strain relation of the steel reinforcement consists of two straight lines according to Fig. III-2.

The stress-strain diagram of both concrete and steel reinforcement are of course data for the calculations.

III.2 Derivation of the formulas

The formulas will be developped for a relative general case: a cross section of a flanged beam with compressive reinforcement too.
The method suggests the steel strain ε_a being a given value. Herewith, from given relations between the deformations and from equilibrium of forces the depth of the neutral axis can be found.
After the determination of the neutral axis it is possible to calculate all stresses and strains and at last the actual curvature and moment.
In this way and for increasing values of ε_a the M-$\varkappa$ diagram of the

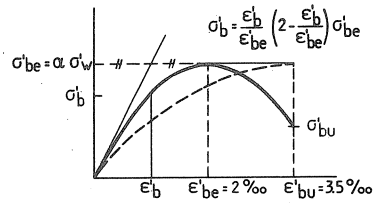

- α = 0.6 according to the G.B.V.
- α = 0.83 used in this paper for the interpretation of tests

Fig. III-1

Concrete stress-strain diagram.
(dotted curve = diagram according to the G.B.V. 1962)

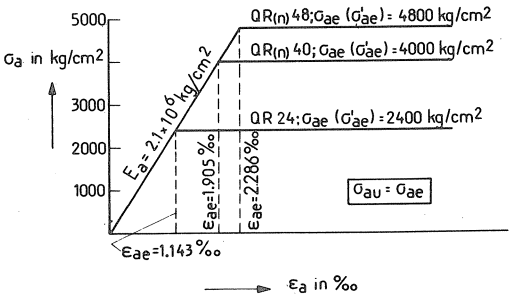

Fig. III-2 Steel stress-strain diagrams.

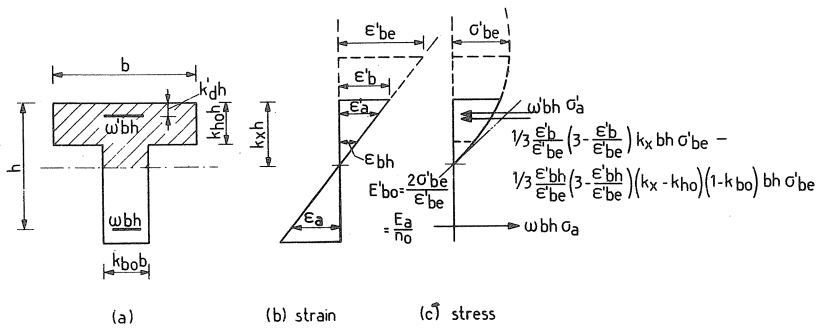

Fig. III-3

cracked section is known also.
For $\varepsilon_a = \varepsilon_{ae}$ (= yield strain of the tensile reinforcement and $\sigma_a = \sigma_{ae}$) the calculations are of course directly related to the yield moment of the cross section.

From Fig. III-3, since the deformations are directly proportional to their distances from the neutral axis:

a) $$\varepsilon'_b = \varepsilon_a \frac{k_x}{1 - k_x} \quad \text{or} \quad \frac{\varepsilon'_b}{\varepsilon'_{be}} = \frac{\varepsilon_a}{\varepsilon'_{be}} \cdot \frac{k_x}{1 - k_x} \qquad \ldots\ldots (1)$$

b) $$\frac{\varepsilon'_{bh}}{\varepsilon'_{be}} = \frac{\varepsilon_a}{\varepsilon'_{be}} \cdot \frac{k_x - k_{ho}}{1 - k_x} = \frac{\varepsilon'_b}{\varepsilon'_{be}} \cdot \frac{k_x - k_{ho}}{k_x} \qquad \ldots\ldots (2)$$

c) $$\varepsilon'_a = \varepsilon_a \cdot \frac{k_x - k'_d}{1 - k_x} = \varepsilon'_b \cdot \frac{k_x - k'_d}{k_x} \qquad \ldots\ldots (3)$$

The concrete-compressive force

With the equations (1) and (2) (see Fig. III-3c):

$$\frac{N'_b}{bh} = \frac{1}{3} \frac{\varepsilon_a}{\varepsilon'_{be}} \cdot \frac{k_x}{1 - k_x} \Big(3 - \underbrace{\frac{\varepsilon_a}{\varepsilon'_{be}} \cdot \frac{k_x}{1 - k_x}}_{= r_d}\Big) k_x \, \sigma'_{be}$$

$$- \frac{a}{3} \frac{\varepsilon_a}{\varepsilon'_{be}} \frac{k_x - k_{ho}}{1 - k_x} \Big(3 - \frac{\varepsilon_a}{\varepsilon'_{be}} \frac{k_x - k_{ho}}{1 - k_x}\Big)(k_x - k_{ho})(1 - k_{bo}) \, \sigma'_{be} \quad \ldots (4)$$

Herein is:

$$a = 0 \quad \text{if} \quad k_x \leqq k_{ho} \qquad \ldots\ldots (5a)$$

and $$a = 1 \quad \text{if} \quad k_x > k_{ho} \qquad \ldots\ldots (5b)$$

Substitution of

$$\frac{\sigma'_{be}}{\varepsilon'_{be}} \cdot \varepsilon_a = \frac{1}{2} E'_{bo} \frac{\sigma_a}{E_a} = \frac{\sigma_a}{2n_o} \quad \text{(a consequence of the parabolic stress-strain diagram)} \qquad \ldots\ldots (6)$$

and $$\frac{\varepsilon_a}{\varepsilon'_{be}} = r_a \qquad \ldots\ldots (7)$$

yield after transposing:

$$\frac{N'_b}{bh} = \frac{\sigma_a}{6n_o(1 - k_x)^2}\Big[\Big[-\Big\{(3 + r_a) - a(1 - k_{bo})(3 + r_a)\Big\}k_x^3 + 3\Big[1 - a\,(1 - k_{bo})\Big\{1 + k_{ho}(2 + r_a)\Big\}\Big]k_x^2 + 3\,a\,k_{ho}\,(1 - k_{bo})\Big\{2 + k_{ho}(1 + r_a)\Big\}\,k_x - a\,k_{ho}^2\,(1 - k_{bo})(3 + k_{ho}.r_a)\Big]\Big] \qquad \ldots\ldots (8)$$

Compressive force in top reinforcement

Assuming the steel grades of the tensile - and compressive reinforcement are aqual and using equation (3):

$$\frac{N'_a}{bh} = \omega' \cdot \sigma_a \cdot \frac{n_o - 1}{n_o} \cdot \frac{k_x - k'_d}{1 - k_x} \qquad \ldots\ldots (9)$$

Herein is, as defined in equation (6), $n_o = \frac{E_a}{E'_{bo}}$.

This equation is only valid if $\varepsilon'_a < \varepsilon_{ae}$.
The other case, $\varepsilon'_a \geqq \varepsilon_{ae}$, will normally not occur before the tensile reinforcement yield and under that circumstances, where both tensile and compressive reinforcement yield:

$$\frac{N'_a}{bh} = \omega' \cdot \frac{n_o - 1}{n_o} \cdot \sigma_{ae} \qquad \ldots\ldots (10)$$

The equations (9) and (10) are summarised in one equation:

$$\frac{N'_a}{bh} = \frac{\sigma_a}{6n_o\,(1 - k_x)^2}\Big[\Big[6(n_o - 1)\omega'\Big\{-\ell_1 k_x^2 + \ell_2 k_x(1 + k'_d) - \ell_3 k'_d\Big\}\Big]\Big] \qquad \ldots\ldots (11)$$

in which

$$\ell_1 = \ell_2 = \ell_3 = 1 \quad \text{if} \quad \varepsilon'_a < \varepsilon_{ae} \qquad \ldots\ldots (12)$$

and

$$\left.\begin{aligned} \ell_1 &= -1 \\ \ell_2 &= -\frac{2}{1 + k'_d} \\ \ell_3 &= -\frac{1}{k'_d} \end{aligned}\right\} \quad \begin{aligned} &\text{if } \varepsilon'_a \geqq \varepsilon_{ae} \\ &\text{(in that case} \\ &\sigma_a \text{ becomes } \sigma_{ae}) \end{aligned} \qquad \ldots\ldots (13)$$

Tensile force in the bottom reinforcement

This force is simply $\frac{N_a}{bh} = \omega \sigma_a$, which gives, provided with the same denominator as equations (8) and (11):

$$\frac{N_a}{bh} = \frac{\sigma_a}{6n_o (1 - k_x)^2} \left\{6n_o (1 - 2 k_x + k_x^2)\omega\right\} \quad \ldots\ldots (14)$$

Equilibrium of forces

From $N'_b + N'_a - N_a = 0$ is found:

$$\begin{aligned} &- \left\{(3 + r_a) - a(1 - k_{bo})(3 + r_a)\right\}k_x^3 \\ &+ \left[\left[3\left[1 - a(1 - k_{bo})\left\{1 + k_{ho}(2 + r_a)\right\}\right] - 6(n_o - 1)\ell_1\omega' - 6 n_o \omega\right]\right]k_x^2 \\ &+ \left[3a k_{ho}(1 - k_{bo})\left\{2 + k_{ho}(1 + r_a)\right\} + 6(n_o - 1)(1 + k'_d)\ell_2\omega' \right. \\ &\qquad \left. + 12 n_o \omega\right] k_x \\ &- \left[a k_{ho}^2 (1 - k_{bo})(3 + k_{ho} \cdot r_a) + 6(n_o - 1)k'_d \ell_3 \omega' + 6n_o\omega\right] = 0 \end{aligned}$$

$\ldots\ldots (15)$

After solving this equation for k_x it must be checked if the right values for a and ℓ_1 to ℓ_3 were taken into account. If not, the calculations must be repeated.

Concrete strain and curvature

With the right solution for k_x, $r_d = \frac{\varepsilon'_b}{\varepsilon'_{be}}$ can be found using equation (1).

The actual curvature ratio is

$$\varkappa.h = \frac{\varepsilon'_b}{k_x} = \frac{\varepsilon_a}{(1 - k_x)}$$

Resisting bending moment

Furthermore the bending moment is obtained from moment equilibrium with respect to the tensile reinforcement.

$$\frac{M}{bh^2} = \frac{\sigma_a}{6n_o(1 - k_x)} \left[(3 - r_d)\, k_x^2 \left\{1 - \frac{4 - r_d}{4(3 - r_d)}\, k_x\right\}\right.$$

$$- a(3 - r_d \frac{k_x - k_{ho}}{k_x})(k_x - k_{ho})^2 \,(1 - k_{bo})$$

$$\times\left\{(1 - k_{ho}) - \frac{4 - r_d \dfrac{k_x - k_{ho}}{k_x}}{4(3 - r_d \dfrac{k_x - k_{ho}}{k_x})} (k_x - k_{ho})\right\}$$

$$\left. + 6m\, \omega' \,(n_o - 1)(k_x - k'_d)(1 - k'_d)\right] \qquad \ldots\ldots (16)$$

in which

$$m = 1 \qquad \text{if} \qquad \varepsilon'_a < \varepsilon_{ae} \qquad \ldots\ldots (17)$$

and

$$m = \frac{1 - k_x}{k_x - k'_d} \qquad \text{if} \qquad \varepsilon'_a \geqq \varepsilon_{ae} \qquad \ldots\ldots (18)$$

Equation (16) can be simplified into:

$$\frac{M}{bh^2} = \frac{\sigma_a}{24n_o\,(1 - k_x)k_x} \left[\left\{4(3 - r_d) - (4 - r_d)k_x\right\} k_x^3\right.$$

$$- a\,(1 - k_{bo})(k_x - k_{ho})^2 \left[4(1 - k_{ho}) \left\{3k_x - r_d\,(k_x - k_{ho})\right\}\right.$$

$$\left. - \left\{4\,k_x - r_d\,(k_x - k_{ho})\right\} (k_x - k_{ho})\right]$$

$$\left. + 24\, m\omega' \,(n_o - 1)(k_x - k'_d)\, k_x\, (1 - k'_d)\right] \qquad \ldots\ldots (19)$$

Samenvatting

In deze publikatie wordt zowel het experimentele als theoretische onderzoek beschreven, dat is uitgevoerd met betrekking tot het moment-kromming diagram van gewapend beton. Het onderzoek betreft rechthoekige doorsneden onder buigend moment. Ook het M-$\varkappa$ diagram voor de verschillende stadia in een bepaalde belasting-historie (b.v. met wisselingen) komt ter sprake, mèt de regels op grond waarvan het geïdealiseerde diagram daarvoor kan worden bepaald.

Theoretische beschouwingen betreffende het M-$\varkappa$ diagram komen vervolgens aan de orde. In deze beschouwingen wordt de bepaling van het M-$\varkappa$ diagram gebaseerd op de vorm van het geïdealiseerde, gemeten diagram bij een eerste belasting, dat uit 3 rechte lijnen is opgebouwd. Het gezochte M-$\varkappa$ diagram volgt dan na kombinatie van de eigenschappen van de ongescheurde en gescheurde doorsnede. Hiervoor wordt zowel de 'exacte' berekening als een aantal benaderingsformules gegeven.

Een volledig overzicht van de uitgevoerde proeven wordt in Appendix I en II vastgelegd.

De theoretische interpretatie van het experimentele onderzoek is nog maar ten dele uitgewerkt. De volgende konklusies kunnen worden getrokken:

- de werkelijke buigstijfheid van gewapend beton in het gescheurde stadium en bij een eerste belasting is een betrekkelijke eenvoudige funktie van het wapeningpercentage;
- het M-$\varkappa$ diagram voor meer ingewikkelde gevallen, zoals voor een bepaalde 'belasting-historie' (dus b.v. bij lastwisselingen) kan op bevredigende wijze uit het diagram voor een eerste belasting worden afgeleid;
- door de CEB-formule voor de buigstijfheid in het gescheurde stadium wordt de werkelijke waarde onderschat, met name bij de lagere betonkwaliteiten en voor de hogere wapeningpercentages.